FINITE ELEMENT ANALYSIS ON MAGNETO-HYDRODYNAMIC MIXED CONVECTION FLOW IN A TRIANGULAR ENCLOSURE

by

Aki Farhana
Student No. 0409093009F
Registration No. 0409093009, Session: April-2009

MASTER OF PHILOSOPHY
IN
MATHEMATICS

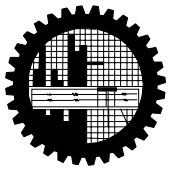

Department of Mathematics
BANGLADESH UNIVERSITY OF ENGINEERING AND TECHNOLOGY (BUET), DHAKA-1000
JANUARY- 2012

The thesis titled

FINITE ELEMENT ANALYSIS ON MAGNETO-HYDRODYNAMIC MIXED CONVECTION FLOW IN A TRIANGULAR ENCLOSURE

Submitted by

AKI FARHANA

Student No. 0409093009F, Registration No. 0409093009, Session: April-2009, a full time student of M. Phil (Mathematics) has been accepted as satisfactory in partial fulfillment for the degree of

Master of Philosophy in Mathematics

On **17th** January- 2012

BOARD OF EXAMINERS

1. _____
   Dr. Md. Abdul Alim — Chairman
   Associate Professor — (Supervisor)
   Dept. of Mathematics, BUET, Dhaka-1000

2. _____
   Head — Member
   Dr. Md. Elias — (Ex-Officio)
   Dept. of Mathematics
   BUET, Dhaka-1000

3. _____
   Dr. Md. Mustafa Kamal Chowdhury — Member
   Professor
   Dept. of Mathematics, BUET, Dhaka-1000

4. _____
   Dr. Md. Monirul Alam Sarker — Member
   Professor
   Dept. of Mathematics, BUET, Dhaka-1000

5. _____
   Dr. Md. Ashraf Uddin — Member
   Professor — (External)
   Department of Mathematics
   Shahjalal University of Science & Technology, Sylhet-3114.

AUTHOR'S DECLARATION

I hereby announce that the work which is being presented in this thesis entitled "**Finite Element Analysis on Magneto-hydrodynamic Mixed Convection Flow in a Triangular Enclosure**" submitted in partial fulfillment of the requirements for the decoration of the degree of Master of Philosophy, department of Mathematics, BUET, Dhaka, is an authentic record of my own work.

The object presented in this thesis has not been submitted by me for the award of any other degree in this university or any other university.

(Aki Farhana)

Date: 17th January, 2012

PERMIT OF RESEARCH

This is to endorse that the work presented in this thesis is carried out by the author under the supervision of Dr. Md. Abdul Alim, Associate Professor, Department of Mathematics, Bangladesh University of Engineering & Technology, Dhaka.

---------- ----------

Dr. Md. Abdul Alim **Aki Farhana**

Dedicated to Almighty Allah(swt),

My Parents & Brother

ACKNOWLEDGEMENT

I would like to affirm the notable recognizance of Almighty's continual mercy and help without which no work would have been possible to accomplish the goal line. I am pleased to acknowledge with gratefulness to my supervisor Dr. Md. Abdul Alim, Associate Professor, Department of Mathematics, Bangladesh University of Engineering and Technology, for his guidance, constant support, intuitive suggestions and relentless encouragement which have been found very benevolent for the outcome of the research.

I would also like to express my thanks to Dr. Md. Mustafizur Rahman, Associate Professor, Department of Mathematics, Bangladesh University of Engineering and Technology, for his outstanding recommendation and counsel in the thesis of being successful to reach the objectives of this dissertation.

I am also deeply indebted to Professor and Head Dr. Md. Elias, Head of the Department of Mathematics, Prof. Dr. Md. Mustafa Kamal Chowdhury, and Prof. Dr. Md. Monirul Alam Sarker, Department of Mathematics, BUET for their support in allowing me to use the departmental facilities in various stages of my work. I wish to thank to the all staff of the Department of Mathematics, Bangladesh University of Engineering and Technology, for their cooperation in this work.

I am obliged to Salma Parvin, Assistant Professor, Department of Mathematics, BUET for her encouragement and helping mentality in all affairs specially in my research work.

I am in debt of gratitude to Md. Nasir Uddin, M. Phil. Student, Department of Mathematics, BUET, who have assisted me by providing relevant books, programming and valuable suggestions.

Finally I express my devoted respect to my mother Mrs. Rowshon Ara Begum, father Golam Akbar, my husband M. A. Rased and all my family members specially my only brother Md. Rashedul Islam Rana and relatives for creating a delightful atmosphere as well as excusing me from family duties in order to complete the courses, research studies and final production of the thesis work.

ABSTRACT

Combined effect of free and forced convection i.e. mixed convection occurs in many heat transfer devices, such as the cooling system of a nuclear power plant, large heat exchangers, cooling of electronic equipment, ventilation and heat or pollution agent clearance.

In this thesis under the title “Finite Element Analysis on Magneto-hydrodynamic Mixed Convection Flow in a Triangular Enclosure”, two problems have been studied. The relative direction between the buoyancy force and the externally forced flow is important. In the case the fluid is externally forced to flow as the buoyancy force, the mode of heat transfer is termed combined forced and natural convection. The studies as well as depending on various flow and geometrical conditions are abstracted below.

Initially, the effect of conduction in mixed convection flow in a triangular enclosure has been investigated numerically. The left vertical wall which is moving from the bottom corner of the cavity is kept at a uniform constant cold temperature and the bottom wall is heat generating, while the other inclined wall is assumed to be adiabatic or insulated. An external flow enters into the enclosure through the bottom portion of the left vertical wall. The fluid is concerned with Prandtl numbers 0.71, 2.0, 3.0 and 6.0. The properties of the fluid were presumed to be constant.

The physical problems have been represented mathematically by different sets of governing equations along with the corresponding boundary conditions. The non-dimensional governing equations are discretized by using Galerkin weighted residual method of finite element formulation. Results are presented in terms of streamlines, isotherms, average Nusselt number along the hot wall and average bulk temperature of the fluid in the cavity for different combinations of the governing parameters namely Reynolds number (*Re)*, Prandtl number (*Pr)*, Hartmann number (*Ha)* and Rayleigh number *Ra*, varying from 10^3 to 10^4. This range of *Ra* is selected on the basis of calculation covering forced convection, mixed convection and free convection dominated regimes. The computational results also indicate that the average Nusselt number at the hot wall of the cavity is depending on the dimensionless parameters. Comparisons with previously published work are performed and the results are found to be in excellent agreement.

In conclusion, the consequences of conduction with magneto-hydrodynamics (MHD) mixed convection flow in a triangular enclosure have been investigated. The cavity consists of the same condition like previous one i.e. the effect of conduction in mixed convection flow in a triangular enclosure with left moving wall, adiabatic right inclined wall and heated bottom wall are considered. A uniform magnetic field is applied in the horizontal direction normal to the moving wall. Heat flow patterns in the presence of magnetic field within triangular enclosures have been analyzed with heatlines concept. The fluid is concerned with wide range of magnetic effect i.e. Hartmann numbers 5, 10, 20, 50 and Prandtl numbers 0.71, 2.0, 3.0, 6.0 at the three values of Rayleigh number *Ra*, varying from 10^3 to 10^4 which have been selected on the source of estimation of covering forced convection, mixed convection and free convection dominated regimes.

Outcome of the numerical analysis has been presented in terms of streamline, isotherms, average Nusselt number and average bulk temperature along the heated bottom wall. The results indicate that both the flow and the thermal fields strongly depend on the parameters, Reynolds number (*Re)*, Hartmann number (*Ha)*, Prandlt number (*Pr)*, at the convective regimes. It is also observed that the Prandtl number (*Pr)* influence on the flow field and have significant effect on the thermal field at the convective regimes. The computational results in both cases found that the flow and thermal field inside the cavity strongly depend on the relevant dimensionless numbers. For the purpose of comparison of the effect of MHD on heat transfer, the results in terms of average Nusselt number and average bulk temperature are shown in tabular form. The achieved results exposed that the effect of MHD has more influence than the case of without MHD on average Nusselt number and bulk temperature at the hot bottom wall.

CONTENTS

NOMENCLATURE

θ_{av}	average temperature
B_0	magnetic induction
C_p	Specific heat at constant pressure (J/kg K)
g	gravitational acceleration (m/s^2)
Gr	Grashof number
h	convective heat transfer coefficient (W/m^2 K)
Ha	Hartmann number
k	thermal conductivity of fluid(W/m K)
K	thermal conductivity ratio fluid
N	non-dimensional distance
Nu	Average Nusselt number
Nu_{local}	Local Nusselt number
P	non-dimensional pressure
p	pressure
Pr	Prandtl number
Ra	Rayleigh number
Re	Reynolds number
T	non-dimensional temperature
U	dimensionless horizontal velocity
u	velocity in x-direction (m/s)
V	dimensionless vertical velocity
v	velocity in y-direction (m/s)
V_0	Lid velocity
x, y	Cartesian coordinates
X, Y	dimensionless Cartesian coordinates

Greek symbols

β	Coefficient of thermal expansion (K^{-1})
ρ	Density of the fluid (kg/m^3)
α	Thermal diffusivity (m^2/s)
Δθ	Temperature difference
θ	Fluid temperature
μ	Dynamic viscosity of the fluid (Pa s)
ν	Kinematic viscosity of the fluid (m^2/s)
σ	Fluid electrical conductivity($\Omega^{-1}m^{-1}$)

LIST OF TABLES

LIST OF FIGURES

CHAPTER 1
INTORDUCTION

1.1 OVERVIEW

The phenomenon of heat transfer was known to human being even in the primitive age when they used solar energy as a source of heat. Heat transfer in its initial stage was conceived with the invention of fire in the early age of human civilization. Since then its knowledge and use has been progressively increasing each day as it is directly related to the growth of human civilization. With the invention of stream engine by James watt in 1765 A. D., the phenomenon of heat transfer got its first industrial recognition and after that its use extended to a great extent and spread out in different spheres of engineering fields. In the past three decades, digital computers, numerical techniques and improvement of numerical models of heat transfer have made it possible to calculate heat transfer of considerable Maze and thereby create a new approach to the design of heat transfer equipment.

Study of the universe has led to the realization that all physical phenomena are subject to natural laws. The term natural might well be used to describe the framework or system of fundamental and universal importance within this system is the mechanisms for the transfer of heat. Heat transfer is a branch of applied thermodynamics. It estimates the rate at which heat is transferred across the system boundaries subjected to specific temperature differences and the temperature distribution of the system during the process. Whereas classical thermodynamics deals with the amount of heat transferred during the process. Heat transfer processes have always been an integral part of our environment.

1.2 FLOW WITHIN AN ENCLOSURE

The flow within an enclosure consisting of two walls, at different temperatures, is an important circumstance encountered quite frequently in practice. In all the applications having this kind of situation, heat transfer occurs due to the temperature difference across the fluid layer, one horizontal solid surface being at a temperature higher than the other. If the upper plate is the hot surface, then the lower surface has heavier fluid and by virtue

of buoyancy the fluid would not come to the lower plate. Because in this case the heat transfer mode is restricted to only conduction. But if the fluid is enclosed between two horizontal surfaces of which the upper surface is at lower temperature, there will be the existence of cellular natural convective currents which are called as Benard cells. For fluids whose density decreases with increasing temperature, this leads to an unstable situation. Benard mentioned this instability as a “top heavy” situation. In that case fluid is completely stationary and heat is transferred across the layer by the conduction mechanism only. Rayleigh recognized that this unstable situation must break down at a certain value of Rayleigh number above which convective motion must be generated. Jeffreys calculated this limiting value of Ra to be 1708, when air layer is bounded on both sides by solid walls.

1.3 A REGULAR SHAPE AND AN IRREGULAR SHAPE

"Regular' has both a general meaning and a specific geometric meaning. In all cases, it concerns how much the various parts of the objects are 'the same'.

Consider the rectangle:

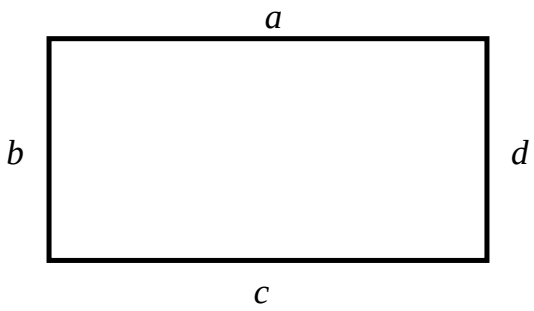

The sides *a* and *c* have the same length. The sides *b* and *d* have the same length. All the angles are the same. A sense of the regularity comes from how it pick up and turn it, and drop it back down and it still look the same. These are called symmetries of the object. If it pick up and turn it 180 degrees: *a* goes to *c*, *b* goes to *d*. The property 'same length' now means something more that can rigidly move it so those sides coincide. If it pick up and flip it over around a vertical line through the center through *ac*.

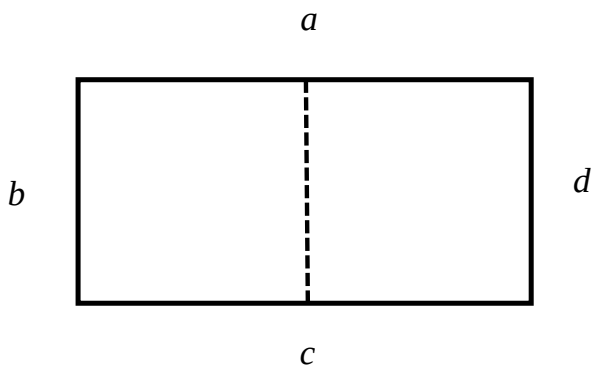

Side *b* goes to side *d*, sides *a* and *d* go on top of themselves. Symmetry a final reflection would involve turning through the line *bd*.

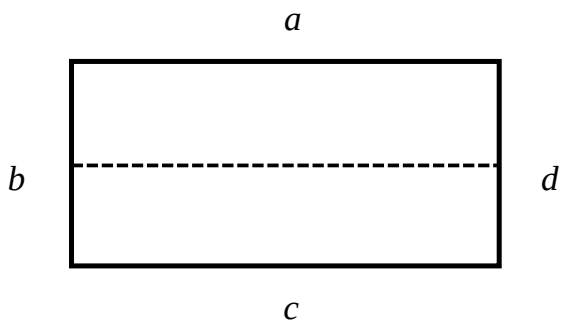

This takes side *a* to side *c*. In fact, trying combinations of these, we can take any corner of the rectangle onto any other corner. All the corners are sort of 'the same'.

A square would have more symmetries than a rectangle. Any side could be taken to any other side, any corner to any other corner. This has quarter turns as well as half-turns, mirrors through the corners as well as the vertical and horizontal mirrors of the rectangle. That is the square is more regular than the rectangle, because there are more symmetries. As a related fact, more parts are the same.

For triangles:

1. Some have no two sides the same, so they are not regular.
2. Some have two sides the same. That also guarantees that two of the angles are the same. These are isosceles. Such triangles do have a mirror through the vertex (corner) where the equal sides meet and the middle of the edge opposite this vertex. That edge joins the two equal angles.
3. Some have all three sides the same. That goes with having all three angles the same. (Get one and the other follows.) For these 'equilateral triangles', there are lots of symmetries: taking any side to any side, any corner to any other corner. This would certainly be called regular.

1.3.1 APPLICATIONS OF AN IRREGULAR TRIANGULAR ENCLOSURE

In recent years, triangular enclosures have received a good attention because of its applicability in various fields. For this reason the present problem is customized under triangular enclosure. The important natural phenomenon of triangular enclosure such as building and thermal insulation systems (air conditioning, load calculations for pitched roofs with horizontal suspended ceiling), solar engineering applications (triangular built-in-storage solar collector), geophysical fluid mechanics (heat transfer and exchange of nutrients or pollutants from the coastal region to the interior waters of lakes or reservoirs, pollutants diffusion in sea and also use in the Ultrasonic Grinding Machine in the industry.

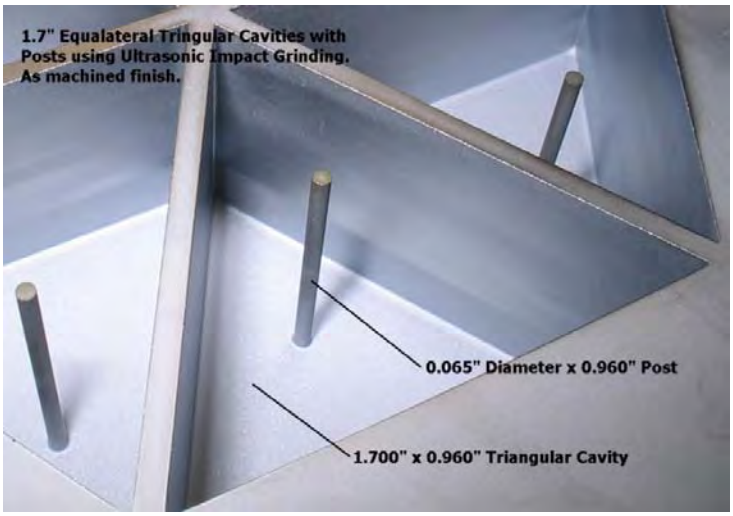

Figure 1.1: Triangular Cavity using in Ultrasonic Impact Grinding Machine (bullentech.com)

1.4 HEAT TRANSFER MECHANISMS

Heat transfer is the transport of thermal energy from one region to another as a result of temperature difference. A thermodynamic analysis is concerned with the amount of heat transfer as a system undergoes a process from one equilibrium state to another. The science that deals with the determination of the rates of such energy transfers is the heat transfer. The transfer of energy as heat is always from the higher temperature medium to the lower temperature one, and heat transfer stops when the two mediums reach the same temperature.

Heat can be transferred in three distinct mechanisms or modes: conduction, convection and radiation.

1.4.1 CONVECTION

Convection is the movement of molecules within fluids (i.e. liquids, gases) and rheids. It cannot take place in solids, since neither bulk current flows nor significant diffusion can take place in solids.

Convection is one of the major modes of heat transfer and mass transfer. Convective heat and mass transfer take place through both diffusion – the random Brownian motion of individual particles in the fluid – and by advection, in which matter or heat is transported by the larger-scale motion of currents in the fluid. In the context of heat and mass transfer, the term "convection" is used to refer to the sum of advective and diffusive transfer. The term "convection" may have slightly different but related usages in different contexts. The broader sense is in fluid mechanics, where "convection" refers to the motion of fluid (regardless of cause). However in thermodynamics "convection" often refers specifically to heat transfer by convection. Additionally, convection includes fluid movement both by bulk motion (advection) and by the motion of individual particles (diffusion). However in some cases, convection is taken to mean only advective phenomena. For instance, in the transport equation, which describes a number of different transport phenomena, terms are separated into "convective" and "diffusive" effects. A similar differentiation is made in the Navier–Stokes equations. In such cases the precise meaning of the term may be clear only from context. Convection occurs on a large scale in atmospheres, oceans, and planetary mantles. Fluid movement during convection may be invisibly slow, or it may be obvious and rapid, as in a hurricane. On astronomical scales, convection of gas and dust is thought to occur in the accretion disks of black holes, at speeds which may closely approach that of light.

Convective heat transfer is a mechanism of heat transfer occurring because of bulk motion (observable movement) of fluids. Heat is the entity of interest being advected (carried), and diffused (dispersed). This can be contrasted with conductive heat transfer, which is the transfer of energy by vibrations at a molecular level through a solid or fluid, and radiative heat transfer, the transfer of energy through electromagnetic waves. Heat is transferred by convection in numerous examples of naturally occurring fluid flow, such as: wind, oceanic currents, and movements within the Earth's mantle. Convection is also

used in engineering practices to provide desired temperature changes, as in heating of homes, industrial processes, cooling of equipment, etc.

The rate of convective heat transfer may be improved by the use of a heat sink, often in conjunction with a fan. For instance, a typical computer CPU will have a purpose-made fan to ensure its operating temperature is kept within tolerable limits.

A **convection cell**, also known as a **Bénard cell** is a characteristic fluid flow pattern in many convection systems. A rising body of fluid typically loses heat because it encounters a cold surface; because it exchanges heat with colder liquid through direct exchange; or in the example of the Earth's atmosphere, because it radiates heat. Because of this heat loss the fluid becomes denser than the fluid underneath it, which is still rising. Since it cannot descend through the rising fluid, it moves to one side. At some distance, its downward force overcomes the rising force beneath it, and the fluid begins to descend. As it descends, it warms again and the cycle repeats itself. In Convection mechanisms convection may happen in fluids at all scales larger than a few atoms. There are a variety of circumstances in which the forces required for natural and forced convection arise, leading to different types of convection, described below. In broad terms, convection arises because of body forces acting within the fluid, such as gravity (buoyancy), or surface forces acting at a boundary of the fluid.

The causes of convection are generally described as one of either "natural" ("free") or "forced", although other mechanisms also exist (discussed below). However the distinction between natural and forced convection is particularly important for convective heat transfer.

1.4.2 NATURAL CONVECTION

Natural convection, or free convection, occurs due to temperature differences which affect the density, and thus relative buoyancy, of the fluid. Heavier (more dense) components will fall while lighter (less dense) components rise, leading to bulk fluid movement. Natural convection can only occur, therefore, in a gravitational field. A common example of natural convection is a pot of boiling water in which the hot and less-dense water on the bottom layer moves upwards in plumes, and the cool and denser water near the top of the pot likewise sinks.

Natural convection will be more likely and/or more rapid with a greater variation in density between the two fluids, a larger acceleration due to gravity that drives the convection, and/or a larger distance through the convecting medium. Convection will be less likely and/or less rapid with more rapid diffusion (thereby diffusing away the gradient that is causing the convection) and/or a more viscous (sticky) fluid. The onset of natural convection can be determined by the Rayleigh number (*Ra*).The differences in buoyancy within a fluid can arise for reasons other than temperature variations, in which case the fluid motion is called gravitational convection.

1.4.3 FORCED CONVECTION

In forced convection, also called heat advection, fluid movement results from external surface forces such as a fan or pump. Forced convection is typically used to increase the rate of heat exchange. Many types of mixing also utilize forced convection to distribute one substance within another. Forced convection also occurs as a by-product to other processes, such as the action of a propeller in a fluid or aerodynamic heating. Fluid radiator systems, and also heating and cooling of parts of the body by blood circulation, are other familiar examples of forced convection.

Forced convection may produce results more quickly than free convection. For instance, a convection oven works by forced convection, as a fan which rapidly circulates hot air forces heat into food faster than would naturally happen due to simple heating without the fan.

1.4.4 THERMO MEGNETIC CONVECTION

Thermo magnetic convection can occur when an external magnetic field is imposed on a ferro-fluid with varying magnetic susceptibility. In the presence of a temperature gradient this results in a non-uniform magnetic body force, which leads to fluid movement. A ferro-fluid is a liquid which becomes strongly magnetized in the presence of a magnetic field.

This form of heat transfer can be useful for cases where conventional convection fails to provide adequate heat transfer, e.g., in miniature micro-scale devices or under reduced gravity conditions.

1.4.5 MIXED CONVECTION

The convection heat transfer which is neither dominated by pure forced nor pure free convection, but is rather a combination of the two is referred as combined or mixed convection. The buoyancy forces that arise as the results of the temperature differences and which cause the fluid flow in free convection also exist when there is a forced flow. The effects of these buoyancy forces are however; usually negligible when there is a forced flow. For example, heat transfer from one fluid to another fluid through the walls of pipe occurs in many practical devices. Heat is then transferred by conduction through the walls of the pipe. Finally, heat is transferred by convection from the other surface to the colder fluid.

1.4.6 MIXED CONVECTION HEAT TRANSFER IN CAVITIES

Mixed convection in cavities is a topic of contemporary importance, because cavities filled with fluid are central components in a long list of engineering and geophysical systems. The flow and heat transfer induced in a cavity differs fundamentally from the external mixed convection boundary layer. Mixed convection in a cavity unlike the external mixed convection boundary layer that is caused by the heat transfer interaction between a single wall and a very large fluid reservoir is the result of the complex interaction between finite size fluid systems in thermal communication with all the walls that confine it. The complexity of this internal interaction is responsible for the diversity of flows that can exist inside cavity.

The phenomenon of mixed convection in cavities is varied by the geometry and the orientation of the cavity. Judging by the potential engineering applications, the cavity phenomena can loosely be organized into two classes.

1. Vented cavity and 2. Lid-driven cavity

In a vented cavity, where the interaction between the external forced stream provided by the inlet and the buoyancy driven flows induced by the heat source leads to the possibility of complex flows. Therefore it is important to understand the fluid flow and heat transfer characteristics of mixed convection in a vented cavity. On the other hand, the fluid flow and heat transfer in a lid-driven cavity where the flow is induced by a shear force resulting from the motion of a lid combined with the buoyancy force due to non-homogeneous temperature of the cavity wall, provides another problem, studied

extensively by researchers to understand the interaction between buoyancy and shearing forces in such flow situation. The interaction between buoyancy driven and shear driven flows inside a closed cavity in a mixed convection regime is quite complex. Therefore it is also important to understand the fluid flow and heat transfer characteristics of mixed convection in a lid-driven cavity.

1.4.7 BOUSSINESQ APPROXIMATION

The governing equations for convection flow are coupled elliptic partial differential equations and are, therefore, of considerable complexity. The major problems in obtaining a solution to these equations lie in the inevitable variation of density with temperature, or concentration, and in their partial, elliptic nature. Several approximations are generally made to considerably simplify these equations. Among them Boussinesq approximation attributed to Boussinesq (1903) is considered here. In flows accompanied by heat transfer, the fluid properties are normally functions of temperature. The variations may be small and yet be the cause of the fluid motion. If the density variation is not large, one may treat the density as constant in the unsteady and convection terms, and treat it as variable only in the gravitational term. This is called the Boussinesq approximation.

1.5 SOME DEFINITIONS

We present here some basic definitions which are related to the current study

1.5.1 THERMAL DIFFUSIVITY

Thermal diffusivity represents how fast heat diffuses through a material and is defined as, $\alpha = \dfrac{\text{Heat conducted}}{\text{Heat stored}} = \dfrac{\kappa}{\rho \; C_p} \qquad \left(m^2/s\right)$

Here the thermal conductivity κ represents how well a material conducts heat, and the heat capacity C_p represents how much energy a material stores per unit volume. Therefore, the thermal diffusivity of a material can be viewed as the ratio of the heat conducted through the material to the heat stored per unit volume. A material that has a high thermal conductivity or a low heat capacity will obviously have a large thermal diffusivity. The larger thermal diffusivity means that the propagation of heat into the

medium is faster. A small value of thermal diffusivity means the heat is mostly absorbed by the material and a small amount of heat is conducted further

1.5.2 INTERNAL AND EXTERNAL FLOWS

A fluid flow is classified into two types; internal and external, depending on whether the fluid is forced to flow in a confined channel or over a surface. An internal flow is in a channel bounded on all sides by solid surfaces except, possibly, for an inlet and exit. Flows through a pipe or in an air-conditioning duct are the examples of internal flow. Internal flows are dominated by the influence of viscosity throughout the flow field. The internal flow configuration represents a convenient geometry for the heating and cooling of fluids used in the chemical processing, environmental control, and energy conversion areas. The flow of an unbounded fluid over a surface is external flow.

1.5.3 BOUNDARY LAYER

The boundary layer was first defined by Ludwig Prandtl in a paper presented on August 12, 1904 at the third International Congress of Mathematicians in Heidelbere, Germany. It allows aerodynamicists to simplify the equations of fluid flow by dividing the flow field into two areas: one inside the boundary layer, where viscosity is dominant and the majority of the drag experienced by a body immersed in a fluid is created and one outside the boundary layer where viscosity can be neglected without significant effects on the solution. This allows a closed-form solution for the flow in both areas, which is a significant simplification over the solution of the full Navier–Stokes equations. The majority of the heat transfer to and from a body also takes place within the boundary layer, again allowing the equations to be simplified in the flow field outside the boundary layer.

The thickness of the velocity boundary layer is normally defined as the distance from the solid body at which the flow velocity is 99% of the freestream velocity, that is, the velocity that is calculated at the surface of the body in an inviscid flow solution. An alternative definition, the displacement thickness, recognises the fact that the boundary layer represents a deficit in mass flow compared to an inviscid case with slip at the wall. It is the distance by which the wall would have to be displaced in the inviscid case to give the same total mass flow as the viscous case. The no-slip condition requires the flow velocity at the surface of a solid object be zero and the fluid temperature be equal to the

temperature of the surface. The flow velocity will then increase rapidly within the boundary layer, governed by the boundary layer equations, below. The thermal boundary layer thickness is similarly the distance from the body at which the temperature is 99% of the temperature found from an inviscid solution. The ratio of the two thicknesses is governed by the Prandtl number. If the Prandtl number is 1, the two boundary layers are the same thickness. If the Prandtl number is greater than 1, the thermal boundary layer is thinner than the velocity boundary layer. If the Prandtl number is less than 1, which is the case for air at standard conditions, the thermal boundary layer is thicker than the velocity boundary layer.

1.5.4 MAGNETO HYDRODYNAMICS

Magneto-hydrodynamics (MHD) is the academic discipline which studies the dynamics of electrically conducting fluids. Examples of such fluids include plasmas, liquid metals and salt water. The word Magneto-hydrodynamics (MHD) is derived from “magneto-” meaning “magnetic field”, and “hydro” meaning “liquid”, and “dynamics” meaning “movement”. The field of MHD was initiated by Hannes Alfven, for which he received the Noble Prize in Physics in 1970.The idea of MHD is that magnetic fields can induce currents in a moving conducting fluid, which create forces on the fluid, and also change the magnetic field itself. The set of equations which describe MHD are a combination of the Nevier-Stokes equations of fluid dynamics and Maxwell’s equations of electromagnetism. These differential equations have to be solved simultaneously, either analytically or numerically. MHD is a continuum theory and as such it cannot treat kinetic phenomena, i.e. those in which the existence of discrete particles or of a non-thermal velocities distribution are important. The simple form of MHD, Ideal MHD, assumes that fluid has so little resistivity that it can be treated as a perfect conductor. This is the limit of infinite magnetic Reynolds number in ideal MHD, Lenz’s law dictates that the fluid is in a sense tied to the magnetic fields lines. To explain, in ideal MHD a small rope like volume of the fluid surrounding a field line will continue to lie along a magnetic field line, even as it is twisted and distorted by fluid flows in the system The connection between magnetic field lines and fluid in ideal MHD fixes the topology of the magnetic field in the fluid-for example, if a set of magnetic field lines are tied into a knot, then they will remain so as long as the fluid/plasma has negligible resistivity. This difficulty in reconnecting magnetic field lines makes it possible to store energy by moving the fluid or the source of the magnetic field. The energy can then become

available if the conditions for ideal MHD break down allowing magnetic reconnection that release the stored energy from the magnetic field.

The ideal MHD equations consist of the continuity equation, the momentum equation, and Ampere's Law in the limit of no electric field and no electron diffusivity, and a temperature evolution equation. As with any fluid description to a kinetic system, a closure approximation must be applied to highest moment of the particle distribution equation. This is often accomplished with approximations to the heat flux through a condition of adiabaticity or isothermality.

Ideal MHD is only strictly applicable when:

1. The plasma is strongly collisional, so that the time scale of collisions is shorter than the other characteristic times in the system, and the particle distributions are therefore close to Maxwellian.

2. The resistivity due to these collisions is small. In particular, the typical magnetic diffusion times over any scale length present in the system must be longer than any time scale of interest.

3. We are interested in length scales much longer than the ion skin depth and Larmor radius perpendicular to the field, long enough along the field to ignore Landau damping, and time scales much longer than the ion gyration time (system is smooth and slowly evolving).

1.5.4(A) APPLICATIONS OF MHD:

Geophysics

The fluid core of the Earth and other planets is theorized to be a huge MHD dynamo that generates the Earth's magnetic field. due to the motion of liquid iron.

Astrophysics

MHD applies quite well to astrophysics since over 99% of baryonic matter content of the Universe is made up of plasma, including stars, the interplanetary medium (space between the planets), the interstellar medium (space between the stars), nebulae and jets. Many astrophysical systems are not in local thermal equilibrium, and therefore require an additional kinematic treatment to describe all the phenomena within the system. Sunspots are caused by the Sun's magnetic fields, as Joseph Larmor theorized in 1919. The solar wind is also governed by MHD. The differential solar rotation may be the long

term effect of magnetic drag at the poles of the Sun, an MHD phenomenon due to the Parker spiral shape assumed by the extended magnetic field of the Sun. Previously, theories describing the formation of the Sun and planets could not explain how the Sun has 99.87% of the mass, yet only 0.54% of the angular momentum in the solar system. In a closed system such as the cloud of gas and dust from which the Sun was formed, mass and angular momentum are both conserved.

That conservation would imply that as the mass concentrated in the center of the cloud to form the Sun, it would spin up, much like a skater pulling their arms in. The high speed of rotation predicted by early theories would have flung the proto-Sun apart before it could have formed. However, magneto hydrodynamic effects transfer the Sun's angular momentum into the outer solar system, slowing its rotation. Breakdown of ideal MHD (in the form of magnetic reconnection) is known to be the cause of solar flares, the largest explosions in the solar system. The magnetic field in a solar active region over a sunspot can become quite stressed over time, storing energy that is released suddenly as a burst of motion, X-rays, and radiation when the main current sheet collapses, reconnecting the field.

Engineering

MHD is related to engineering problems such as plasma confinement, liquid-metal cooling of nuclear reactors, and electromagnetic casting (among others).The first prototype of this kind of propulsion was built and tested in 1965 by Steward Way, a professor of mechanical engineering at the University of California, Santa Barbara. Way, on leave from his job at Westinghouse Electric, assigned his senior year undergraduate students to develop a submarine with this new propulsion system. In early 1990s, Mitsubishi built a boat, the 'Yamato,' which uses a magneto hydrodynamic drive, is driven by a liquid helium-cooled superconductor, and can travel at 15 km/h. MHD power generation fueled by potassium-seeded coal combustion gas showed potential for more efficient energy conversion (the absence of solid moving parts allows operation at higher temperatures), but failed due to cost prohibitive technical difficulties. In micro fluidic devices, the MHD pump is so far the most effective for producing a continuous, no pulsating flow in a complex micro channel design. It was used to implement a PCR protocol.

1.5.5 FLUID MECHANICS ASPECT

The local properties such as pressure and velocity of the fluid should strictly be defined as averages over elements large compared with the microscopic structure of matter but small enough in comparison with the scale of the macroscopic phenomena.

In MHD, the fluid is electrically conducting. It is not magnetic; it affects a magnetic field not by its mere presence but only by virtue of electric currents flowing in it. The fluid conducts because it contains free charges (ions or electrons) that can move indefinitely. According to the non-relativistic electromagnetic theory, a charged particle such as an electron suffers forces of three kinds.

1. It is repelled or attracted by other charged particles, the total force on the particle per unit of its charge due to all the other charges present being the electrostatic field, E's.

2. Charged particles in motion and also magnetic materials produce the phenomenon of magnetism or magnetic field, B.

2(a). A charge particle moving with velocity relative to a certain frame of reference suffers a magnetic force $\overline{V} \times \overline{B}$ per unit of its charge. The force is perpendicular to $\overline{V}$ and $\overline{B}$. The direction of $\overline{B}$ is that in which the particle must travel to feel no magnetic force.

2(b). If the magnetic field B, so identified, is changing with time relative to a certain frame of reference, then per unit of its charge a particle will suffer a further force Ei. The total force on a particle per unit of its charge is $f_e = \overline{E} + \overline{V} \times \overline{B}$. This is known as Lorentz force.

Electromagnetic body forces act on the fluid, and in turn the motion of the fluid in the presence of the electromagnetic field may generate an induced electromotive force and alter the fields. Implicit in this is the assumption of local quasi-equilibrium, which permits the state of the fluid at each point to be described by a few variables, related just as if the fluid were in equilibrium. Thereby the fluid may be assumed to be incompressible, homogeneous and isotropic in the mathematical and electric sense. The mathematical models have no difference from those used in conventional fluid mechanics. The only effect of the electromagnetic field is a coupling through the electromagnetic body force in the equation of motion.

1.6 DIMENSIONLESS PARAMETERS

The dimensionless parameters can be thought of as measures of the relative importance of certain aspects of the flow. Some dimensionless parameters related to our study are discussed below:

1.6.1 REYNOLDS NUMBER, *Re*

In fluid mechanics, the Reynolds number Re is a dimensionless number that gives a measure of the ratio of inertial forces to viscous forces and consequently quantifies the relative importance of these two types of forces for given flow conditions. The concept was introduced by George Gabriel Stokes in 1851, but the Reynolds number is named after Osborne Reynolds (1842–1912), who popularized its use in 1883. Reynolds numbers frequently arise when performing dimensional analysis of fluid dynamics problems, and as such can be used to determine dynamic similitude between different experimental cases. They are also used to characterize different flow regimes, such as laminar or turbulent flow: Laminar flow occurs at low Reynolds numbers, where viscous forces are dominant, and is characterized by smooth, constant fluid motion; while turbulent flow occurs at high Reynolds numbers and is dominated by inertial forces, which tend to produce chaotic eddies, vortices and other flow instabilities. Reynolds number can be defined for a number of different situations where a fluid is in relative motion to a surface (the definition of the Reynolds number is not to be confused with the Reynolds Equation or lubrication equation. These definitions generally include the fluid properties of density and viscosity, plus a velocity and a characteristic length or characteristic dimension. This dimension is a matter of convention – for example a radius or diameter is equally valid for spheres or circles, but one is chosen by convention. For aircraft or ships, the length or width can be used. For flow in a pipe or a sphere moving in a fluid the internal diameter is generally used today. Other shapes (such as rectangular pipes or non-spherical objects) have an equivalent diameter defined. For fluids of variable density (e.g. compressible gases) or variable viscosity (non-Newtonian fluids) special rules apply. The velocity may also be a matter of convention in some circumstances, notably stirred vessels.

$$\mathrm{Re} = \frac{\rho V L}{\mu} = \frac{V L}{\nu}$$

where:

V is the mean velocity of the object relative to the fluid (SI units: m/s)

L is a characteristic linear dimension, (traveled length of the fluid; hydraulic diameter when dealing with river systems) (m)

μ is the dynamic viscosity of the fluid (Pa·s or N·s/m² or kg/(m·s))

ν is the kinematic viscosity ($\nu = \mu / \rho$) (m²/s)

is the density of the fluid (kg/m³)

Example of the importance of the Reynolds number

If an airplane wing needs testing, one can make a scaled down model of the wing and test it in a wind tunnel using the same Reynolds number that the actual airplane is subjected to. If for example the scale model has linear dimensions one quarter of full size, the flow velocity of the model would have to be multiplied by a factor of 4 to obtain similar flow behavior. Alternatively, tests could be conducted in a water tank instead of in air (provided the compressibility effects of air are not significant). As the kinematic viscosity of water is around 13 times less than that of air at 15 °C, in this case the scale model would need to be about one thirteenth the size in all dimensions to maintain the same Reynolds number, assuming the full-scale flow velocity was used. The results of the laboratory model will be similar to those of the actual plane wing results. Thus there is no need to bring a full scale plane into the lab and actually test it. This is an example of "dynamic similarity". Reynolds number is important in the calculation of a body's drag characteristics. A notable example is that of the flow around a cylinder. Above roughly 3×10^6 Re the drag coefficient drops considerably. This is important when calculating the optimal cruise speeds for low drag (and therefore long range) profiles for airplanes.

Where the viscosity is naturally high, such as polymer solutions and polymer melts, flow is normally laminar. The Reynolds number is very small and Stokes' Law can be used to measure the viscosity of the fluid. Spheres are allowed to fall through the fluid and they reach the terminal velocity quickly, from which the viscosity can be determined. The laminar flow of polymer solutions is exploited by animals such as fish and dolphins, who exude viscous solutions from their skin to aid flow over their bodies while swimming. It has been used in yacht racing by owners who want to gain a speed advantage by

pumping a polymer solution such as low molecular weight polyoxyethylene in water, over the wetted surface of the hull. It is however, a problem for mixing of polymers, because turbulence is needed to distribute fine filler (for example) through the material. Inventions such as the "cavity transfer mixer" have been developed to produce multiple folds into a moving melt so as to improve mixing efficiency. The device can be fitted onto extruders to aid mixing.

1.6.2 RAYLEIGH NUMBER, *Ra*

The Rayleigh number for a fluid is a dimensionless number associated with buoyancy driven flow (also known as free convection or natural convection).in fluid mechanics When the Rayleigh number is below the critical value for that fluid, heat transfer is primarily in the form of conduction; when it exceeds the critical value, heat transfer is primarily in the form of convection. The Rayleigh number is named after Lord Rayleigh and is defined as the product of the Grashof number, which describes the relationship between buoyancy and viscosity within a fluid, and the Prandt number, which describes the relationship between momentum diffusivity and thermal diffusivity. Hence the Rayleigh number itself may also be viewed as the ratio of buoyancy forces and (the product of) thermal and momentum diffusivities.

For convection near a vertical wall, this number is

$$Ra_x = Gr_x \,\mathrm{Pr} = \frac{g\beta}{\nu\alpha}(T_s - T_\infty)x^3$$

where

x = Characteristic length (in this case, the distance from the leading edge)

Ra_x = Rayleigh number at position x

Gr_x = Grashof number at position x

Pr = Prandtl number

g = acceleration due to gravity

T_s = Surface temperature (temperature of the wall)

T_∞ = Quiescent temperature (fluid temperature far from the surface of the object)

ν = Kinematic viscosity

α = Thermal diffusivity

β = Thermal expansion coefficient

In the above, the fluid properties Pr, ν, α and β are evaluated at the film temperature, which is defined as,

$$T_f = \frac{T_s + T_\infty}{2}$$

For most engineering purposes, the Rayleigh number is large, somewhere around 10^6 and 10^8.

1.6.3 PRANDTL NUMBER, *Pr*

The Prandtl number Pr is a dimensionless number; the ratio of momentum diffusivity (kinematic viscosity) to thermal diffusivity. It is named after the German physicist Ludwig Prandtl.

It is defined as:

$$Pr = \frac{\nu}{\alpha} = \frac{\text{Viscous Diffusion Rate}}{\text{Thermal Diffusion Rate}} = \frac{c_p \mu}{k}$$

Where:

ν: kinematic viscosity, ν = μ / ρ, (SI units: m^2/s)

α: thermal diffusivity, α = k / (ρc_p), (SI units: m^2/s)

μ: dynamic viscosity (SI units: Pa s = (N s)/m^2)

k: thermal conductivity, (SI units: W/(m K))

c_p: specific heat, (SI units: J/(kg K))

ρ: density, (SI units: kg/m^3).

Whereas the Reynolds number and Grashof number are subscripted with a length scale variable, Prandtl number contains no such length scale in its definition and is dependent only on the fluid and the fluid state. As such, Prandtl number is often found in property tables alongside other properties such as viscosity and thermal conductivity.

In heat transfer problems, the Prandtl number controls the relative thickness of the momentum and thermal boundary layers. When *Pr* is small, it means that the heat

diffuses very quickly compared to the velocity (momentum). This means that for liquid metals the thickness of the thermal boundary layer is much bigger than the velocity boundary layer.

1.6.4 HARTMANN NUMBER, *Ha*

Hartmann number is the ratio of electromagnetic force to the viscous force first introduced by Hartmann. It is defined by:

$$Ha = B_0 L\sqrt{\frac{\sigma}{\mu}}$$

Where, B_0 is the magnetic field, L is the characteristic length scale, σ is the electrical conductivity, μ is the viscosity. In addition, it is a dimensionless quantity characterizing flow of conducting fluid in a transverse magnetic field, being the product of the magnetic flux density, a representative length, and the square root of the ratio of electrical conductivity to viscosity.

1.6.5 GRASHOF NUMBER, *Gr*

The flow regime in free convection is governed by the dimensionless Grashof number, which represent the ratio of the buoyancy force to the viscous forces acting on the fluid, and is defined as

$$Gr = \frac{g\beta L^3 (T_w - T_\infty)}{\nu^2}$$

where g is the acceleration due to gravity, β is the volumetric thermal expansion coefficient, T_w is the wall temperature, T_∞ is the ambient temperature, L is the characteristic length and ν is the kinematics viscosity. The Grashof number Gr plays same role in free convection as the Reynolds number Re plays in forced convection. As such, the Grashof number provides the main criterion in determining whether the fluid flow is laminar or turbulent in free convection. For vertical plates, the critical value of the Grashof number is observed to be about 10^9. Therefore, the flow regime on a vertical plate becomes turbulent at Grashof numbers greater than10^9.

1.6.6 NUSSELT NUMBER, *Nu*

The Nusselt number represents the enhancement of heat transfer through a fluid layer as a result of convection relative to conduction across the same fluid layer, and is defined as

$$Nu = \frac{\text{Convective Heat Transfer}}{\text{Conductive Heat Transfer}} = \frac{hL}{k}$$

where k is the thermal conductivity of the fluid, h is the heat transfer coefficient and L is the characteristics length. The Nusselt number is named after Wilhelm Nusselt, who made significant contributions to convective heat transfer in the first half of the twentieth century, and it is viewed as the dimensionless convection heat transfer coefficient. The larger Nusselt number indicates a large temperature gradient at the surface and hence, high heat transfer by convection. A Nusselt number of $Nu = 1$, for a fluid layer represents heat transfer across the layer by pure conduction. To understand the physical significance of the Nusselt number, consider the following daily life problems. We remedy to forced convection whenever we want to increase the rate of heat transfer from a hot object. In free convection flow velocities are produced by the buoyancy forces hence there are no externally induced flow velocities.

CHAPTER 2

2.1 LITERATURE REVIEW

Analysis of mixed convection usually induced in enclosed cavities or channels containing heating elements on one of its wall or on both walls are important from both theoretical and practical points of view. Most of the common enclosure are used in industries are cylinder, rectangular, trapezoidal and triangular. Because of applicability of triangular enclosures in various fields it has received a considerable attention and the numerous studies related to mixed convection in enclosure cavity have been reported in order to investigate the heat transfer and fluid flow in such geometry

Triangular Cavity:

Akinsete and coleman (1982) first studied the various flow system in triangular cavity They studied the laminar natural convection in triangular cavity. They solved the problem for various aspect ratios and Grashof numbers (Gr) and concluded that heat transfer across the base wall increase towards the hypotenuse and base intersection. It was found that a considerable proportion of the heat transfer acroos the base wall of the region takes place near the intersection of the base and the hypotenuse Then Karyakin and Sokovishin (1988) presented convection patterns in isosceles triangular enclosure. After that Kaushik et al. [1994] studied the performance of a triangular built-in-storage solar water temperature. M. Li and T. Tang (1996) studied the steady viscous flow in a triangular cavity by efficient numerical techniques. They found accurate and efficient calculations of the flow inside a triangular cavity are presented for high Ra numbers. Aside from solving equilateral triangular cavity problem, they also has been able to compute numerical solution for scalene triangular cavity problems. Their coarse-mesh results for the equilateral triangular cavity problem are compared with fixed mesh results in the literature and the agreement was good.

The laminar natural convection in a pitched roof of triangular cross-section for summer day boundary conditions was studied by Asan and Nanli, 2000. They obtained steady sate solutions for height-base ratio and Rayleigh number on the flow structure and heat transfers are investigated. Y.M Hwang and Taylan Altan (2002) studied finite element simulations of the crushing of circular tubes into triangular cross-sections. The objectives were using FE method, the plastic flow patterns of a circular tube hydro dynamically

expanded or crushed into a regular triangular cross-section. Here the relationship of the forming pressurization and loading pass during crushing process was discussed .A few recent studies on natural convection in triangular enclosure have also been carried out for various applications (Varol et al., 2006; Radouance et al., 2006; Tzeng et al., 2005; Joudi et al., 2004). A numerical model from the simulation of double-diffusive natural convection in a triangular cavity using equal-order and control volume based on the finite element method was studied by Hazri et al. (2007).They used the configuration in their research was encountered in green house solar stills, where vertical temperature and concentration gradients between the saline water and transparent cover induce flow in a confined space. This phenomenon played a decisive role in the water distillation process and in the biological comfort. Varol et al. (2006) studied free convection in porous media right-angle triangular enclosure. They considered steady-state free convection heat transfer in a right-angle triangular enclosure, whose vertical wall insulated and inclined and bottom walls are differentially heated. In this study they showed the effect of aspect ratios ranging from 0.25 to 1.0 and Rayleigh numbers $50 \leq Ra \leq 1000$ was investigated as governing parameters on heat transfer and flow field. A Finite Element Analysis of natural convection flow in an isosceles triangular enclosure due to uniform and non-uniform heating at the side walls was studied by Basak et al. (2008).In this study they used penalty finite element analysis with bi-quadratic elements. Two cases of thermal boundary conditions are considered Case-1: two inclined walls are uniformly heated while the bottom wall is cold isothermal and Case-2: two inclined walls are non-uniformly heated while the bottom wall is cold isothermal. The numerical solution of the problem was presented for various Rayleigh numbers ($10^3 \leq Ra \leq 10^6$) and Prandlt numbers ($0.007 \leq Pr \leq 1000$). They found that at small Prandlt numbers, geometry does not have much influence on flow structure while at $Pr = 1000$, geometry has considerable effect on the flow pattern. In the meantime Basak et al. (2006) studied natural convection and flow simulation in differentially heated isosceles triangular enclosures filled with porous medium. In this investigation the numerical procedure adopted yields consistent performance over a wide range of parameters of Darcy number, Da ($10^{-5} \leq Da \leq 10^{-3}$), Rayleigh number, Ra ($10^3 \leq Ra \leq 10^6$), Prandlt number, Pr ($0.026 \leq Pr \leq 1000$) in all cases. It observed that at small Darcy number, the heat transfer is primarily due to conduction irrespective of Pr. As the Darcy number increases; there is a change from conduction dominant regime to convection dominant regime. Flow circulations are also found to be strong functions of Pr at large $Da = 10^3$and multiple

circulation cells occur at small *Pr* with *Ra* = $10^{6.}$Varol and Oztop et al. (2008) studied visualization of natural convection heat transport using heat line method in porous non-isothermally heated triangular cavity. In this investigation three different boundary conditions were applied for the vertical and inclined boundaries of triangular enclosures. The study was performed for different aspect ratios numbers ($100 \leq Ra \leq 1000$). It was observed that the heat transfer enhancement was formed when vertical and inclined walls were isothermal while bottom wall was at non-uniform temperature. Heat transfer from bottom wall did not vary when the value of aspect ratio was higher than 0.50. A numerical analysis of laminar natural convection in isosceles triangular enclosures for cold base and hot inclined walls was solved by Fuad Kent (2009). In this study base angles varying from 15° to 75° have been used for different Rayleigh numbers ranging from 103to 105. Effects of Rayleigh number and aspect ratio on the flow field and heat transfer were analyzed. It is observed that the enclosures with a low aspect ratio have higher heat transfer rates from the bottom surface of the triangular enclosure. Chen et al. (2009) carried out a numerical study of the effects of lid oscillation on the periodic flow pattern and convection heat transfer in a triangular cavity. In this study is concern with a periodic flow pattern with mixed convection in a triangular cavity caused by the effects of lid oscillation and buoyancy. Attention is in particular focused on the flow behavior under the interaction between the frequency of the oscillation of the lid velocity and the frequency of the natural periodic flow. Numerical predictions of the thermal characteristics represented by local and average Nusselt numbers on the walls as well as the transient flow pattern are also provided. Visualization of heat flow due to natural convection within triangular cavities using Bejan's heat line concept was deduced by Basak et al. (2009). This was based on comprehensive analysis of heat flow pattern using Bejan's heat line concept Xu and Yu (2010) carried out a numerical solution for laminar natural convective heat transfer around a horizontal cylinder inside a concentric cylinder inside a concentric air filled triangular enclosures. In this study the buoyancy effect was modeled by Boussinesq approximation. The effects of Rayleigh number and the aspect ratio were examined. Basak et al. (2010) analysis heat line analysis of heat recovery and thermal transport in materials confined within triangular cavity. The concept of heat line used to visualize the heat energy trajectory. At low Rayleigh number, it is founded that the heat line are smooth and perfectly normal to the isotherms including the dominance of conduction. At high Rayleigh number flow slowly becomes convection dominant. Fluid with any Prandlt number may be useful for enhanced heat transfer within the upper

triangle but fluid with high Prandlt number may be preferred for the lower triangle. Roy and Pop et al. (2010) extended this work as visualization of heat transport due to natural convection for hot materials confined within to entrapped porous triangular cavities via hotline concept. The parameters for this study are *Re*, *Pr* and *Ra*, Average Nusselt number. Heat transfer rates are explained based on heat lines.

Mixed Convection

The numerical study to investigate the combined forced and natural convective cooling of heat dissipating electronic components located in rectangular enclosure and cooled by an external through flow of air carried out a series by Papanicolaou and Jaluria (1990, 1992, 1994 and 1995). In mixed convection, structures of laminar wakes and heat transfer in a horizontal channel with a built-in square cylinder were studied numerically by Biswas et al. (1990). In their study, they found that the channel walls and the surface of the bluff body have higher temperatures than the incoming flow and the mixed convection initiate periodicity and asymmetry in the wake at a lower *Re* than forced convection alone. They also found that the mixed convection can enhance the heating of the fluid within the channel up to a certain *Gr* and further increase in *Gr* leads to the deterioration in the heat transfer rate. Related studies of mixed convection in a partially divided rectangular enclosure were respectively carried out by How and Hsu (1998) and Calmidi and Mahajan (1998). The simulation was conducted for wide range of Reynolds and Grashof numbers. They indicated that the average Nusselt number and the dimensionless surface temperature depended on the location and height of the divider. Moreover, Raji and Hasnaoui (1998a, 1998b) obtained numerical results by using a finite difference procedure for opposing flows mixed (forced and natural) convection flow in a rectangular cavity heated from the side with a constant heat flux and submitted to a laminar cold jet from the bottom of its heated wall. The fluid leaves the cavity via the top or the bottom of the opposite vertical wall. Also, Omri and Nasrallah (1999) performed numerical analysis by a control volume finite element method on mixed convection in a rectangular enclosure with differentially heated vertical sidewalls. The laminar flow of an incompressible fluid in a channel past a single heated normal flat plate as well as cascades of heated normal plates were studied numerically by Lin and Sharif (1997). They showed that both *Re* and blockage ratio have significant effects on the flow and the temperature field, especially in the wake region. At the same time, Gowda et al. (1997) studied numerically the heat transfer and fluid flow over a row of in-line cylinders placed

between two parallel plates. They concluded that there are considerable effects of buoyancy and the blockage on the flow heat transfer over the cylinders. Later on, Raji and Hasnaoui (2000) investigated the mixed convection in ventilated cavities where the horizontal top wall and the vertical left wall were prescribed with equal heat fluxes. At the same time, Angirasa (2000) numerically studied and explained the complex interaction between buoyancy and forced flow in a square enclosure with an inlet and a vent situated respectively, at the bottom and top edges of the vertical isothermal surface, where the other three walls are adiabatic. Singh and Sharif (2003) extended their works by considering six placement configurations of the inlet and outlet of a differentially heated rectangular enclosure whereas the previous work was limited to only two different configurations of inlet and outlet. Hsu and Wang (2000) investigated the mixed convective heat transfer where the heat source was embedded on a board mounted vertically on the bottom wall at the middle in the enclosure. The cooling airflow enters and exits the enclosure through the openings near the top of the vertical sidewalls. Gau et al. (2000) performed experiments on mixed convection in a horizontal rectangular channel with side heating. A numerical study of mixed convection heat transfer in two dimensional open-ended enclosures were investigated by Khanafer et al. (2002) for three different forced flow angle of attack. Wang and Jaluria (2002) numerically investigated the characteristics of the instability and the resulting effect on the heat transfer in mixed convection flow in a horizontal duct with discrete heat sources. A numerical analysis of laminar mixed convection in a channel with an open cavity and a heated wall bounded by a horizontally insulted plate was presented in Manca et al. (2003), where they considered three heating modes: assisting flow, opposing flow and heating from below. Later on, similar problem for the case of assisting forced flow configuration was tested experimentally by Manca et al. (2006). The flow and temperature field for a two-dimensional confined slot jet impinging on an isothermal hot surface computed by Sahoo and Sharif (2004). Bhoite et al. (2005) studied numerically the problem of mixed convection flow and heat transfer in a shallow enclosure with a series of block-like heat generating component for a range of Reynolds and Grashof numbers and block-to-fluid thermal conductivity ratios. They showed that higher Reynolds number tend to create a recirculation region of increasing strength at the core region and the effect of buoyancy becomes insignificant beyond a Reynolds number of typically 600, and the thermal conductivity ratio has a negligible effect on the velocity fields. A finite-volume based computational study of steady laminar forced convection inside a square cavity with inlet

and outlet ports was presented in Saeidi and Khodadadi (2006). Hossain and Gorla (2006) investigated the effects of viscous dissipation on unsteady combined convective heat transfer to water near its density maximum in a rectangular cavity with isothermal wall. Two-dimensional flow in a two-sided lid-driven cavity containing a temperature gradient was investigated numerically by Luo and Yang (2007). Recently Rahman et al. (2007) studied numerically the opposing mixed convection in a vented enclosure. They found that with the increase of Reynolds and Richardson numbers the convective heat transfer becomes predominant over the conduction heat transfer and the rate of heat transfer from the heated wall is significantly depended on the position of the inlet port.

MHD Mixed Convection:

Many scientists, versed engineers and researchers studied the problems of MHD mixed convection for different types of cavity. Amongst them, Oreper and Szekely (1983) studied the effect of an externally imposed magnetic field on buoyancy driven flow in a rectangular cavity. They found that the presence of a magnetic field can suppress natural convection currents and that the strength of the magnetic field is one of the important factors in determining the quality of the crystal. Ozoe and Maruo (1987) investigated magnetic and gravitational natural convection of melted silicon two-dimensional numerical computations for the rate of heat transfer. Rudraiah et al. (1995a) investigated the effect of surface tension on buoyancy driven flow of an electrically conducting fluid in a rectangular cavity in the presence of a vertical transverse magnetic field to see how this force damps hydrodynamic movements. At the same time, Rudraiah et al. (1995b) also studied the effect of a magnetic field on free convection in a rectangular enclosure. The problem of unsteady laminar combined forced and free convection flow and heat transfer of an electrically conducting and heat generating or absorbing fluid in a vertical liddriven cavity in the presence of a magnetic field was formulated by Chamkha (2002).Recently, Rahman et al. (2009a) studied the effect of a heat conducting horizontal circular cylinder on MHD mixed convection in a lid-driven cavity along with Joule Heating. The author considered the cavity consists of adiabatic horizontal walls and differentially heated vertical walls, but it also contains a heat conducting horizontal circular cylinder located somewhere inside the cavity. The results indicated that both the flow and thermal fields strongly depend on the size and locations of the inner cylinder, but the thermal conductivity of the cylinder has significant effect only on the thermal field. Rahman et al.(2009b) investigated the effect on magnetohydrodynamic (MHD)

mixed convection around a heat conducting Horizontal circular cylinder placed at the center of a rectangular cavity along with joule heating. They observed that the streamlines, isotherms, average Nusselt number, average fluid temperature and dimensionless temperature at the cylinder center strongly depend on the Richardson number, Hartmann number and the cavity aspect ratio. Very recently, Rahman et al. (2010) made numerical investigation on the effect of magneto hydrodynamic (MHD) mixed convection flow in a vertical lid driven square enclosure including a heat conducting horizontal circular cylinder with Joule heating. The author found that the Hartmann number, Reynolds number and Richardson number have strong influence on the streamlines and isotherms.

To the best of our knowledge in the light of the above literatures, it has been pointed out that no work has been paid on MHD mixed convection inside a triangular cavity yet.

2.2 OBJECTIVE OF THE PRESENT STUDY

The aim proposed research is to investigate the effects of Magneto-hydrodynamic (MHD) mixed convection flow in a triangular cavity. Results will be presented for different non-dimensional governing and physical parameters in terms of streamlines, isotherms, heat transfer rate as well as the average temperature of the fluid in the cavity.

- To modify the mathematical model regarding the effect of MHD on mixed convection flow in a triangular vented cavity under different boundary conditions.
- To investigate the effects of the physical parameters such as the size, shape, location, thermal conductivity of the heat generating component, direction of moving lid and aspect ratio of the cavity on aforesaid cases in the cavity.
- To investigate the effects of the governing parameters namely, Reynolds number *Re*, Rayleigh number *Ra*, Prandtl number *Pr* and Hartmann number *Ha* on the flow and thermal field in the cavity.
- To compare the present results with other published works.

2.3 OUTLINE OF THE THESIS

This dissertation contains five chapters this thesis is concerned with the analysis of flow and heat transfer characteristics of a steady laminar mixed convection heat transfer in a

triangular cavity. There are many cavity configurations for the study of conjugate effect of conduction and mixed convection flow. In this study we have considered a triangular cavity.

In Chapter 1, A general framework for the description of convective heat transfers has been presented and discussed their properties, also relevant discussion on dimensionless parameter.

In Chapter 2, In this chapter a brief introduction is presented with aim and objective. There is nothing new to say about it. This chapter also consists a literature review of the past studies on fluid flow and heat transfer in cavities or channels. In this state-of-the art review, different aspects of the previous studies have been mentioned categorically. This is followed by the post-mortem of a recent historical event for the illustration of fluid flow and heat transfer effects in cavities

In Chapter 3 effect on mixed convection flow in a triangular cavity have been investigated numerically. Mathematical modeling and Finite Element Formulation for the problem have been presented. Lastly, results of the relevant parametric study have been performed.

In Chapter 4, MHD effects on mixed convection in a triangular cavity have been investigated numerically. Mathematical modeling and Finite Element Formulation for the problem have been presented. Lastly, results of the relevant parametric study have been performed.

Finally, in Chapter 5 the main achievements and some ideas of further work have been summarized.

2.4 ELETROMAGNETIC FIELD

Electromagnetism is the physics of the electromagnetic field: a field which exerts a force on particles that possess the property of electric charge, and is in turn affected by the presence and motion of those particles. The force that the electromagnetic field exerts on electrically charged particles, called the electromagnetic force, is one of the four fundamental forces.

There are at least three ways in which force due to magnetic fields can be experienced. The force can be (a) due to a moving charged particle in a B field, (b) on a current element in an external B field, or (c) between two current elements. The present study is

concerned with the first case (i.e. force on a charged particle). The electric force $\overline{F_e}$ on a stationary or moving electric charge Q in an electric field is given by Coulomb's experimental law and is related to the electric field intensity $\overline{E}$ as

$$\overline{F_e} = Q\overline{E} \tag{2.1}$$

This shows that if Q is positive, $\overline{F_e}$ and $\overline{E}$ has the same direction.

A magnetic field can exert force only on a moving charge. From experiments, it is found that the magnetic force $\overline{F_m}$ experienced by a charge Q moving with a velocity $\bar{v}$ in a magnetic field $\overline{B}$ is

$$\overline{F_m} = Q\bar{v} \times \overline{B} \tag{2.2}$$

This clearly shows that $\overline{F_m}$ is perpendicular to both $\bar{u}$ and $\overline{B}$. $\overline{F_e}$ is independent of the velocity of the charge and can perform work on the charge and change its kinetic energy. Unlike $\overline{F_e}$, $\overline{F_m}$ depends on the charge velocity and is normal to it. $\overline{F_m}$ Cannot perform work because it is at right angles to the direction of motion of the charge $(\bar{F}.\bar{dl} = 0)$; it does not cause an increase in kinetic energy of the charge. The magnitude of $\overline{F_m}$ is generally small compared to $\overline{F_e}$ except at high velocities. For a moving charge Q in the presence of both electric and magnetic fields, the total force on the charge is given by

$$\overline{F} = \overline{F_e} + \overline{F_m} \tag{2.3}$$

Or

$$\overline{F} = \sigma\left(\overline{E} + \bar{v} \times \overline{B}\right) \tag{2.4}$$

This is known as the Lorentz force equation. It relates mechanical force to electrical force. If the mass of the charged particle moving in E and B fields is m, by Newton's second law of motion.

$$\overline{F} = m\frac{d\bar{v}}{dt} = Q\left(\overline{E} + \bar{v} \times \overline{B}\right) \tag{2.5}$$

The solution to this equation is important in determining the motion of charged particles in $\overline{E}$ and $\overline{B}$ fields. It should be remembered that in such fields, energy transfer can be only by means of the electric field.

2.4.1 ELECTROMAGNETIC FIELD IN HYDRODYNAMICS

Electromagnetic field has an important influence on the hydrodynamics. One of the main purposes of the electromagnetic control is to stabilize the flow and suppress oscillatory instabilities, which degrades the resulting crystal. To incorporate the electromagnetic force with the fluid flow model, the Lorentz force for moving axes has been taken in consideration.

$$\overline{F} = q\overline{E} + \overline{j} \times \overline{B} \tag{2.6}$$

$$\overline{j} = \sigma_e \left(\overline{E} + \overline{v} \times \overline{B} \right) \tag{2.7}$$

where $\overline{j}$ is the current density, σ_e is the electrical conductivity of the fluid and $\overline{E} = -\nabla\varphi$ is the electric field and φ is the electric potential and $\overline{u}$ is the field velocity. Electrical insulation is present in the practical applications. So $\nabla\varphi$ becomes zero (i.e. $\nabla\varphi = 0$) indicating the absence of the electric field. Now the modified Lorentz force becomes

$$\overline{F_m} = \sigma_e \left(\overline{v} \times \overline{B} \right) \times \overline{B} \tag{2.8}$$

Therefore the magneto-hydrodynamic (MHD) flow model has be

$$\rho_f (\overline{v}\nabla).\overline{v} = -\nabla p + \mu_f \nabla^2 \overline{v} - \frac{\mu_f}{\kappa}\overline{v} + \sigma_\epsilon \left(\overline{v} \times \overline{B} \right) \times \overline{B} + \overline{F_B}) \tag{2.9}$$

where $\overline{F_B}$ is body force, μ_f and ρ_f are dynamic viscosity and density of fluid respectively.

2.5 COMPUTATIONAL DETAILS

The governing equations in fluid dynamics and heat transfer, including conservation forms of the Navier-Stokes system of equations as derived from the first law of thermodynamics, are expressed in terms of the control volume / surface integral equations, which represent various physical phenomena. To visualize these thermo-fluid

flow scenarios, an approximate numerical solution is needed, which can be obtained by the CFD (Computational Fluid Dynamics) code. The partial differential equations of fluid mechanics and heat transfer are discretized in order to obtain a system of approximate algebraic equations, which then can be solved on a computer. The approximations are applied to small domains in space and / or time so the numerical solution provides results at discrete locations in space and time. Much as accuracy of experimental data depends on the quality of the tools used, the accuracy of numerical solution is dependent on the quality of discretization used.

CFD computation involves the creation of a set numbers that constitutes a realistic approximation of a real life system. The outcome of computation process improves the understanding of the behavior of a system. Thereby, engineers need CFD codes that can produce physically realistic results with good accuracy in simulations with finite grids. Contained within the broad field of computational fluid dynamics are activities that cover the range from the automation of well established engineering design methods to the use of detailed solutions of the Navier-Stokes equations as substitutes for experimental research into the nature of complex flows. CFD have been used for solving wide range of fluid dynamics problem. It is more frequently used in fields of engineering where the geometry is complicated or some important feature that cannot be dealt with standard methods.

The complete Navier-Stokes equations are considered to be the correct mathematical description of the governing equations of fluid motion. The most accurate numerical computations in fluid dynamics come from solving the Navier-Stokes equations. The equations represent the conservation of mass and momentum.

There are several discritization methods available for the high performance numerical computation in CFD.

- Finite volume method (FVM)
- Finite element method (FEM)
- Finite difference method (FDM)
- Boundary element method (BEM)
- Boundary volume method (BVM)

- In the present numerical computation, Galerkin finite element method (FEM) has been used.

2.5.1 FINITE ELEMENT METHOD

The finite element method (FEM) is a powerful computational technique for solving problems which are described by partial differential equations or can be formulated as functional minimization. The basic idea of the finite element method is to view a given domain as an assemblage of simple geometric shapes, called finite elements, for which it is possible to systematically generate the approximation functions needed in the solution of partial differential equations by the variational or weighted residual method. The computational domains with irregular geometries by a collection of finite elements makes the method a valuable practical tool for the solution of boundary, initial and eigen value problems arising in various fields of engineering. The approximation functions, which satisfy the governing equations and boundary conditions, are often constructed using ideas from interpolation theory. Approximating functions in finite elements are determined in terms of nodal values of a physical field which is sought. A continuous physical problem is transformed into a discretized finite element problem with unknown nodal values. For a linear problem, a system of linear algebraic equations should be solved. Values inside finite elements can be recovered using nodal values.

The major steps involved in finite element analysis of a typical problem are:

1. Discretization of the domain into a set of finite elements (mesh generation).
2. Weighted-integral or weak formulation of the differential equation to be analyzed.
3. Development of the finite element model of the problem using its weighted-integral or weak form.
4. Assembly of finite elements to obtain the global system of algebraic equations.
5. Imposition of boundary conditions.
6. Solution of equations.
7. Post-computation of solution and quantities of interest.

2.5.2 MESH GENERATION

In finite element method, the mesh generation is the technique to subdivide a domain into a set of subdomains, called finite elements. Figure 2.1 shows a domain, Λ is subdivided into a set of subdomains, Λ^e with boundary Γ^e.

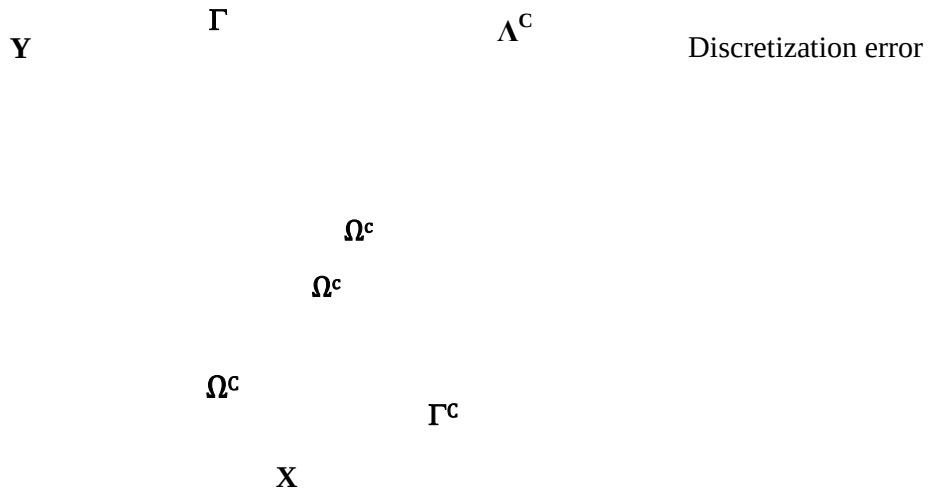

Figure 2.1: Finite element discretization of a domain

The present numerical technique will discretize the computational domain into unstructured triangles by Delaunay Triangular method. The Delaunay triangulation is a geometric structure that has enjoyed great popularity in mesh generation since the mesh generation was in its infancy. In two dimensions, the Delaunay triangulation of a vertex set maximizes the minimum angle among all possible triangulations of that vertex set.

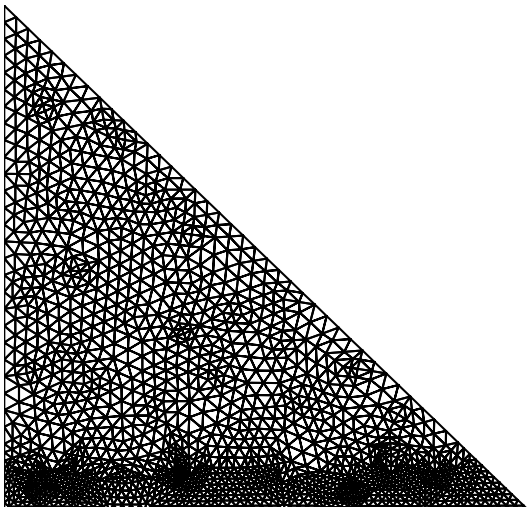

Figure 2.2: Current mesh structure of elements for triangular cavity.

2.5.3 ALGORITHM

The algorithm was originally put forward by the iterative Newton-Raphson algorithm; the discrete forms of the continuity, momentum and energy equations are solved to find out the value of the velocity and the temperature. It is essential to guess the initial values of the variables. Then the numerical solutions of the variables are obtained while the convergent criterion is fulfilled. The simple algorithm is shown by the flow chart below.

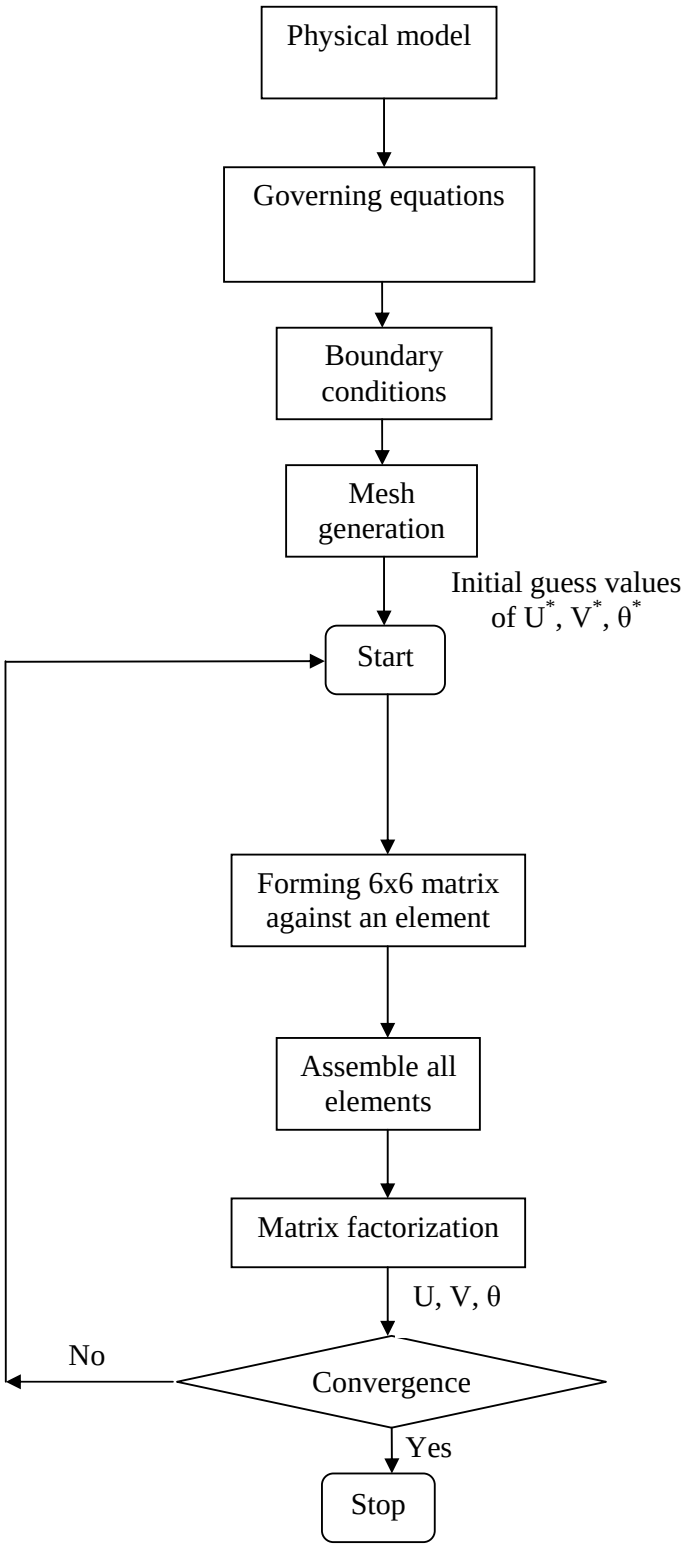

Figure 2.3: Flow chart of the computational procedure

2.5.4 SOLUTION OF SYSTEM OF EQUATIONS

A system of linear algebraic equations has been solved by the UMFPACK with MATLAB interface. UMFPACK is a set of routines for solving asymmetric sparse linear systems Ax = b, using the Asymmetric MultiFrontal method and direct sparse LU factorization. Five primary UMFPACK routines are required to factorize A or Ax = b:

1. Pre-orders the columns of A to reduce fill-in and performs a symbolic analysis.
2. Numerically scales and then factorizes a sparse matrix.
3. Solves a sparse linear system using the numeric factorization.
4. Frees the Symbolic object.
5. Frees the Numeric object.

Additional routines are:

1. Passing a different column ordering
2. Changing default parameters
3. Manipulating sparse matrices
4. Getting LU factors
5. Solving the LU factors
6. Computing determinant

UMFPACK factorizes PAQ, PRAQ, or $PR^{-1}AQ$ into the product LU, where L and U are lower and upper triangular, respectively, P and Q are permutation matrices, and R is a diagonal matrix of row scaling factors (or R = I if row-scaling is not used). Both P and Q are chosen to reduce fill-in (new nonzeros in L and U that are not present in A). The permutation P has the dual role of reducing fill-in and maintaining numerical accuracy (via relaxed partial pivoting and row interchanges). The sparse matrix A can be square or rectangular, singular or non-singular, and real or complex (or any combination). Only square matrices A can be used to solve Ax = b or related systems. Rectangular matrices can only be factorized. UMFPACK first finds a column pre-ordering that reduces fill-in, without regard to numerical values. It scales and analyzes the matrix, and then automatically selects one of three strategies for pre-ordering the rows and columns: asymmetric, 2-by-2 and symmetric. These strategies are described below.

One notable attribute of the UMFPACK is that whenever a matrix is factored, the factorization is stored as a part of the original matrix so that further operations on the matrix can reuse this factorization. Whenever a factorization or decomposition is calculated, it is preserved as a list (element) in the factor slot of the original object. In

this way a sequence of operations, such as determining the condition number of a matrix and then solving a linear system based on the matrix, do not require multiple factorizations of the intermediate results.

Conceptually, the simplest representation of a sparse matrix is as a triplet of an integer vector **i** giving the row numbers, an integer vector **j** giving the column numbers, and a numeric vector **x** giving the non-zero values in the matrix. The triplet representation is row-oriented if elements in the same row were adjacent and column-oriented if elements in the same column were adjacent. The compressed sparse row (csr) or compressed sparse column (csc) representation is similar to row-oriented triplet or column-oriented triplet respectively. These compressed representations remove the redundant row or column in indices and provide faster access to a given location in the matrix.

2.6 CHAPTER SUMMARY

This chapter has presented a tutorial introduction to computational method with advantages of numerical investigation, because numerical method has played a central role in this thesis. Various components of numerical method have been also explained. Finally, the major steps involved in finite element analysis of a typical problem have been discussed.

CHAPTER 3
FINITE ELEMENT ANALYSIS ON MIXED CONVECTION FLOW IN A TRIANGULAR ENCLOSURE

3.1 MATHEMATICAL MODELLING

The convection heat transfer which is neither dominated by pure forced nor pure free convection, rather a combination of the two, is referred to as combined or mixed convection. The starting point of any numerical method is the mathematical model, i.e. the set of partial differential equations and boundary conditions. A solution method is usually designed for a particular set of equations. Trying to produce a general-purpose solution method, i.e. one which is applicable to all flows, is impractical, is not impossible and as with most general purpose tools, they are usually not optimum for any one application.

The generalized governing equations are used based on the conservation laws of mass, momentum and energy. As the heat transfer depends upon a number of factors, a dimensional analysis is presented to show the important non-dimensional parameters which will influence the dimensionless heat transfer parameter, i.e. Nusselt number.

3.2 PHYSICAL MODEL

The physical model considered here is shown in Fig. 3.1, along with the important geometric parameters. The heat transfer and the fluid flow in a two-dimensional triangular cavity with a fluid whose left wall and bottom wall are subjected to cold T_c and hot T_h temperatures respectively while the inclined walls are kept adiabatic. The fluid was assumed with Prandtl number (Pr = 0.71 - 6.0), Reynols number (Re = 40 - 100) and Newtonian, and the fluid flow is considered to be laminar. The properties of the fluid were assumed to be constant.

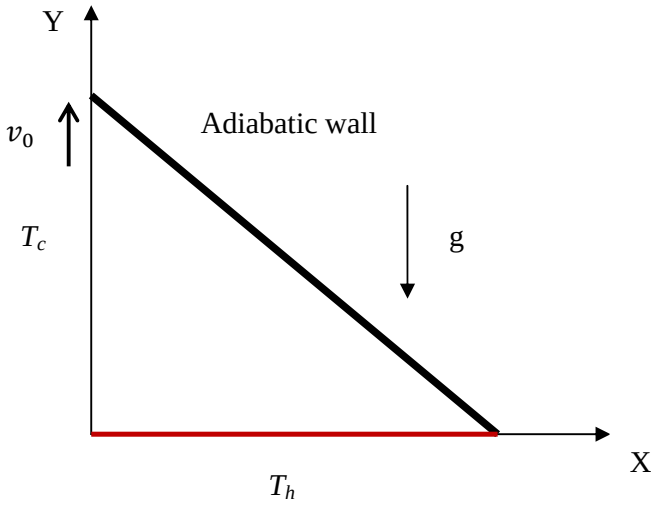

Figure-3.1: Schematic diagram of the physical system

3.3 MATHEMATICAL FORMULATION

The several steps of the mathematical formulation for the above physical configurations are shown as follows

3.3.1 GOVERNING EQUATIONS

The fundamental laws used to solve the fluid flow and heat transfer problems are the conservation of mass (continuity equations), conservation of momentums (momentum equations), and conservation of energy (energy equations), which constitute a set of coupled, nonlinear, partial differential equations. For laminar incompressible thermal flow, the buoyancy force is included here as a body force in the *v*-momentum equation. The governing equations for the two-dimensional steady flow after invoking the Boussinesq approximation and neglecting radiation and viscous dissipation can be expressed as

Continuity Equation

$$\frac{\partial u}{\partial x}+\frac{\partial v}{\partial y}=0 \qquad (3.1)$$

Momentum Equations

$$u\frac{\partial u}{\partial x}+v\frac{\partial u}{\partial y}=-\frac{1}{\rho}\frac{\partial p}{\partial x}+\upsilon\left(\frac{\partial^2 u}{\partial x^2}+\frac{\partial^2 u}{\partial y^2}\right) \tag{3.2}$$

$$u\frac{\partial v}{\partial x}+v\frac{\partial v}{\partial y}=-\frac{1}{\rho}\frac{\partial p}{\partial y}+\nu(\frac{\partial^2 v}{\partial x^2}+\frac{\partial^2 v}{\partial y^2})+g\beta(T-T_c) \tag{3.3}$$

Energy Equations

$$u\frac{\partial T}{\partial x}+v\frac{\partial T}{\partial y}=\frac{k}{\rho c_p}\left(\frac{\partial^2 T}{\partial x^2}+\frac{\partial^2 T}{\partial y^2}\right) \tag{3.4}$$

where x and y are the distances measured along the horizontal and vertical directions respectively; u and v are the velocity components in the x and y directions respectively; T denote the fluid temperature, T_c denotes the reference temperature for which buoyant force vanishes, p is the pressure and ρ is the fluid density, g is the gravitational constant, β is the volumetric coefficient of thermal expansion, c_p is the fluid specific heat, k is the thermal conductivity of fluid.

3.3.2 BOUNDARY CONDITIONS

The boundary conditions for the present problem are specified as follows:

At the cool left vertical wall: $u(0,y)=0, v(0,y)=v_0, T=T_c$

At the bottom wall: $u(x,0)=0=v(x,0), \quad T=T_h$

At the inclined wall: $u(x,y)=0=v(x,y), \frac{\partial T}{\partial n}=0$

Where n is the non-dimensional distances either along x or y direction acting normal to the surface and k is the thermal conductivity of the fluid.

The local Nusselt number at the heated surface of the cavity which is defined by the following expression:

$$Nu_l=-\frac{h(x)L}{k}$$

Such local values have been further averaged over the entire heated surface to obtain the surface averaged or overall mean Nusselt number

$$Nu = \int_0^L Nu_l dx$$

where L and $h(x)$ are the length and the local convection heat transfer coefficient of the heated wall respectively. The average Nusselt number can be used in process engineering design calculations to estimate the rate transfer from the heated surface.

3.3.3 DIMENSIONAL ANALYSIS

Non-dimensional variables are used for making the governing equations (3.1 − 3.4) into dimensionless form are stated as follows:

$$X = \frac{x}{L}, Y = \frac{y}{L}, U = \frac{u}{v_0}, V = \frac{v}{v_0}, P = \frac{p}{\rho v_0^2}, \theta = \frac{(T - T_c)}{(T_h - T_c)}$$

Where X and Y are the coordinates varying along horizontal and vertical directions, respectively, U and V are the velocity components in the X and Y directions, respectively, θ is the dimensionless temperature and P is the dimensionless pressure. After substitution the dimensionless variables into the equations (3.1 - 3.4), we get the following dimensionless equations as

Continuity Equation

$$\frac{\partial U}{\partial X} + \frac{\partial V}{\partial Y} = 0 \tag{3.5}$$

Momentum Equations

$$U\frac{\partial U}{\partial X} + V\frac{\partial U}{\partial Y} = -\frac{\partial P}{\partial X} + \frac{1}{Re}\left(\frac{\partial^2 U}{\partial X^2} + \frac{\partial^2 U}{\partial Y^2}\right) \tag{3.6}$$

$$U\frac{\partial U}{\partial X} + V\frac{\partial U}{\partial Y} = -\frac{\partial P}{\partial Y} + \frac{1}{Re}\left(\frac{\partial^2 V}{\partial X^2} + \frac{\partial^2 V}{\partial Y^2}\right) + Ra\,Pr\,\theta \tag{3.7}$$

Energy Equations

$$U\frac{\partial \theta}{\partial X} + V\frac{\partial \theta}{\partial Y} = \frac{1}{Re\,Pr}\left(\frac{\partial^2 \theta}{\partial X^2} + \frac{\partial^2 \theta}{\partial Y^2}\right) \tag{3.8}$$

The dimensionless parameters appearing in the equations (3.5) through (3.8) are the Reynolds number *Re*, Grashof number *Gr*, Prandtl number *Pr* and Rayleigh number *Ra*. They are respectively defined as follows:

$$Re = \frac{u_i L}{\nu}, Pr = \frac{\nu}{\alpha}, Gr = \frac{\beta g \Delta T L^3}{\nu^2}, Ra = Gr \times Pr$$

where $\Delta T = T_h - T_c$ and $\alpha = \frac{\kappa}{\rho C_p}$ are the temperature difference and thermal diffusivity of the fluid respectively.

The dimensionless boundary conditions under consideration can be written as:

3.3.4 NON-DIMENSIONAL BOUNDARY CONDITIONS

At the left vertical wall: U=0, V=1, $\theta = 0$

At the bottom wall: U=0, V=0, $\theta = 1$

At the inclined wall: U=0, V=0, $\frac{\partial \theta}{\partial N} = 0$

Where N is the non-dimensional distances either along X or Y direction acting normal to the surface and K is the dimensionless thermal conductivity. According to Singh and Sharif (2003), the average Nusselt number at the heated wall of the cavity based on the non-dimensional variables may be expressed as $Nu = \int_0^1 \left(\frac{\partial \theta}{\partial Y} \right)_{y=0} dX$ and the bulk average temperature defined as $\theta_{av} = \int \theta \, d\overline{V} / \overline{V}$, where $\overline{V}$ is the cavity volume.

3.4 NUMERICAL ANALYSIS

The governing equations along with the boundary conditions are solved numerically, employing Galerkin weighted residual finite element techniques discussed below.

3.4.1 FINITE ELEMENT FORMULATION

To derive the finite element equations, the method of weighted residuals Zienkiewicz (1991) is applied to the equations (3.5) – (3.8) as

$$\int_A N_\alpha \left(\frac{\partial U}{\partial X} + \frac{\partial V}{\partial Y} \right) dA = 0 \tag{3.9}$$

$$\int_A N_\alpha \left(U \frac{\partial U}{\partial X} + V \frac{\partial U}{\partial Y} \right) dA = -\int_A H_\lambda \left(\frac{\partial P}{\partial X} \right) dA + \frac{1}{Re} \int_A N_\alpha \left(\frac{\partial^2 U}{\partial X^2} + \frac{\partial^2 U}{\partial Y^2} \right) dA \tag{3.10}$$

$$\int_A N_\alpha (U \frac{\partial V}{\partial X} + V \frac{\partial V}{\partial Y}) dA = -\int_A H_\lambda (\frac{\partial P}{\partial Y}) dA + \frac{1}{Re} \int_A N_\alpha (\frac{\partial^2 V}{\partial X^2} + \frac{\partial^2 V}{\partial Y^2}) dA + Ra\, Pr \int_A N_\alpha \theta dA \tag{3.11}$$

$$\int_A N_\alpha \left(U \frac{\partial \theta}{\partial X} + V \frac{\partial \theta}{\partial Y} \right) dA = \frac{1}{Re\, Pr} \int_A N_\alpha \left(\frac{\partial^2 \theta}{\partial X^2} + \frac{\partial^2 \theta}{\partial Y^2} \right) dA \tag{3.12}$$

Where A is the element area, N_α (α = 1, 2, … … , 6) are the element interpolation functions for the velocity components and the temperature, and H_λ (λ = 1, 2, 3) are the element interpolation functions for the pressure.

Gauss's theorem is then applied to equations (3.10).-.(3.12) to generate the boundary integral terms associated with the surface tractions and heat flux. Then equations (3.9) - (3.12) become,

$$\int_A N_\alpha \left(U \frac{\partial U}{\partial X} + V \frac{\partial U}{\partial Y} \right) dA + \int_A H_\lambda \left(\frac{\partial P}{\partial X} \right) dA + \frac{1}{Re} \int_A \left(\frac{\partial N_\alpha}{\partial X} \frac{\partial U}{\partial X} + \frac{\partial N_\alpha}{\partial Y} \frac{\partial U}{\partial Y} \right) dA = \int_{S_0} N_\alpha S_x dS_0 \tag{3.13}$$

$$\int_A N_\alpha (U \frac{\partial V}{\partial X} + V \frac{\partial V}{\partial Y}) dA + \int_A H_\lambda (\frac{\partial P}{\partial Y}) dA + \frac{1}{Re} \int_A (\frac{\partial N_\alpha}{\partial X} \frac{\partial V}{\partial X} + \frac{\partial N_\alpha}{\partial Y} \frac{\partial V}{\partial Y}) - Ra\, Pr \int_\alpha N_\alpha \theta dA = \int_{s_{00}} N_\alpha S_y dS_0 \tag{3.14}$$

(2.14)

$$\int_\alpha N_\alpha (U \frac{\partial \theta}{\partial X} + V \frac{\partial \theta}{\partial Y}) dA + \frac{1}{Re.Pr} \int_\alpha (\frac{\partial N_\alpha}{\partial X} \frac{\partial \theta}{\partial X} + \frac{\partial N_\alpha}{\partial Y} \frac{\partial \theta}{\partial Y}) dA = \int_{S_w} N_\alpha q_{lw} dS_w \tag{3.15}$$

Here (3.13).-.(3.14) specifying surface tractions (S_x, S_y) along outflow boundary S_0 and (3.15) specifying velocity components and fluid temperature or heat flux (q_w) that flows into or out from domain along wall boundary S_w.

The basic unknowns for the above differential equations are the velocity components *U*, *V* the temperature, θ and the pressure, *P*. The six node triangular element is used in this work for the development of the finite element equations. All six nodes are associated with velocities as well as temperature; only the corner nodes are associated with pressure. This means that a lower order polynomial is chosen for pressure and which is satisfied through continuity equation. The velocity component and the temperature distributions and linear interpolation for the pressure distribution according to their highest derivative orders in the differential equations (3.9) - (3.12) as

$$U(X,Y) = N_\beta U_\beta \tag{3.16}$$

$$V(X,Y) = N_\beta V_\beta \tag{3.17}$$

$$\theta(X,Y) = N_\beta \theta_\beta \tag{3.18}$$

$$P(X,Y) = H_\lambda P_\lambda \tag{3.19}$$

where β = 1, 2, … … , 6; λ = 1, 2, 3.

Substituting the element velocity component distributions, the temperature distribution, and the pressure distribution from equations (3.20) - (3.24), the finite element equations can be written in the form,

$$K_{\alpha\beta^x} U_\beta + K_{\alpha\beta^y} V_\beta = 0 \tag{3.20}$$

$$K_{\alpha\beta\gamma^x} U_\beta U_\gamma + K_{\alpha\beta\gamma^y} V_\gamma U_\gamma + M_{\alpha\mu^x} P_\mu + \frac{1}{Re}\left(S_{\alpha\beta^{xx}} + S_{\alpha\beta^{yy}}\right) U_\beta = Q_{\alpha^u} \tag{3.21}$$

$$K_{\alpha\beta\gamma^x} U_\beta V_\gamma + K_{\alpha\beta\gamma^y} V_\gamma V_\gamma + M_{\alpha\mu^y} P_\mu + \frac{1}{Re}(S_{\alpha\beta^{xx}} + S_{\alpha\beta^{yy}}) V_\beta - Ra\,Pr\,K_{\alpha\beta}\theta_\beta = Q_{\alpha^v} \tag{3.22}$$

$$K_{\alpha\beta\gamma^x} U_\beta \theta_\gamma + K_{\alpha\beta\gamma^y} V_\beta \theta_\gamma + \frac{1}{Re.Pr}\left(S_{\alpha\beta^{xx}} + S_{\alpha\beta^{yy}}\right)\theta_\beta = Q_{\alpha^\theta} \tag{3.23}$$

where the coefficients in element matrices are in the form of the integrals over the element area and along the element edges S_0 and S_w as

$$K_{\alpha\beta^x} = \int_A N_\alpha N_{\beta,x} dA \tag{3.24a}$$

$$K_{\alpha\beta^y} = \int_A N_\alpha N_{\beta,y} dA \tag{3.24b}$$

$$K_{\alpha\beta\gamma^x} = \int_A N_\alpha N_\beta N_{\gamma,x} dA \tag{3.24c}$$

$$K_{\alpha\beta\gamma^y} = \int_A N_\alpha N_\beta N_{\gamma,y} dA \tag{3.24d}$$

$$K_{\alpha\beta} = \int_A N_\alpha N_\beta dA \tag{3.24e}$$

$$S_{\alpha\beta^{xx}} = \int_A N_{\alpha,x} N_{\beta,x} dA \tag{3.24f}$$

$$S_{\alpha\beta^{yy}} = \int_A N_{\alpha,y} N_{\beta,y} dA \tag{3.24g}$$

$$M_{\alpha\mu^x} = \int_A H_\alpha H_{\mu,x} dA \tag{3.24h}$$

$$M_{\alpha\mu^y} = \int_A H_\alpha H_{\mu,y} dA \tag{3.24i}$$

$$Q_{\alpha^u} = \int_{S_0} N_\alpha S_x dS_0 \tag{3.24j}$$

$$Q_{\alpha^v} = \int_{S_0} N_\alpha S_y dS_0 \tag{3.24k}$$

$$Q_{\alpha\theta} = \int_{S_w} N_\alpha \, q_{1w} dS_w \tag{3.24*l*}$$

$$Q_{\alpha\theta s} = \int_{S_w} N_\alpha \, q_{2w} dS_w \tag{3.24m}$$

These element matrices are evaluated in closed form ready for numerical simulation. Details of the derivation for these element matrices are omitted herein.

The derived finite element equations (3.20) - (3.23) are nonlinear. These nonlinear algebraic equations are solved by applying the Newton-Raphson iteration technique by first writing the unbalanced values from the set of the finite element equations (3.20) - (3.23) as,

$$F_{\alpha^p} = K_{\alpha\beta^x} U_\beta + K_{\alpha\beta^y} V_\beta \tag{3.25a}$$

$$\begin{aligned} F_{\alpha^u} &= K_{\alpha\beta\gamma^x} U_\beta U_\gamma + K_{\alpha\beta\gamma^y} V_\gamma U_\gamma + M_{\alpha\mu^x} P_\mu \\ &\quad + \frac{1}{Re}(S_{\alpha\beta^{xx}} + S_{\alpha\beta^{yy}}) U_\beta - Q_{\alpha^u} \end{aligned} \tag{3.25b}$$

$$F_{\alpha^v} = K_{\alpha\beta\gamma^x} U_\beta V_\gamma + K_{\alpha\beta\gamma^y} V_\gamma V_\gamma + M_{\alpha\mu^y} P_\mu + \frac{1}{Re}(S_{\alpha\beta^{xx}} + S_{\alpha\beta^{yy}})V_\beta - Ra\,Pr\,K_{\alpha\beta}\theta_\beta - Q_{\alpha^\theta} \quad (3.25c)$$

$$F_{\alpha^\theta} = K_{\alpha\beta\gamma^x} U_\beta \theta_\gamma + K_{\alpha\beta\gamma^y} V_\beta \theta_\gamma + \frac{1}{Re.Pr}\left(S_{\alpha\beta^{xx}} + S_{\alpha\beta^{yy}}\right)\theta_\beta - Q_{\alpha^\theta} \quad (3.25d)$$

This leads to a set of algebraic equations with the incremental unknowns of the element nodal velocity components, temperatures, and pressures in the form,

$$\begin{bmatrix} K_{pu} & K_{pv} & 0 & 0 \\ K_{uu} & K_{uv} & 0 & K_{up} \\ K_{\theta u} & K_{\theta v} & K_{\theta\theta} & 0 \\ K_{vu} & K_{vv} & K_{v\theta} & K_{vp} \end{bmatrix} \begin{bmatrix} \Delta p \\ \Delta u \\ \Delta\theta \\ \Delta v \end{bmatrix} = -\begin{bmatrix} F_\alpha p \\ F_\alpha u \\ F_\alpha \theta \\ F_\alpha v \end{bmatrix} \quad (3.26)$$

where $K_{uu} = K_{\alpha\beta\gamma^x} U_\beta + K_{\alpha\gamma\beta^x} U_\gamma + K_{\alpha\beta\gamma^y} V_\beta + \frac{1}{Re}\left(S_{\alpha\beta^{xx}} + S_{\alpha\beta^{yy}}\right)$

$K_{uv} = K_{\alpha\beta\gamma^y} U\gamma$

$K_{u\theta} = 0$, $K_{up} = M_{\alpha\mu^x}$

$K_{vu} = K_{\alpha\beta\gamma^x} V\gamma$

$K_{vv} = K_{\alpha\beta\gamma^x} U_\gamma + K_{\alpha\beta\gamma^y} V_\gamma + K_{\alpha\beta\gamma^y} V_\gamma + \frac{1}{Re}(S_{\alpha\beta^{xx}} + S_{\alpha\beta^{yy}})$

$K_{v\theta} = -Ra\,Pr\,K_{\alpha\beta}$, $K_{vp} = M_{\alpha\mu^y}$

$K_{\theta u} = K_{\alpha\beta\gamma^x}\theta\gamma$, $K_{\theta v} = K_{\alpha\beta\gamma^y}\theta\gamma$

$K_{\theta\theta} = K_{\alpha\beta\gamma^x} U_\beta + K_{\alpha\beta\gamma^y} V_\beta + \frac{1}{Re.Pr}(S_{\alpha\beta^{xx}} + S_{\alpha\beta^{yy}})$

$K_{\theta p} = 0$,

$K_{pu} = K_{\alpha\beta^x}$, $K_{pv} = K_{\alpha\beta^y}$ and $K_{p\theta} = 0 = K_{pp}$

The iteration process is terminated if the percentage of the overall change compared to the previous iteration is less than the specified value.

To solve the sets of the global nonlinear algebraic equations in the form of matrix, the Newton-Raphson iteration technique has been adapted through PDE solver with MATLAB interface. The convergence of solutions is assumed when the relative error for each variable between consecutive iterations is recorded below the convergence criterion ε such that $\left|\Psi^{n+1}-\Psi^{n}\right|<\varepsilon$, where n is number of iteration and $\Psi = U, V, \theta$. The convergence criterion was set to $\varepsilon = 10^{-4}$.

3.4.2 GRID INDEPENDENCE TEST

Preliminary results are obtained to inspect the field variables grid independency solutions. Test for the accuracy of grid fineness has been carried out to find out the optimum grid number.

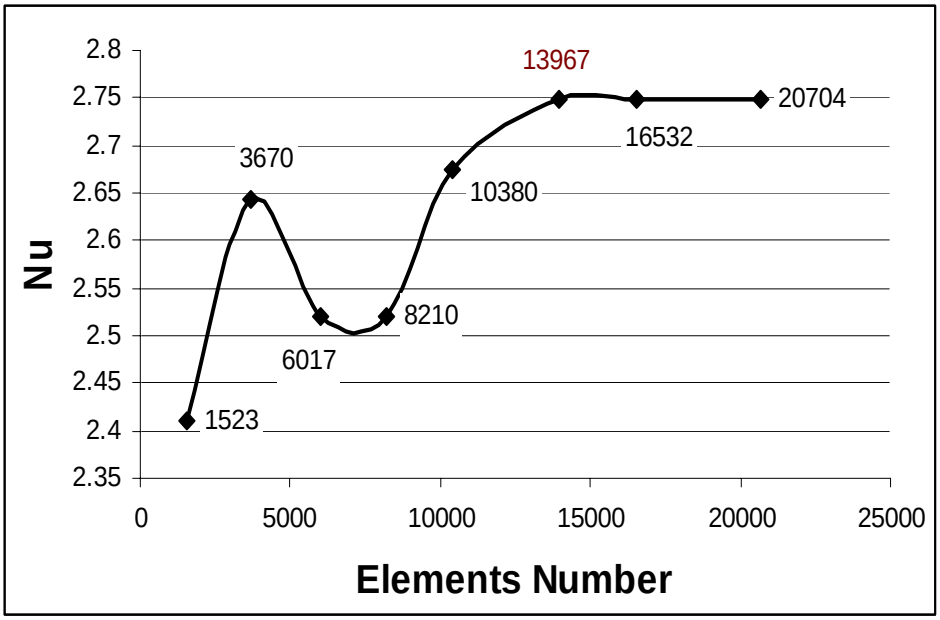

Figure 3.2: Convergence of average Nusselt number with grid refinement for *Pr* = 0.71, *Re* = 50 and *Ra* = 10^4.

In order to obtain grid independent solution, a grid refinement study is performed for a triangular cavity with *Pr* = 0.71, *Re* = 50 and *Ra* = 10^3. Figure 3.2 shows the convergence of the average Nusselt number, Nu_{av} at the heated surface with grid refinement. It is observed that grid independence is achieved with 13967 elements where

there is insignificant change in Nu with further increase of mesh elements. I believe that for this inconsequential change before the element 13967 should not taken as for grid independence. Six different non-uniform grids with the following number of nodes and elements were considered for the grid refinement tests: 9138 nodes, 1523 elements; 22020 nodes, 3670 elements; 36102 nodes, 6017 elements; 49260 nodes, 8210 elements; 62280 nodes, 10380 elements; 83802 nodes, 13967 elements; 99192 nodes, 16532elements. From these values, 83802 nodes, 13967 elements can be chosen throughout the simulation to optimize the relation between the accuracy required and the computing time.

Nodes (Elements)	9138 1523	22020 3670	36102 6017	49260 8210	62280 10380	83802 13967	99192 16532
Nu	2.4095029	2.6431469	2.5207933	2.5207523	2.6746807	2.7484171	2.748417
Time (s)	8.297	19.609	34.0	47.703	67.297	94.828	112.25

Table 3.1: Grid Sensitivity Check at $Pr = 0.71$, $Re = 50$ and $Ra = 10^4$.

3.4.3 CODE VALIDATION

Obviously for high values of *Ra* number the errors encountered are appreciable and hence it is necessary to perform some grid size testing in order to establish a suitable grid size. Grid independent solution is ensured by comparing the results of different grid meshes for $Ra = 10^5$, which was the highest Raylaigh number. The total domain is discretized into 53592 elements that results in 80388 nodes. In order to validate the numerical code, pure natural convection with $Pr = 0.71$ in a triangular cavity was solved and the average Nusselt numbers is presented by graphically. The results were compared with those reported by Basak et al., obtained with an extended computational domain. In Table1, a comparison between the average Nusselt numbers is presented. The results from the present experiment are almost same as Basak et.al.

Table 3.2: Comparison of the results for the constant surface temperature with Pr = 0.71.

Ra	Nu_{av}	
	Present work	Basak et al. (2007)
10^3	5.49	5.40
10^4	5.77	5.56
10^5	7.08	7.54

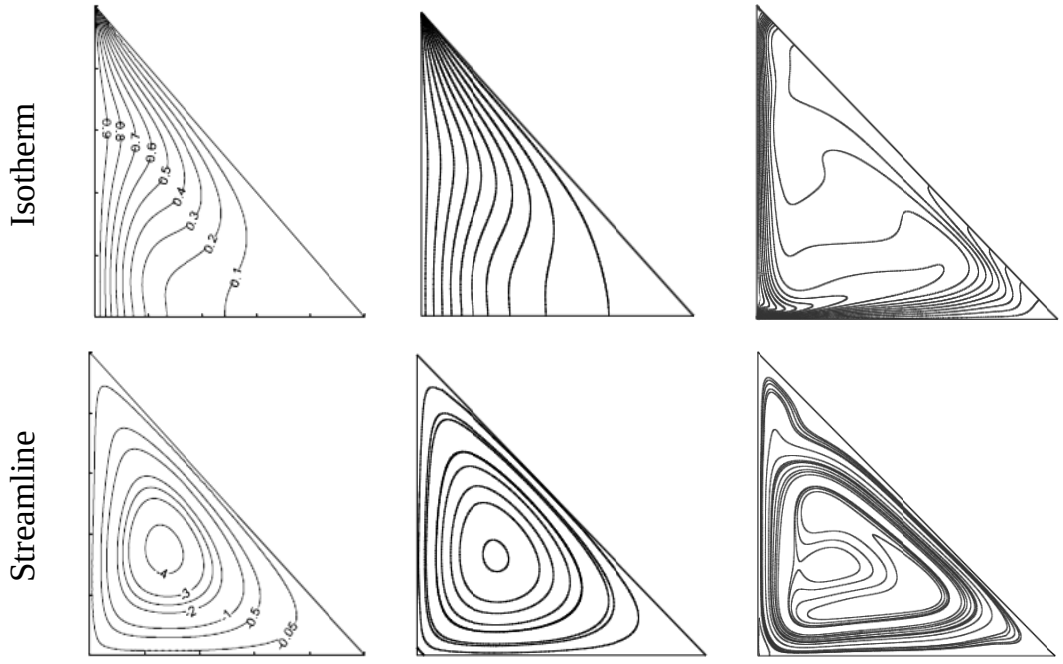

Basak et. Al. (2007) | Regenerate program of Basak et. al. (2007**)** | Present Work with MHD effect

3.5 RESULTS AND DISCUSSION

Numerical results are presented in order to conclude the properties of the presence of dimensionless parameters in triangular cavity with a heat conducting horizontal bottom wall and the other two remaining walls were kept cooled Temperature T_c (left wall) and

adiabatic (inclined wall). Two-dimensional forms of Navier-Stokes equations along with the energy equations are solved using Galerkin finite element method. The dimensionless parameters that must be specified for the system are Reynolds number *Re*, Rayleigh number *Ra*, Prandtl number *Pr*. Since so many basic dimensionless parameters are required to characterize a system, an analysis of all combinations of these parameters is not practical. The numerical results have been aimed to explain the effect of several parameters at a small fraction of the possible situations by simplifying the configuration. Results are obtained for a range of Rayleigh number from 10^3 to 10^4 at Pr = 0.71 - 6.0 and Re = 40 - 100, with constant physical properties. The parametric studies for a wide range of governing parameters show consistent performance of the present numerical approach to obtain as stream functions and temperature profiles. The computational results indicate that the heat transfer coefficient is strongly affected by Rayleigh number.

The average Nusselt number at heated surface and average bulk temperature of the fluid has been presented in figure (3.7, 3.8, 3.13 and 3.14.) and table (3.3 – 3.6).

3.5.1 EFECT OF REYNOLDS NUMBER

The fluid flow patterns inside the cavity are presented in terms of streamlines and isotherms in the figure 3.3 - 3.6 at the four values of Reynolds number *Re* (*Re* = 40, 50, 70, and 100) and the three different values of *Ra* (*Ra* = 10^3, 5×10^3 and 10^4), while *Pr* = 0.71. Using the definition of stream function (ψ), the streamlines with 'positive value' of stream function corresponds to anti-clockwise circulation, and those with 'negative value' of stream function correspond to clockwise circulation. As expected due to the upward motion of the bottom wall fluid rise up along the side of the cold vertical wall and flow down along the right vertical wall forming a roll with anti-clockwise rotation inside the cavity for the three values of *Ra at* *Re* = 40. It is also observed that the orientation of the core in the recirculation cell changes as Reynolds number *Re* changes. Next at *Re* = 50, secondary rotating cells are developed in the cavity for all values of *Ra*, which indicates both the conducting force and buoyant force are present in the cavity. In this folder at low *Ra* = 10^3 the '+ψ' value is low in the cell, which is due to conductive force occupies most of the part of the cavity and other two secondary rotating cells due to buoyant force are developed at the bottom and inclined wall. However, as *Ra* increases the value of ψ stream function also increased and the cells become larger in size. It is

also seen from figure 3.5 - 3.6 that value of ψ of the anticlockwise rotating cell increases sharply and more tightened to the neighboring boundary wall, indicating a sign of supremacy of free convection in the cavity at *Re* = 100 and different value of *Ra*.

Now we draw the attention to see the effect of increasing Reynolds number *Re* on the temperature distribution in the cavity. From the figures 3.3 - 3.6, it can be seen that isothermal lines are nearly parallel to the hot wall at *Re* = 40 and $Ra = 10^3$, which is similar to conduction-like distribution. It is also seen that isothermal lines start to turn back from the hot wall to the cold wall near the bottom wall at $Ra = 5\times10^3$ and *Re* = 40 due to the dominating influence of conduction and forced convection in the lower part of the cavity. More significant distortion in isothermal lines near the left bottom corner of the cavity is observed at the higher values of *Ra*. The isotherm patterns reflects a conductive pattern of energy transfer at the lower values of *Re* (*Re* = 40, 50) and a convective pattern of energy transfer at the higher values of *Re* (*Re* = 70, 100). On the other hand, the convective distortion of isothermal lines start to appear at $Ra = 5\times10^3$ and *Re* = 40. At $Ra = 5\times10^3$ and *Re* = 70, it is seen that the isothermal lines turn back towards the left cold wall near the top of the cavity and a thermal boundary layer is developed near the left vertical (cold) wall due to the dominating influence of the convective current in the upper part of the cavity. Finally at $Ra = 10^4$, the convective distortion in the isotherms become more intensive and the thermal boundary layer near the cold wall becomes more concentrated with further increasing the values of Reynolds number due to the strong influence of the convective current.

The effect of Reynolds number on average Nusselt number (*Nu*) at the heated bottom wall, average fluid temperature (θ_{av}) in the cavity are displayed as a function of Rayleigh number at some particular Reynolds number in figure 3.7 & 3.8 for the above mentioned cavity. It is observed that the average Nusselt number at the hot wall increases considerably in the forced convection dominated region and increases very penetratingly in the free convection dominated region with increasing *Ra* for the higher values of Reynolds number *Re* (*Re* = 50, 70 and 100). However, maximum values of *Nu* is found for the highest value of *Re* (*Re* = 100) at free convection dominated region. On the other hand, the average fluid temperature (θ_{av}) in the cavity increases gradually for higher values of *Re* (*Re* = 50, 70, 100) and but suddenly fall dramatically for the all value of *Re* with increasing *Ra*. In addition, the values of θ_{av} are found minimum for *Re* = 40 at *Ra* =

10^4, in free convection dominated region. However, a visual examination of the figure 3.8 show qualitatively similar plots for both of the cases at different values of *Re* and *Ra*.

Finally, the quantitative differences of the values of *Nu* at different values of *Re* are indicated in Tables 3.3 and 3.4.

Table 3.3: Average Nusselt numbers for different Reynolds number while *Re* = 40, 50, 70, 100 and *Pr* = 0.71.

Nu_{av}			
Re	$Ra = 10^3$	$Ra = 5\times10^3$	$Ra = 10^4$
40	2.161478	2.586721	2.952413
50	2.248317	2.674681	3.055404
70	2.397222	2.397222	3.227744
100	2.580004	3.015424	3.432453

Table 3.4: Average Bulk temperature for different Reynolds number while *Re* = 40, 50, 70, 100 and *Pr* = 0.71.

θ_{av}			
Re	$Ra = 10^3$	$Ra = 5\times10^3$	$Ra = 10^4$
40	0.458247	0.586141	0.301202
50	0.467239	0.585775	0.301637
70	0.477203	0.584899	0.302132
100	0.485564	0.583535	0.302443

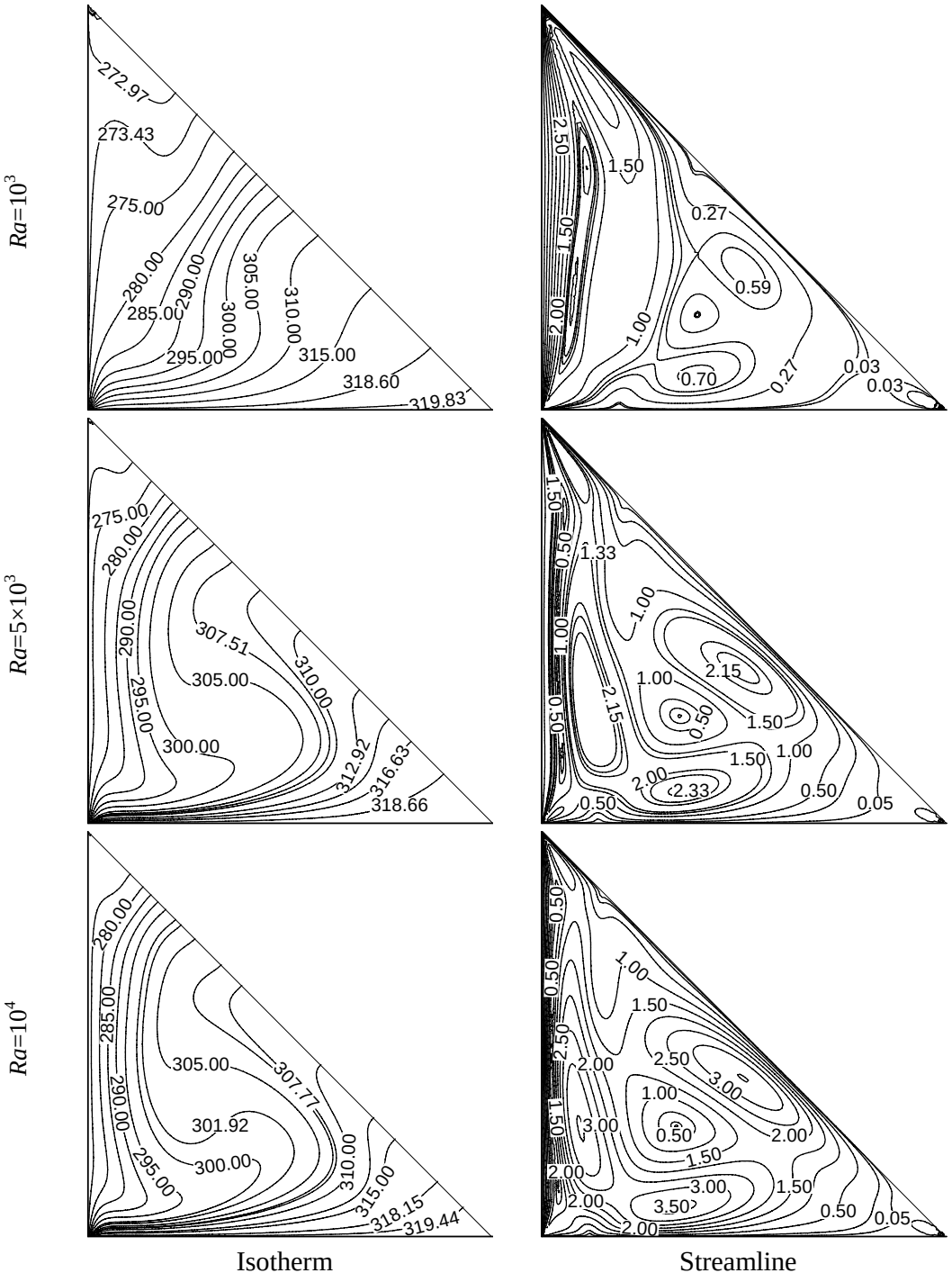

Fig 3.3: Isotherms and streamlines patterns for *Re* = 40 *and Pr* = 0.71

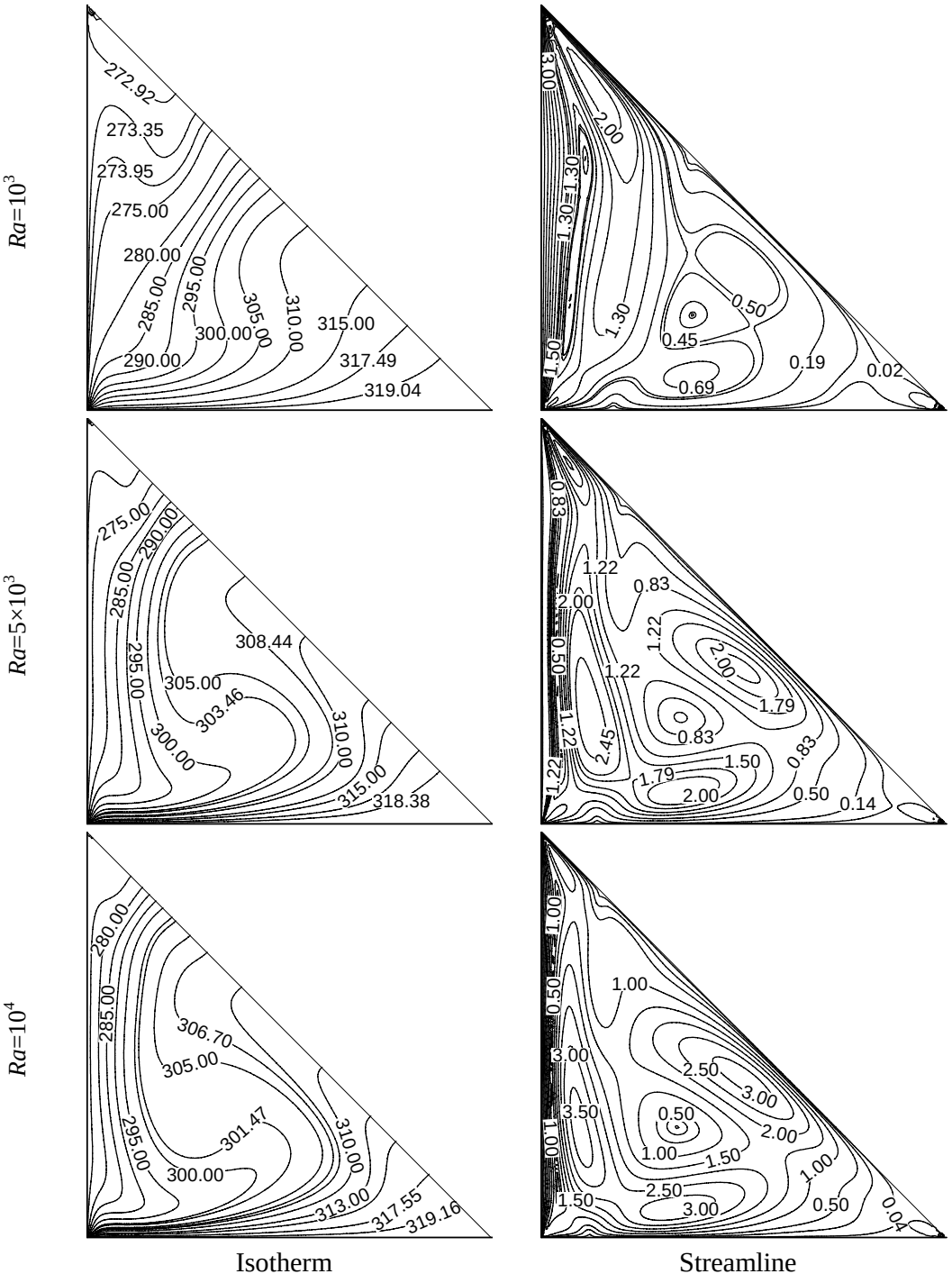

Fig 3.4: Isotherms and streamlines patterns for Re = 50 and Pr = 0.71

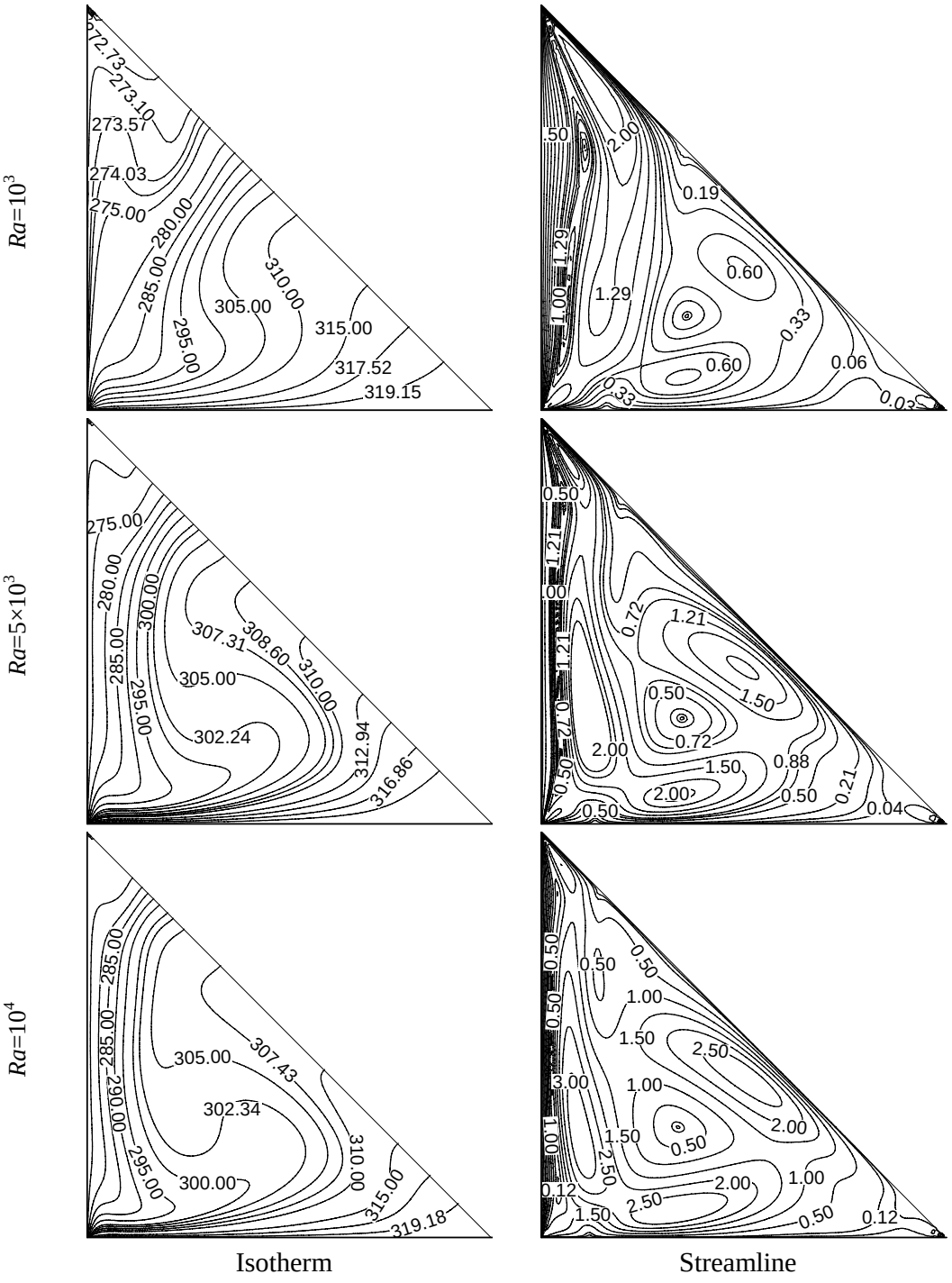

Fig 3.5: Isotherms and streamlines patterns for *Re* = 70 and *Pr* = 0.71

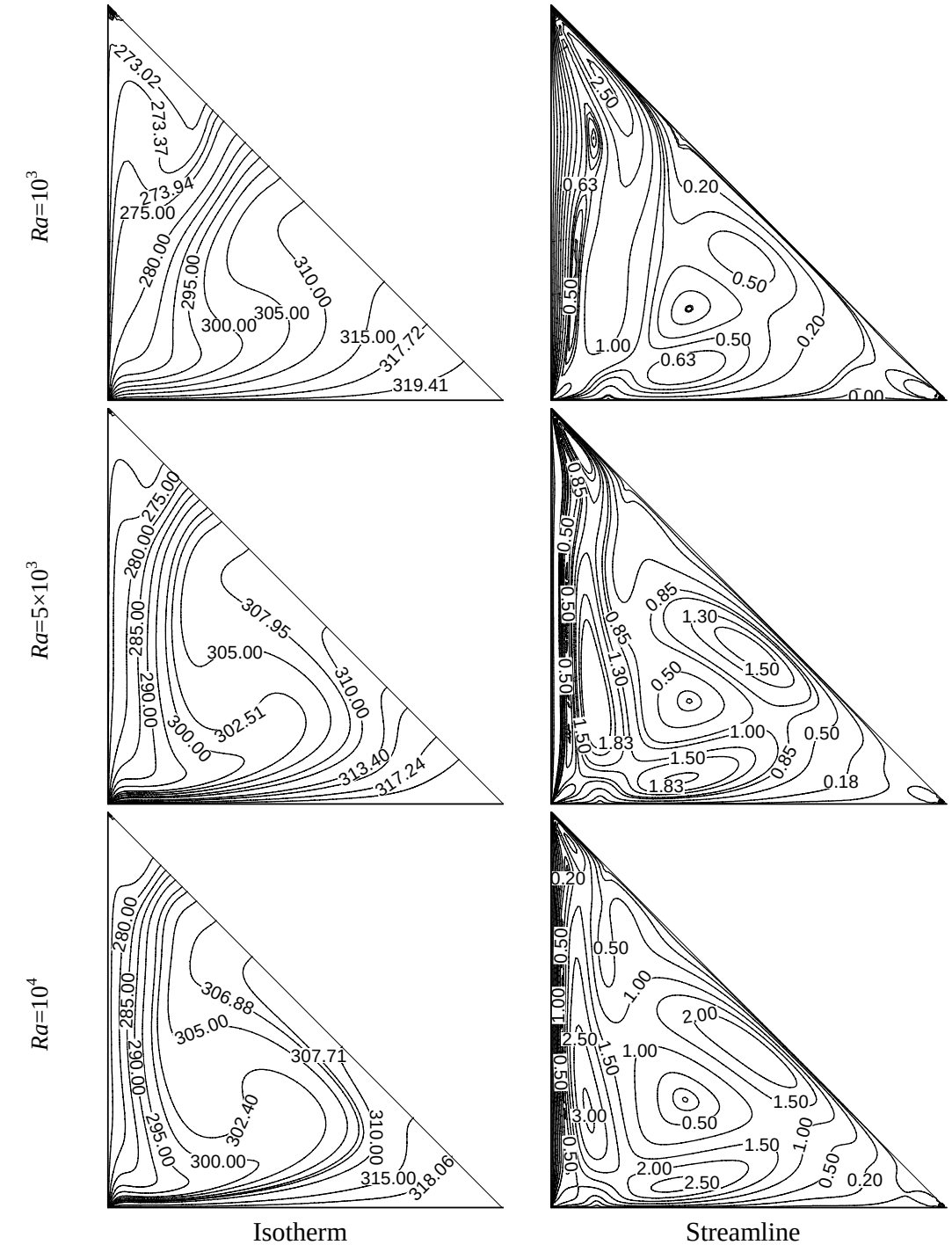

Fig 3.6: Isotherms and streamlines patterns for *Re* = 100 and *Pr* = 0.71

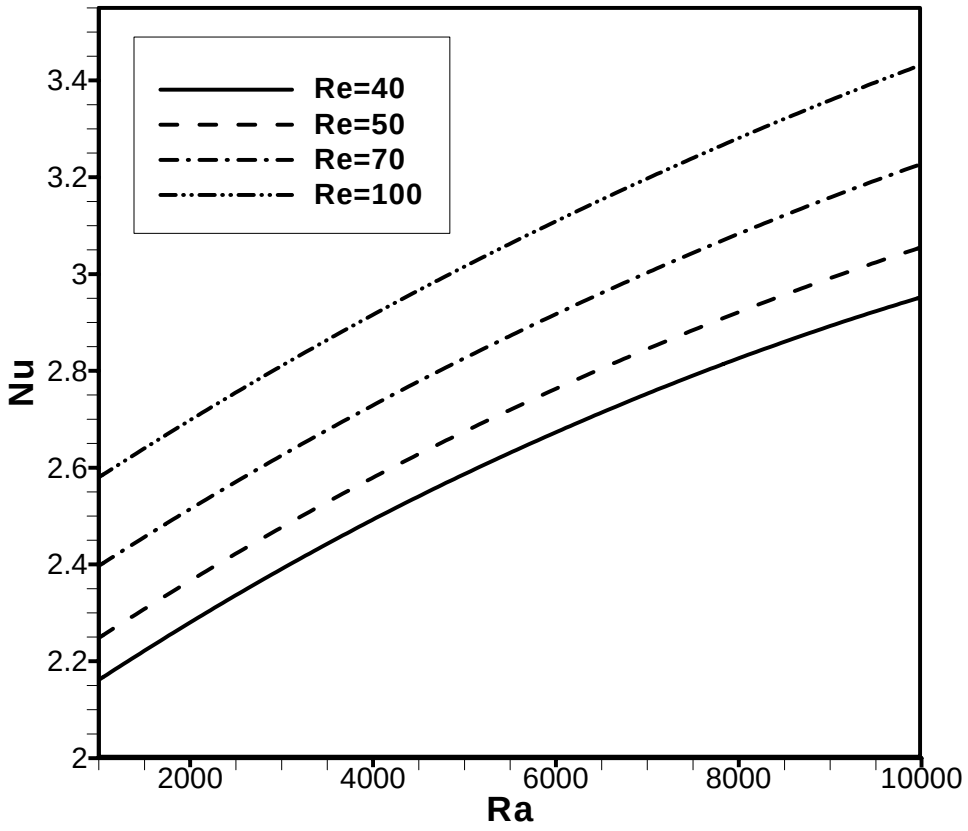

Fig.3.7: Effect of average Nusselt number and Rayleigh number while Pr = 0.71.

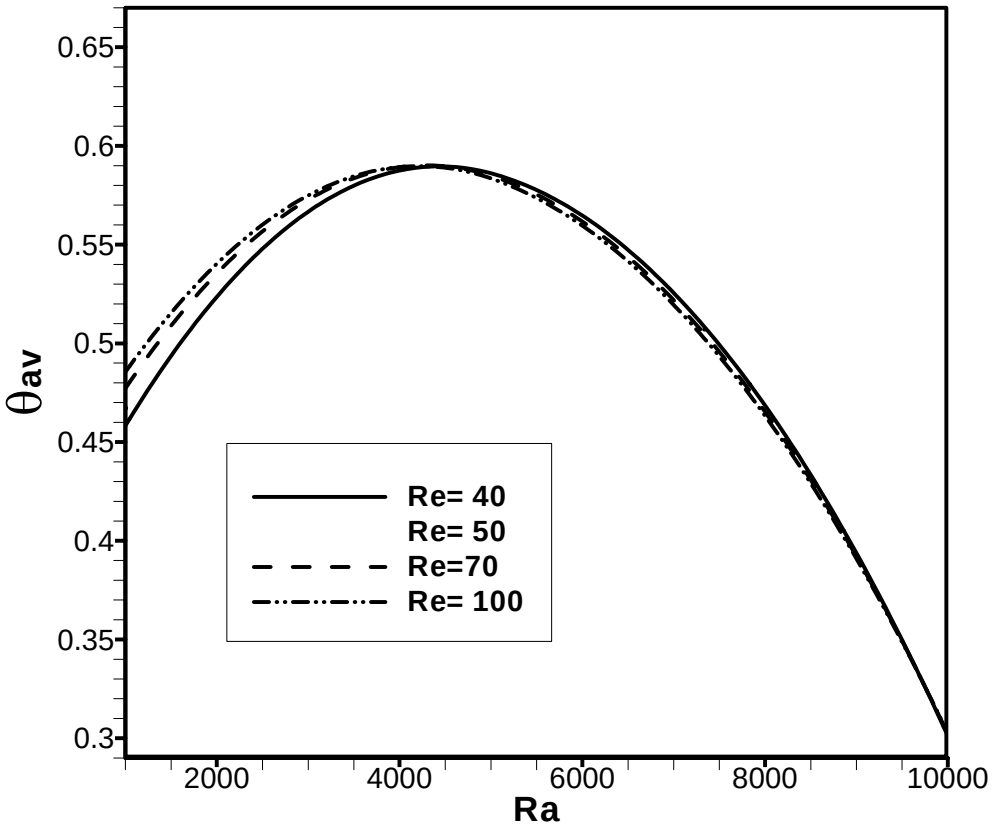

Fig.3.8: Effect of average bulk temperature and Rayleigh number while *Pr* = 0.71

3.5.2 EFFECT OF PRANDLT NUMBER

Fig. 3.9 – 3.12 display the effects of *Ra* (*Ra* = 10^3 – 10^4) and *Pr* (*Pr* = 0.71 – 6.0) when the bottom wall is heated while the left moving wall is maintained at cold temperature. The fluid near the hot (bottom) wall has lower density, so it moves upward while the relatively heavy fluid near to cold (left) wall moves downward and this fluid is heated up. Thus the fluid motion completes a circulation. As mentioned before by the definition of stream function, the streamlines with 'positive value' of stream function corresponds to anti-clockwise circulation, and those with 'negative value' of stream function correspond to clockwise circulation. It has been seen that for steady flow, stream lines are equivalent to the paths followed by the individual particles in the fluid. Results indicate that at low Rayleigh number (*Ra* = 10^3), the isotherm lines are smooth and monotonic as shown for *Pr* = 0.71 in Fig. 3.9. The magnitudes of the stream function contours are very low. This illustrates that at low *Ra* the flow is mostly due to conduction.

At *Ra* = 5×10^3 and *Pr* = 0.71, the circulations near the central regime are stronger and consequently, the thermal boundary layer start getting shifted towards the left wall (Fig. 3.10 - 3.12).The presence of significant convection is also exhibited in the temperature profile which get pushed towards the upper portion of left wall. As Rayleigh number increases to 10^4, the buoyancy driven circulation inside the cavity is also increased as seen from greater magnitudes of the stream function (Fig. 3.9 - 3.12). It is remarkable that fig. 3.12 for *Pr* = 6.0 shows the circulations are bigger near the center due to convection and least at the vicinity wall due to no-slip boundary conditions. The greater circulation in central regime follows a progressive packaging around the center of rotation, and a more and more pronounced compression of the isotherms occurs towards the bottom and left wall of triangular cavity. Due to high circulations, the temperature contours with 300.00 condensed in a very small regime at the bottom wall and this may cause bigger heat transfer rates at the bottom wall. It may also be noted that the higher circulation pushes fluid near the upper region of the left wall, and the fluid is pulled away from the central region of the left wall. Consequently, at *Ra* = 10^4, the temperature gradients near the bottom wall are found to be significantly high.

The effects of Prandtl number on average Nusselt number *Nu* at the heated surface and average bulk temperature θ_{av} in the cavity is illustrated in Fig. 3.13 & 3.14 with *Re* = 50.

From this figure, it is found that the average Nusselt number *Nu* moves up calmly with increasing *Pr*. Moreover, it is also to be highlighted that the highest heat transfer rate occurs for the highest values of *Pr* (= 6.0). On the other hand, the average bulk temperature of the fluid in the cavity increases very sharply in forced convection dominated region inside the cavity and reached to the highest bulk temperature rate at *Pr* = 0.71.But in the free dominated region bulk temperature rate is slower for the higher values of *Pr* .

Table 3.5: Average Nusselt numbers for different Prandtl number while *Pr* = 0.71, 2.0, 3.0, 6.0 and *Re* = 50.

Nu_{av}			
Pr	$Ra = 10^3$	$Ra = 5\times10^3$	$Ra = 10^4$
0.71	2.248317	2.674681	3.055404
2.0	3.28083	4.045073	4.731271
3.0	3.887278	4.791325	5.577197
6.0	5.162974	6.307248	7.443361

Table 3.6: Average Bulk temperature for different Prandtl number while *Pr* = 0.71, 2.0, 3.0, 6.0 and *Re* = 50.

θ_{av}			
Pr	$Ra = 10^3$	$Ra = 5\times10^3$	$Ra = 10^4$
0.71	0.467239	0.585775	0.603274
2.0	0.512497	0.592877	0.590195
3.0	0.518236	0.584532	0.570561
6.0	0.522066	0.558371	0.543347

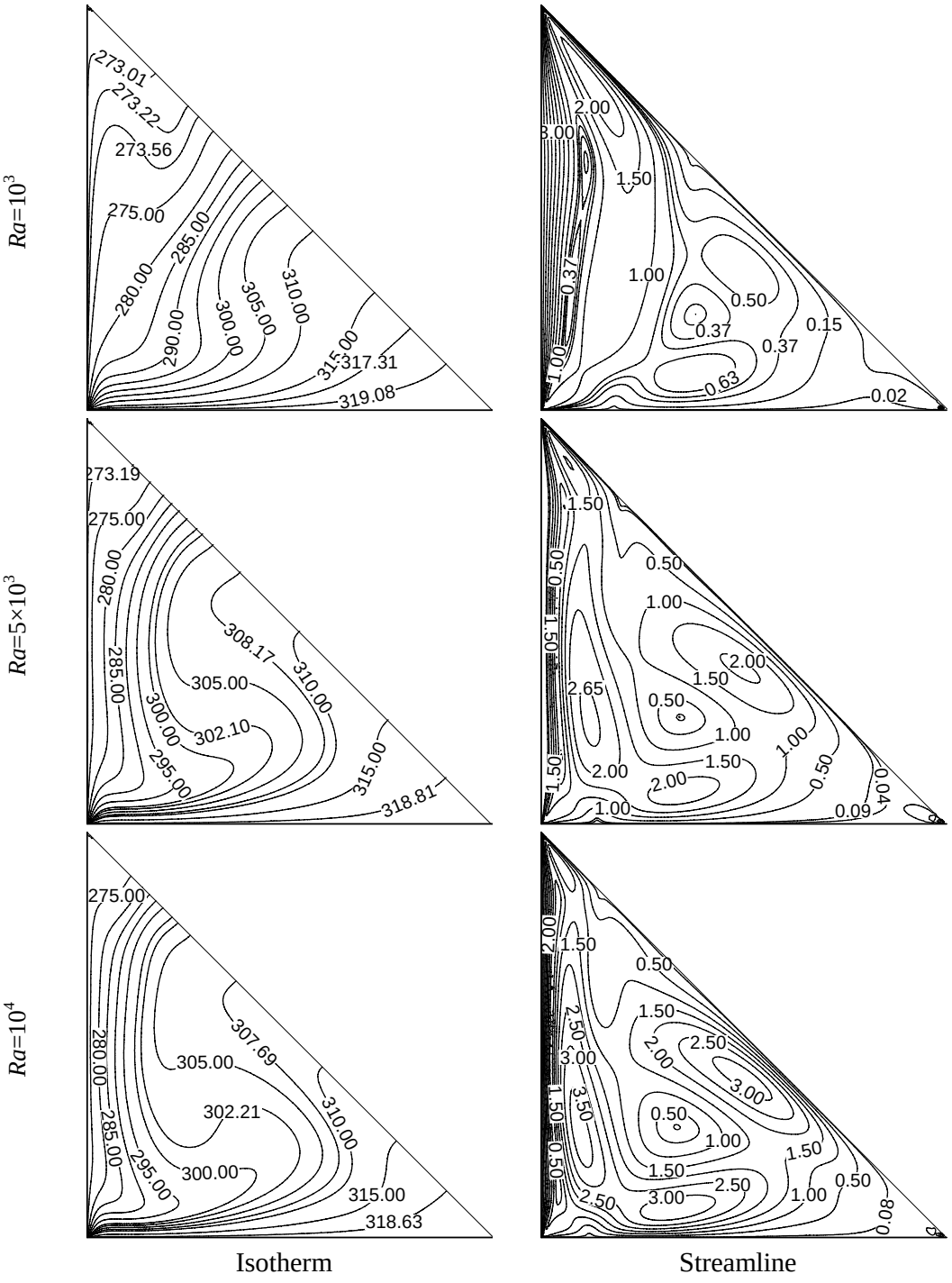

Fig 3.9: Isotherms and streamlines patterns for Re = 50 and Pr = 0.71

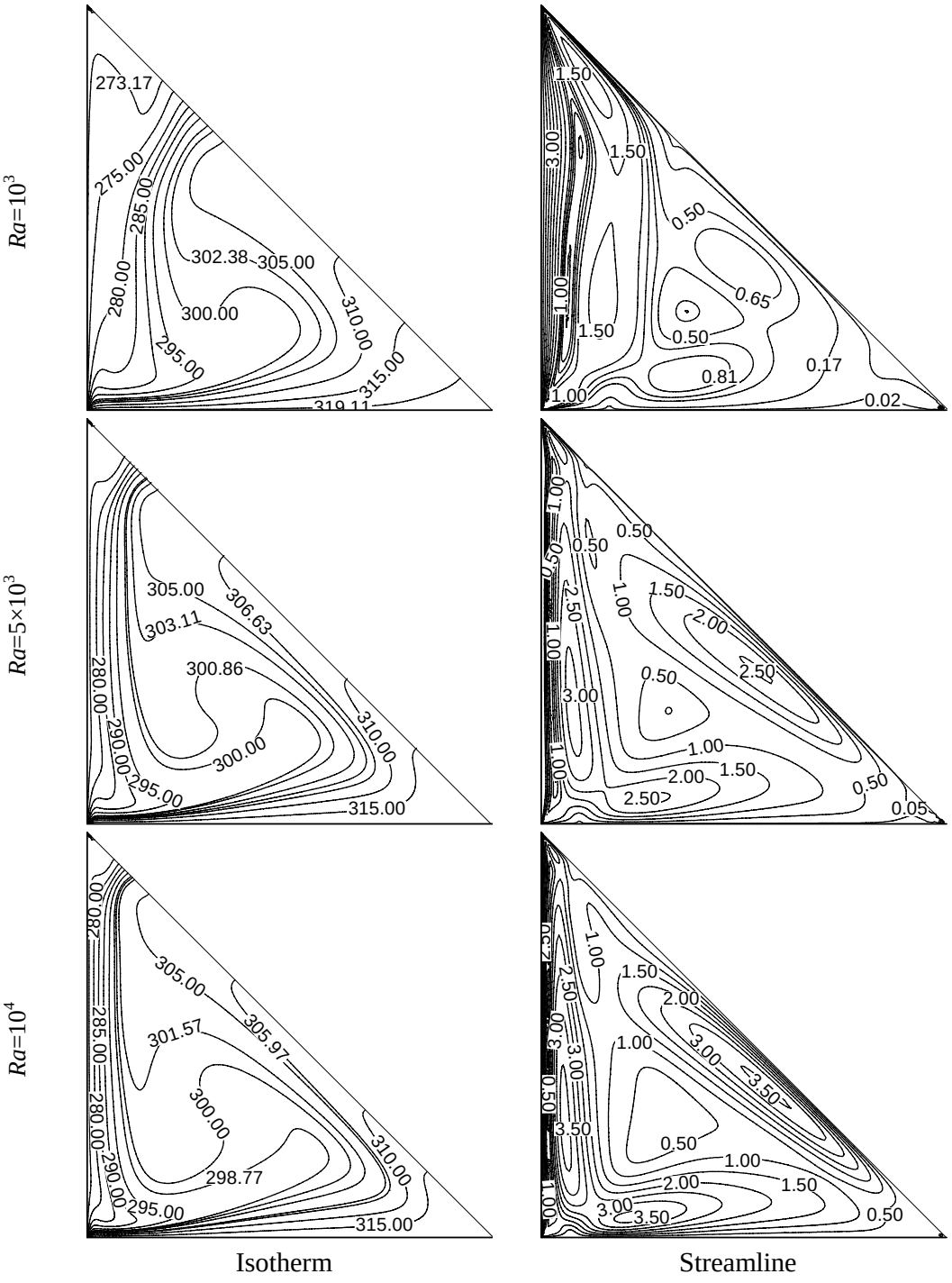

Fig 3.10: Isotherms and streamlines patterns for *Re* = 50 and *Pr* = 2

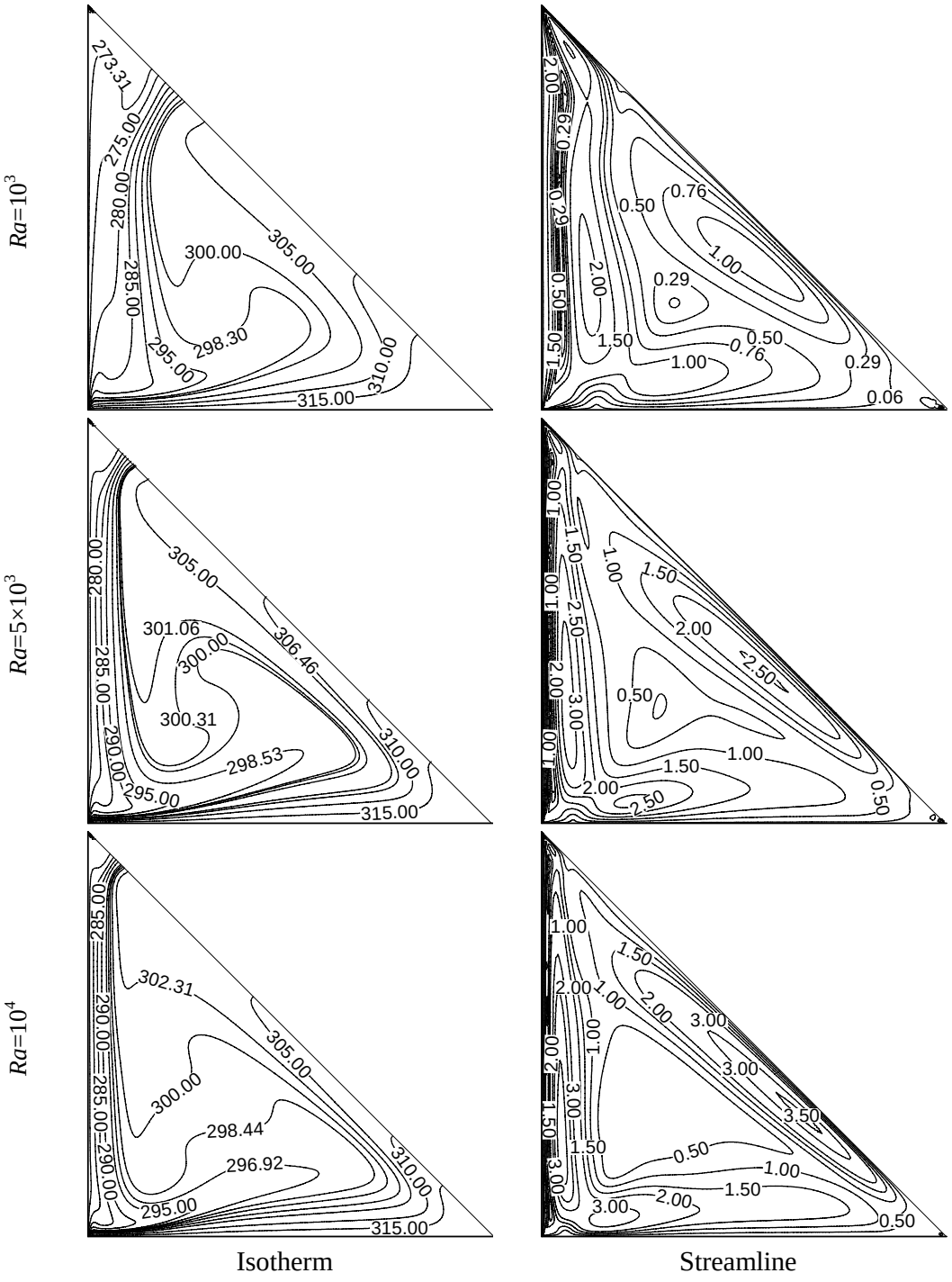

Fig 3.11: Isotherms and streamlines patterns for *Re* = 50 and *Pr* = 3

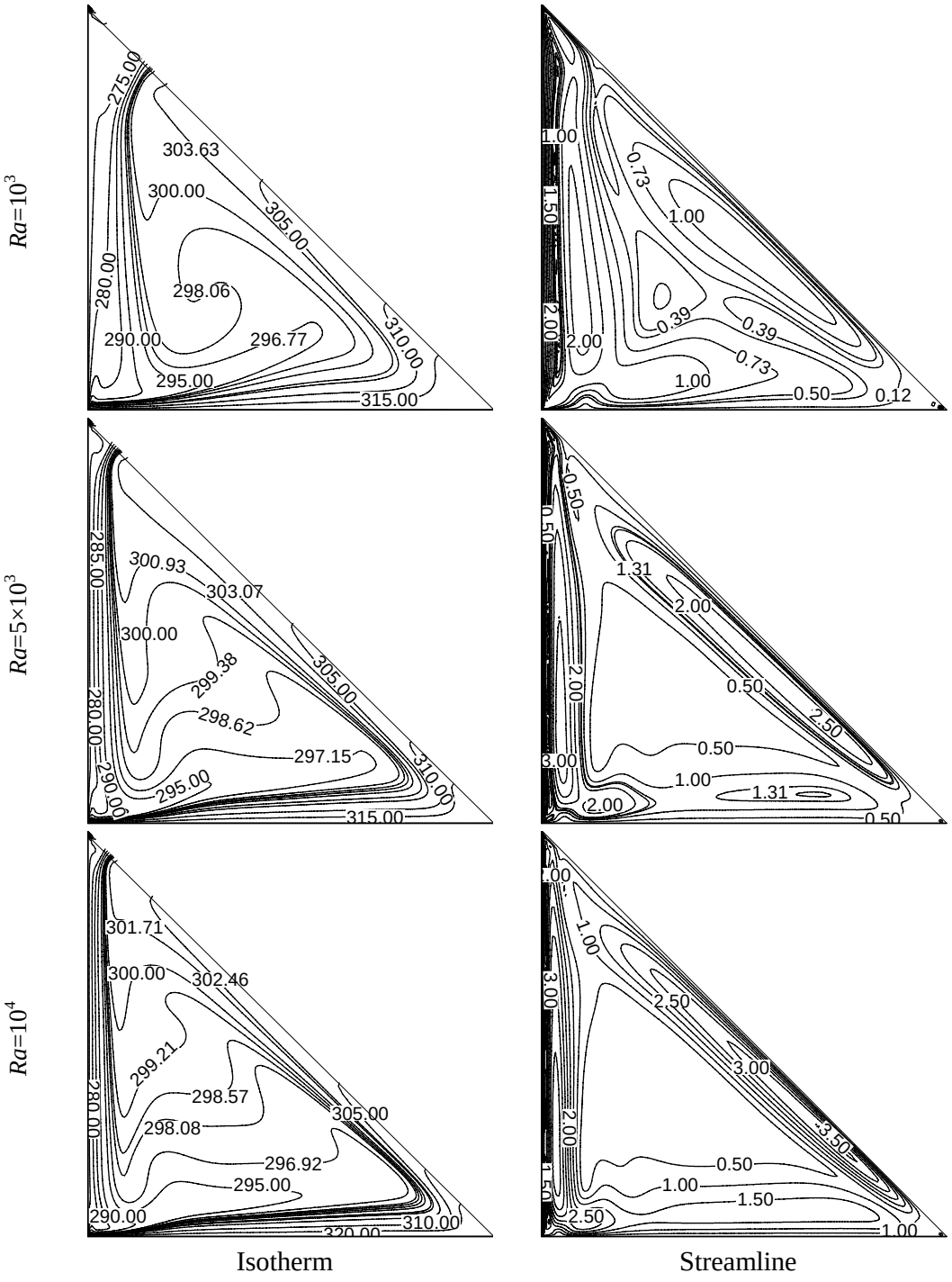

Fig 3.12: Isotherms and streamlines patterns for *Re* = 50 and *Pr* = 6.0

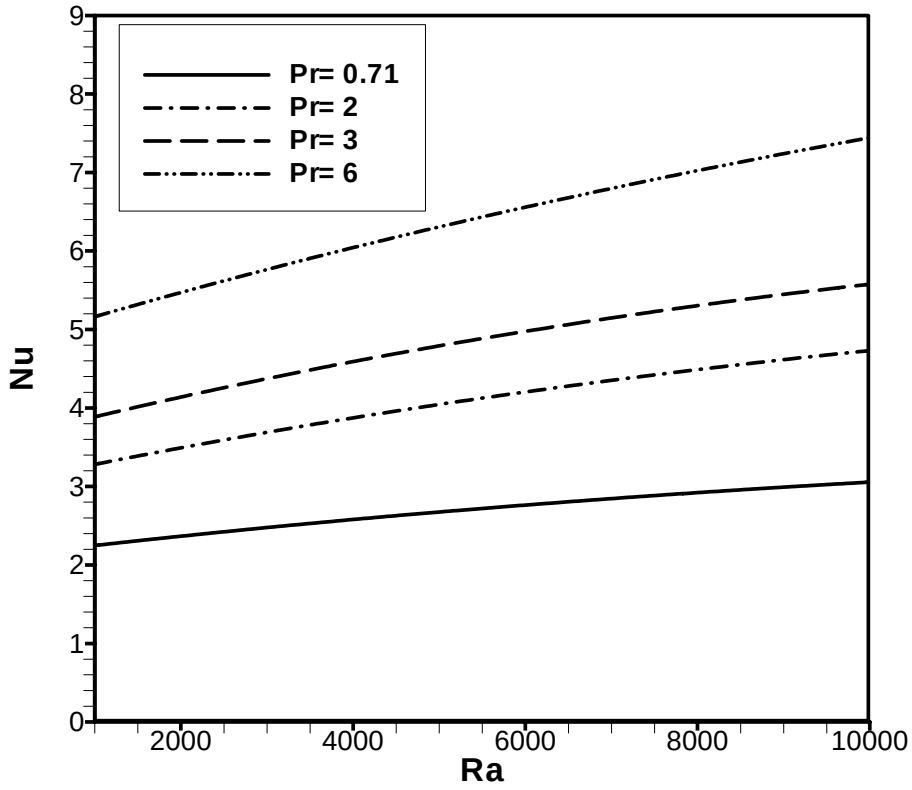

Fig.3.13: Effect of average Nusselt number and Rayleigh number while *Re* = 50.

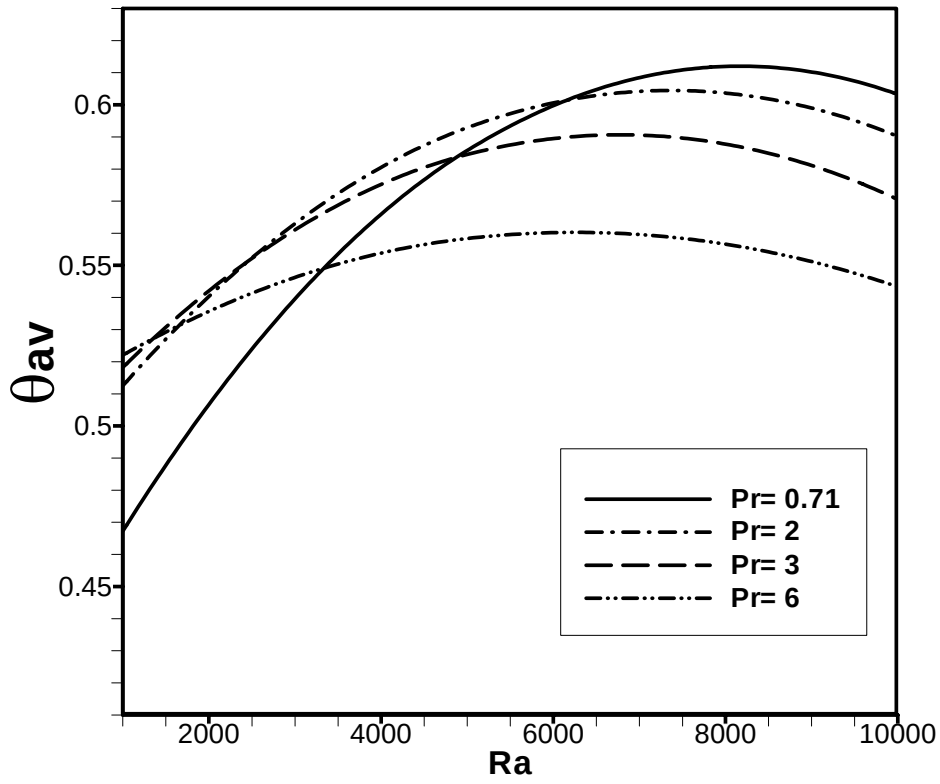

Fig.3.14: Effect of average bulk temperature and Rayleigh number while *Re* = 50.

3.6 CHAPTER SUMMARY

Steady mixed convection flow and heat transfer in a triangular cavity whose left wall is moving and a heat-conducting horizontal bottom wall under laminar regime were numerically investigated. A finite element method for steady-state incompressible mixed convection flow is presented. A detailed analysis of the distribution of streamlines, isotherms, average Nusselt numbers at the heated surface and average bulk temperature in the triangular cavity were carried out to investigate the effect of the dimensionless parameters. The investigation is carried out for a number of relevant dimensionless groups, namely Rayleigh number *Ra*, Hartmann number *Ha*, Reynolds number *Re*, and Prandtl numbers *Pr*. From an examination of heat transfer and fluid flow phenomena revealed by the numerical experiments, the following major conclusions were drawn

- Interesting behavior of the flow and thermal fields with varying Reynolds number is observed. In addition, the numerical solutions indicate that the increasing values of *Re* leads to higher heat transfer rate from the heat source but other side the average bulk temperature decline significantly.
- As *Ra* escalates the value of the magnitude of the stream function is ψ and the cells become larger in size, become more attested to the boundary wall.
- The impact of Prandtl number on the flow and thermal fields in the cavity is found to be more pronounced, if *Re* is kept fixed. The maximum heat transfer is experimented at the highest value of *Pr* for the considered value of *Ra*.
- The average bulk temperature is high for $Pr = 0.71$ in free convection region.
- Thermal boundary layer thickness is thinner for increasing of Rayleigh number because slowly the conductive heat transfer turns into convective heat transfer.
- Various vortices entering into the flow field and a secondary vortex at the inclined and bottom wall of the cavity is seen in the streamlines.

CHAPTER 4
FINITE ELEMENT ANALYSIS ON MAGNETO-HYDRODYNAMIC MIXED CONVECTION FLOW IN A TRIANGULAR ENCLOSURE

4.1 MATHEMATICAL MODELLING

Buoyancy driven flow of an electrically conducting fluid inside a enclosure is analogue to Rayleigh-Benard multi-cellular convective transport phenomenon This chapter describes the MHD effect on mixed convection in a triangular cavity. Numerical solutions are obtained over a wide range of non-dimensional parameters i.e. Hartmann number (*Ha*), Reynolds number (*Re*), Rayleigh number (*Ra*), Prandtl number (*Pr*), and various physical parameters i.e. locations of inlet and outlet opening in the cavity, and aspect ratio of the cavity. Parametric results are presented in terms streamlines and isothermal lines. As the heat transfer at the heated wall depends upon a number of factors, a dimensional analysis is presented to show the importance of non-dimensional parameters which will influence the heat transfer parameter, i.e. Nusselt number. Average temperature in the cavity for all the cases is also presented.

4.2 PHYSICAL MODEL

The physical model considered here is shown in Fig. 4.1, along with the important geometric parameters. The heat transfer and the fluid flow in a two-dimensional triangular cavity with MHD flow whose left wall and bottom wall are subjected to cold T_c and hot T_h temperatures respectively while the inclined walls are kept adiabatic. The fluid was assumed with Prandtl number (*Pr* = 0.71, 2.0, 3.0, 6.0), Reynolds number *(Re* = 40-100), Hartmann number (*Ha* = 5-50) and Newtonian, and the fluid flow is considered to be laminar. The properties of the fluid were assumed to be constant.

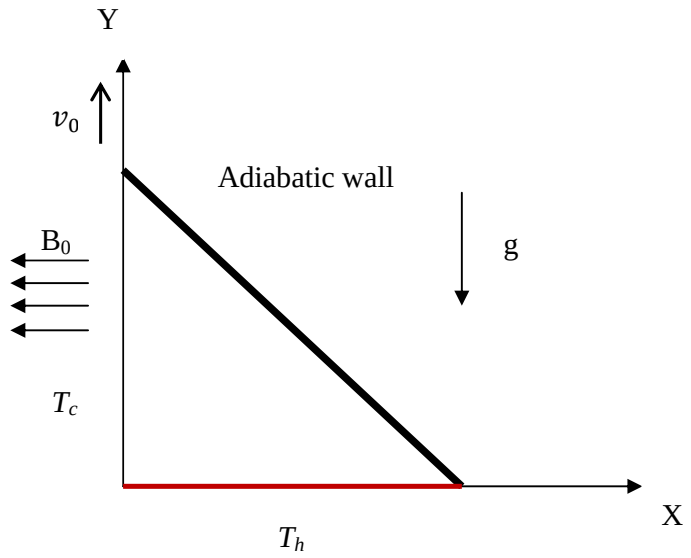

Figure-4.1: Schematic diagram of the physical system

4.3 MATHEMATICAL FORMULATION

The several steps of the mathematical formulation for the above physical configurations are shown as follows

4.3.1 GOVERNING EQUATIONS

The fundamental laws used to solve the fluid flow and heat transfer problems are the conservation of mass (continuity equations), conservation of momentums (momentum equations), and conservation of energy (energy equations), which constitute a set of coupled, nonlinear, partial differential equations. For laminar incompressible thermal flow, the buoyancy force is included here as a body force in the *v*-momentum equation. The governing equations for the two-dimensional steady flow after invoking the Boussinesq approximation and neglecting radiation and viscous dissipation can be expressed as

Continuity Equation

$$\frac{\partial u}{\partial x}+\frac{\partial v}{\partial y}=0 \qquad (4.1)$$

Momentum Equations

$$u\frac{\partial u}{\partial x}+v\frac{\partial u}{\partial y}=-\frac{1}{\rho}\frac{\partial p}{\partial x}+\upsilon\left(\frac{\partial^2 u}{\partial x^2}+\frac{\partial^2 u}{\partial y^2}\right) \tag{4.2}$$

$$u\frac{\partial v}{\partial x}+v\frac{\partial v}{\partial y}=-\frac{1}{\rho}\frac{\partial p}{\partial y}+\nu(\frac{\partial^2 v}{\partial x^2}+\frac{\partial^2 v}{\partial y^2})+g\beta(T-T_c)-\frac{\sigma B_0^2 v}{\rho} \tag{4.3}$$

Energy Equations

$$u\frac{\partial T}{\partial x}+v\frac{\partial T}{\partial y}=\frac{k}{\rho c_p}\left(\frac{\partial^2 T}{\partial x^2}+\frac{\partial^2 T}{\partial y^2}\right) \tag{4.4}$$

where x and y are the distances measured along the horizontal and vertical directions respectively; u and v are the velocity components in the x and y directions respectively; T denote the fluid temperature, T_c denotes the reference temperature for which buoyant force vanishes, p is the pressure and ρ is the fluid density, g is the gravitational constant, β is the volumetric coefficient of thermal expansion, c_p is the fluid specific heat, k is the thermal conductivity of fluid.

4.3.2 BOUNDARY CONDITIONS

The boundary conditions for the present problem are specified as follows:

At the cool left vertical wall: $u(0,y)=0, v(0,y)=v_0,\ T=T_c$

At the bottom wall: $u(x,0)=0=v(x,0),\ T=T_h$

At the inclined wall: $u(x,y)=0=v(x,y), \dfrac{\partial T}{\partial n}=0$

Where n is the non-dimensional distances either along x or y direction acting normal to the surface and k is the thermal conductivity of the fluid.

The local Nusselt number at the heated surface of the cavity which is defined by the following expression:

$$Nu_l=-\frac{h(x)L}{k}$$

Such local values have been further averaged over the entire heated surface to obtain the surface averaged or overall mean Nusselt number

$$Nu = \int_0^L Nu_l dx$$

Where L and $h(x)$ are the length and the local convection heat transfer coefficient of the heated wall respectively. The average Nusselt number can be used in process engineering design calculations to estimate the rate transfer from the heated surface.

4.3.3 DIMENSIONAL ANALYSIS

Non-dimensional variables are used for making the governing equations (4.1−4.4) into dimensionless form are stated as follows:

$$X = \frac{x}{L}, Y = \frac{y}{L}, U = \frac{u}{v_0}, V = \frac{v}{v_0}, P = \frac{p}{\rho v_0^2}, \theta = \frac{(T - T_c)}{(T_h - T_c)}$$

Where X and Y are the coordinates varying along horizontal and vertical directions, respectively, U and V are the velocity components in the X and Y directions, respectively, θ is the dimensionless temperature and P is the dimensionless pressure. After substitution the dimensionless variables into the equations (4.1 - 4.4), we get the following dimensionless equations as

Continuity Equation

$$\frac{\partial U}{\partial X} + \frac{\partial V}{\partial Y} = 0 \tag{4.5}$$

Momentum Equations

$$U\frac{\partial U}{\partial X} + V\frac{\partial U}{\partial Y} = -\frac{\partial P}{\partial X} + \frac{1}{Re}\left(\frac{\partial^2 U}{\partial X^2} + \frac{\partial^2 U}{\partial Y^2}\right) \tag{4.6}$$

$$U\frac{\partial U}{\partial X} + V\frac{\partial U}{\partial Y} = -\frac{\partial P}{\partial Y} + \frac{1}{Re}\left(\frac{\partial^2 V}{\partial X^2} + \frac{\partial^2 V}{\partial Y^2}\right) + Ra\,Pr\,\theta - \frac{Ha^2}{Re}V \tag{4.7}$$

Energy Equations

$$U\frac{\partial\theta}{\partial X}+V\frac{\partial\theta}{\partial Y}=\frac{1}{Re\,Pr}\left(\frac{\partial^2\theta}{\partial X^2}+\frac{\partial^2\theta}{\partial Y^2}\right) \tag{4.8}$$

The dimensionless parameters appearing in the equations (4.5) through (4.8) are the Reynolds number *Re*, Grashof number *Gr*, Prandtl number *Pr* and Rayleigh number *Ra*. They are respectively defined as follows:

$$Re=\frac{u_i L}{\nu},Pr=\frac{\nu}{\alpha},Gr=\frac{\beta g\Delta TL^3}{\nu^2},Ha^2=\frac{\sigma B_0^2 L^2}{\mu},Ra=Gr\times Pr$$

where $\Delta T=T_h-T_c and\alpha=\frac{\kappa}{\rho C_p}$ are the temperature difference and thermal diffusivity of the fluid respectively.

4.3.4 NON-DIMENSIONAL BOUNDARY CONDITIONS

The dimensionless boundary conditions under consideration can be written as:

At the left vertical wall: *U*=0, *V*=1, $\theta=0$

At the bottom wall: *U*=0, *V*=0, $\theta=1$

At the inclined wall: *U*=0, *V*=0, $\frac{\partial\theta}{\partial N}=0$

Where *N* is the non-dimensional distances either along *X* or *Y* direction acting normal to the surface and *K* is the dimensionless thermal conductivity. According to Singh and Sharif (2003), the average Nusselt number at the heated wall of the cavity based on the non-dimensional variables may be expressed as $Nu=\int_0^1\left(\frac{\partial\theta}{\partial Y}\right)_{y=0}dX$ and the bulk average temperature defined as $\theta_{av}=\int\theta\,d\overline{V}/\overline{V}$, where $\overline{V}$ is the cavity volume.

4.4 NUMERICAL ANALYSIS

The governing equations along with the boundary conditions are solved numerically, employing Galerkin weighted residual finite element techniques discussed below.

4.4.1 FINITE ELEMENT FORMULATION

To derive the finite element equations, the method of weighted residuals Zienkiewicz (1991) is applied to the equations (4.5) – (4.8) as

$$\int_A N_\alpha \left(\frac{\partial U}{\partial X} + \frac{\partial V}{\partial Y} \right) dA = 0 \tag{4.9}$$

$$\int_A N_\alpha \left(U \frac{\partial U}{\partial X} + V \frac{\partial U}{\partial Y} \right) dA = -\int_A H_\lambda \left(\frac{\partial P}{\partial X} \right) dA + \frac{1}{Re} \int_A N_\alpha \left(\frac{\partial^2 U}{\partial X^2} + \frac{\partial^2 U}{\partial Y^2} \right) dA \tag{4.10}$$

$$\begin{aligned} &\int_A N_\alpha (U \frac{\partial V}{\partial X} + V \frac{\partial V}{\partial Y}) dA = -\int_A H_\lambda (\frac{\partial P}{\partial Y}) dA + \\ &\frac{1}{Re} \int_A N_\alpha (\frac{\partial^2 V}{\partial X^2} + \frac{\partial^2 V}{\partial Y^2}) dA + Ra\, Pr \int_A N_\alpha \theta dA - \frac{Ha^2}{Re} \int_A N_\alpha V dA \end{aligned} \tag{4.11}$$

$$\int_A N_\alpha \left(U \frac{\partial \theta}{\partial X} + V \frac{\partial \theta}{\partial Y} \right) dA = \frac{1}{Re\, Pr} \int_A N_\alpha \left(\frac{\partial^2 \theta}{\partial X^2} + \frac{\partial^2 \theta}{\partial Y^2} \right) dA \tag{4.12}$$

Where A is the element area, N_α (α = 1, 2, … … , 6) are the element interpolation functions for the velocity components and the temperature, and H_λ (λ = 1, 2, 3) are the element interpolation functions for the pressure.

Gauss's theorem is then applied to equations (4.10) - (4.12) to generate the boundary integral terms associated with the surface tractions and heat flux. Then equations (4.9) - (4.12) become,

$$\begin{aligned} &\int_A N_\alpha \left(U \frac{\partial U}{\partial X} + V \frac{\partial U}{\partial Y} \right) dA + \int_A H_\lambda \left(\frac{\partial P}{\partial X} \right) dA \\ &\quad + \frac{1}{Re} \int_A \left(\frac{\partial N_\alpha}{\partial X} \frac{\partial U}{\partial X} + \frac{\partial N_\alpha}{\partial Y} \frac{\partial U}{\partial Y} \right) dA = \int_{S_0} N_\alpha S_x dS_0 \end{aligned} \tag{4.13}$$

$$\begin{aligned} &\int_A N_\alpha (U \frac{\partial V}{\partial X} + V \frac{\partial V}{\partial Y}) dA + \int_A H_\lambda (\frac{\partial P}{\partial Y}) dA \\ &+ \frac{1}{Re} \int_A (\frac{\partial N_\alpha}{\partial X} \frac{\partial V}{\partial X} + \frac{\partial N_\alpha}{\partial Y} \frac{\partial V}{\partial Y}) - Ra\, Pr \int_\alpha N_\alpha \theta dA + \frac{Ha^2}{Re} \int_\alpha N_\alpha V dA = \int_{s_{00}} N_\alpha S_y dS_0 \end{aligned} \tag{4.14}$$

$$\int_\alpha N_\alpha (U \frac{\partial \theta}{\partial X} + V \frac{\partial \theta}{\partial Y}) dA + \frac{1}{Re.Pr} \int_\alpha (\frac{\partial N_\alpha}{\partial X} \frac{\partial \theta}{\partial X} + \frac{\partial N_\alpha}{\partial Y} \frac{\partial \theta}{\partial Y}) dA = \int_{S_w} N_\alpha q_{lw} dS_w \tag{4.15}$$

Here (4.13) - (4.14) specifying surface tractions (S_x, S_y) along outflow boundary S_0 and (4.15) specifying velocity components and fluid temperature or heat flux (q_w) that flows into or out from domain along wall boundary S_w.

The basic unknowns for the above differential equations are the velocity components U, V the temperature, θ and the pressure, P. The six node triangular element is used in this work for the development of the finite element equations. All six nodes are associated with velocities as well as temperature; only the corner nodes are associated with pressure. This means that a lower order polynomial is chosen for pressure and which is satisfied through continuity equation. The velocity component and the temperature distributions and linear interpolation for the pressure distribution according to their highest derivative orders in the differential equations (4.9) - (4.12) as

$$U(X,Y) = N_\beta U_\beta \tag{4.16}$$

$$V(X,Y) = N_\beta V_\beta \tag{4.17}$$

$$\theta(X,Y) = N_\beta \theta_\beta \tag{4.18}$$

$$P(X,Y) = H_\lambda P_\lambda \tag{4.19}$$

where $\beta = 1, 2, \ldots \ldots, 6$; $\lambda = 1, 2, 3$.

Substituting the element velocity component distributions, the temperature distribution, and the pressure distribution from equations (3.20) - (3.24), the finite element equations can be written in the form,

$$K_{\alpha\beta^x} U_\beta + K_{\alpha\beta^y} V_\beta = 0 \tag{4.20}$$

$$K_{\alpha\beta\gamma^x} U_\beta U_\gamma + K_{\alpha\beta\gamma^y} V_\gamma U_\gamma + M_{\alpha\mu^x} P_\mu + \frac{1}{Re}\left(S_{\alpha\beta^{xx}} + S_{\alpha\beta^{yy}}\right) U_\beta = Q_{\alpha^u} \tag{4.21}$$

$$K_{\alpha\beta\gamma^x} U_\beta V_\gamma + K_{\alpha\beta\gamma^y} V_\gamma V_\gamma + M_{\alpha\mu^y} P_\mu + \frac{1}{Re}(S_{\alpha\beta^{xx}} + S_{\alpha\beta^{yy}} + Ha^2 K_{\alpha\beta}) V_\beta - Ra\,Pr\,K_{\alpha\beta}\theta_\beta = Q_{\alpha^v} \tag{4.22}$$

$$K_{\alpha\beta\gamma^x} U_\beta \theta_\gamma + K_{\alpha\beta\gamma^y} V_\beta \theta_\gamma + \frac{1}{Re.Pr}\left(S_{\alpha\beta^{xx}} + S_{\alpha\beta^{yy}}\right)\theta_\beta = Q_{\alpha\theta} \tag{4.23}$$

where the coefficients in element matrices are in the form of the integrals over the element area and along the element edges S_0 and S_w as

$$K_{\alpha\beta^x} = \int_A N_\alpha N_{\beta,x} dA \tag{4.24a}$$

$$K_{\alpha\beta^y} = \int_A N_\alpha N_{\beta,y} dA \tag{4.24b}$$

$$K_{\alpha\beta\gamma^x} = \int_A N_\alpha N_\beta N_{\gamma,x} dA \tag{4.24c}$$

$$K_{\alpha\beta\gamma^y} = \int_A N_\alpha N_\beta N_{\gamma,y} dA \tag{4.24d}$$

$$K_{\alpha\beta} = \int_A N_\alpha N_\beta dA \tag{4.24e}$$

$$S_{\alpha\beta^{xx}} = \int_A N_{\alpha,x} N_{\beta,x} dA \tag{4.24f}$$

$$S_{\alpha\beta^{yy}} = \int_A N_{\alpha,y} N_{\beta,y} dA \tag{4.24g}$$

$$M_{\alpha\mu^x} = \int_A H_\alpha H_{\mu,x} dA \tag{4.24h}$$

$$M_{\alpha\mu^y} = \int_A H_\alpha H_{\mu,y} dA \tag{4.24i}$$

$$Q_{\alpha^u} = \int_{S_0} N_\alpha S_x dS_0 \tag{4.24j}$$

$$Q_{\alpha^v} = \int_{S_0} N_\alpha S_y dS_0 \tag{4.24k}$$

$$Q_{\alpha\theta} = \int_{S_w} N_\alpha \, q_{1w} dS_w \tag{4.24l}$$

$$Q_{\alpha^{\theta s}} = \int_{S_w} N_\alpha \, q_{2w} dS_w \tag{4.24m}$$

These element matrices are evaluated in closed form ready for numerical simulation. Details of the derivation for these element matrices are omitted herein.

The derived finite element equations (4.20) - (4.23) are nonlinear. These nonlinear algebraic equations are solved by applying the Newton-Raphson iteration technique by first writing the unbalanced values from the set of the finite element equations (4.20) - (4.23) as,

$$F_{\alpha^p} = K_{\alpha\beta^x} U_\beta + K_{\alpha\beta^y} V_\beta \tag{4.25a}$$

$$F_{\alpha^u} = K_{\alpha\beta\gamma^x} U_\beta U_\gamma + K_{\alpha\beta\gamma^y} V_\gamma U_\gamma + M_{\alpha\mu^x} P_\mu + \frac{1}{Re}(S_{\alpha\beta^{xx}} + S_{\alpha\beta^{yy}})U_\beta - Q_{\alpha^u} \quad (4.25b)$$

$$F_{\alpha^v} = K_{\alpha\beta\gamma^x} U_\beta V_\gamma + K_{\alpha\beta\gamma^y} V_\gamma V_\gamma + M_{\alpha\mu^y} P_\mu + \frac{1}{Re}(S_{\alpha\beta^{xx}} + S_{\alpha\beta^{yy}} + Ha^2 K_{\alpha\beta})V_\beta - Ra\,Pr\,K_{\alpha\beta}\theta_\beta - Q_{\alpha^\theta} \quad (4.25c)$$

$$F_{\alpha^\theta} = K_{\alpha\beta\gamma^x} U_\beta \theta_\gamma + K_{\alpha\beta\gamma^y} V_\beta \theta_\gamma + \frac{1}{Re.Pr}\left(S_{\alpha\beta^{xx}} + S_{\alpha\beta^{yy}}\right)\theta_\beta - Q_{\alpha^\theta} \quad (4.25d)$$

This leads to a set of algebraic equations with the incremental unknowns of the element nodal velocity components, temperatures, and pressures in the form,

$$\begin{bmatrix} K_{pu} & K_{pv} & 0 & 0 \\ K_{uu} & K_{uv} & 0 & K_{up} \\ K_{\theta u} & K_{\theta v} & K_{\theta\theta} & 0 \\ K_{vu} & K_{vv} & K_{v\theta} & K_{vp} \end{bmatrix} \begin{bmatrix} \Delta p \\ \Delta u \\ \Delta\theta \\ \Delta v \end{bmatrix} = -\begin{bmatrix} F_\alpha p \\ F_\alpha u \\ F_\alpha \theta \\ F_\alpha v \end{bmatrix} \quad (4.26)$$

where $K_{uu} = K_{\alpha\beta\gamma^x} U_\beta + K_{\alpha\gamma\beta^x} U_\gamma + K_{\alpha\beta\gamma^y} V_\beta + \frac{1}{Re}\left(S_{\alpha\beta^{xx}} + S_{\alpha\beta^{yy}}\right)$

$K_{uv} = K_{\alpha\beta\gamma^y} U\gamma$

$K_{u\theta} = 0$, $K_{up} = M_{\alpha\mu^x}$

$K_{vu} = K_{\alpha\beta\gamma^x} V\gamma$

$K_{vv} = K_{\alpha\beta\gamma^x} U_\gamma + K_{\alpha\beta\gamma^y} V_\gamma + K_{\alpha\beta\gamma^y} V_\gamma + \frac{1}{Re}(S_{\alpha\beta^{xx}} + S_{\alpha\beta^{yy}} + Ha^2 K_{\alpha\beta})$

$K_{v\theta} = -Ra\,Pr\,K_{\alpha\beta}$, $K_{vp} = M_{\alpha\mu^y}$

$K_{\theta u} = K_{\alpha\beta\gamma^x}\theta\gamma$, $K_{\theta v} = K_{\alpha\beta\gamma^y}\theta\gamma$

$K_{\theta\theta} = K_{\alpha\beta\gamma^x} U_\beta + K_{\alpha\beta\gamma^y} V_\beta + \frac{1}{Re.Pr}(S_{\alpha\beta^{xx}} + S_{\alpha\beta^{yy}})$

$K_{\theta p} = 0$,

$K_{pu} = K_{\alpha\beta^x}$, $K_{pv} = K_{\alpha\beta^y}$ and $K_{p\theta} = 0 = K_{pp}$

The iteration process is terminated if the percentage of the overall change compared to the previous iteration is less than the specified value.

To solve the sets of the global nonlinear algebraic equations in the form of matrix, the Newton-Raphson iteration technique has been adapted through PDE solver with MATLAB interface. The convergence of solutions is assumed when the relative error for each variable between consecutive iterations is recorded below the convergence criterion ε such that $\left|\Psi^{n+1} - \Psi^{n}\right| < \varepsilon$, where n is number of iteration and $\Psi = U, V, \theta$. The convergence criterion was set to $\varepsilon = 10^{-4}$.

4.4.2 GRID INDEPENDENCE TEST

Test for the accuracy of grid fineness has been carried out to find out the optimum grid number.

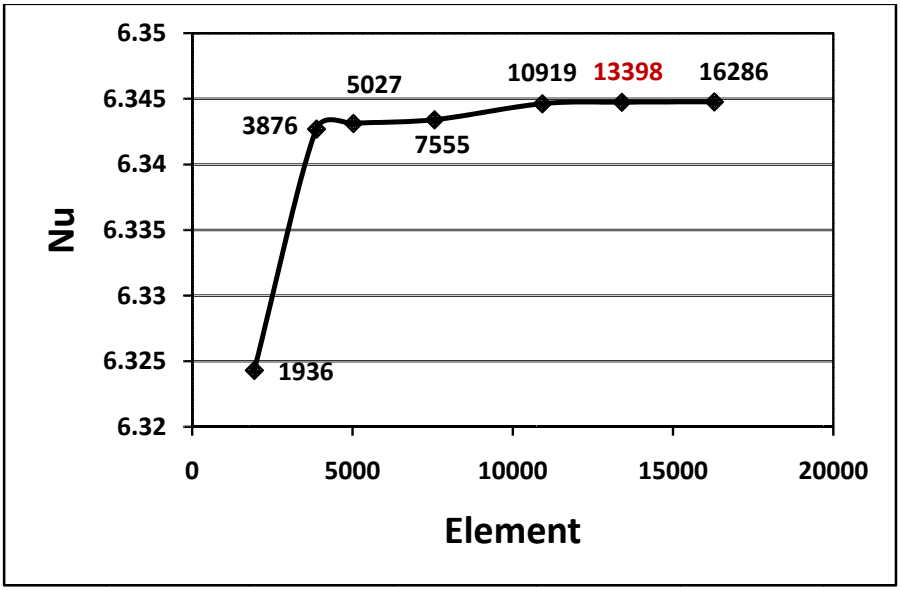

Figure 4.2: Convergence of average Nusselt number with grid refinement for *Pr* = 0.71, *Re* = 50, *Ha* = 20 and *Ra* = 10^4.

In order to obtain grid independent solution, a grid refinement study is performed for a square open cavity with *Pr* = 0.71, *Re* = 50 and *Ra* = 10^4. Figure 3.2 shows the convergence of the average Nusselt number, Nu_{av} at the heated surface with grid refinement. It is observed that grid independence is achieved with 13398 elements where

there is insignificant change in Nu with further increase of mesh elements. Six different non-uniform grids with the following number of nodes and elements were considered for the grid refinement tests: 11616 nodes, 1936 elements; 23256 nodes, 3876 elements; 30162 nodes, 5027 elements; 45330 nodes, 7555 elements; 65514 nodes, 10919 elements; 80388 nodes, 13398 elements, 97716 nodes, 16286 elements. From these values, 80388 nodes, 13398 elements can be chosen throughout the simulation to optimize the relation between the accuracy required and the computing time.

Nodes (Elements)	11616 (1936)	23256 (3876)	30162 (5027)	45330 (7555)	65514 (10919)	80388 (13398)	97716 (16286)
Nu	6.324303	6.342699	6.343124	6.3434096	6.3446291	6.344772	6.3447712
Time (s)	15.422	30.562 s	39.062 s	63.312 s	118.578	159.563	190.016

Table 4.1: Grid Sensitivity Check at $Pr = 0.71$, $Re = 50$, $Ha = 20$ *and* $Ra = 10^4$.

4.5 RESULTS AND DISCUSSION

The MHD mixed convection flow and temperature fields as well as heat transfer rates and bulk temperature of the fluid inside the triangular cavity has been numerically investigated. The MHD mixed convection phenomenon inside the enclosure is strongly influenced by governing as well as physical parameters, namely and Hartman number *Ha*, Reynolds number *Re*, Prandtl number *Pr*, Rayleigh number *Ra*. As the nature of flow and thermo physical properties of fluid strongly influenced on the heat transfer rate, and the numerical computation were performed for a range of *Ha*, *Re* and *Pr* (*Ha* = 5 - 50, *Re* = 40 - 100, *Pr* = 0.71 - 6). In addition, for each value of mentioned parameters, computations are performed at $Ra = 5 \times 10^3$ that focuses on pure mixed convection. Moreover, the results of this study have been presented in terms of streamlines and isotherms. Furthermore, the heat transfer effectiveness of the enclosure is displayed in terms of average Nusselt number *Nu* and the dimensionless average bulk temperature θ_{av}.

4.5.1 EFFECTS OF HARTMAN NUMBER

The special effects of Hartmann number *Ha* on the flow and thermal fields at $Ra = 10^3$ to 10^4 is illustrate in Figure 4.3 - 4.6, while *Pr* = 0.71 and *Re* = 50 were kept fixed. In this folder, the size of the counter clockwise vortex also decreases sharply with increasing of *Ha*. This is because application of a slanting magnetic field has the propensity to slow down the movement of the buoyancy induced flow in the cavity. The effects of Hartmann number *Ha* on isotherms are shown in the Figure 4.3 - 4.6 while *Re* = 50 and *Pr* = 0.71 are kept fixed. It is observed that the higher values isotherms are more tightened at the vicinity of the heated wall of the cavity for the considered value of *Ra*. A similar trend is found for the higher values of *Ha*. From this figure it can easily be seen that isotherms are almost parallel at the vicinity of the bottom horizontal hot wall but it changes to parabolic shape with the increasing distance from inclined wall for the highest value of *Ha* (= 20.0) at *Pr* = 0.71, which indicate that most of the heat transfer process is carried out by conduction. In addition, it is noticed that the isothermal layer near the heated surface becomes slightly thin with the decreasing *Ha*. However in the remaining area near the left wall of the cavity, the temperature gradients are small in order to mechanically driven circulations.

The effects of *Ha* on average Nusselt number *Nu* at the heated surface and average bulk temperature θ_{av} in the cavity is illustrated in Fig. 4.7 & 4.8 with *Re* = 50 and *Pr* = 0.71. From this figure, it is found that the average Nusselt number *Nu* decreases with increasing *Pr*. It is to be highlighted that the highest heat transfer rate occurs for the lowest values of *Ha* (= 5). The average bulk temperature of the fluid in the cavity is high for higher values of *Ha* (10 - 50). It is to be mentioned here that the highest average temperature is documented for the higher value of *Ha* in the free convection dominated region.

Table 4.2: Average Nusselt numbers for different Hartmann number while *Ha* = 5, 10, 20, 50, *Re* = 50 and *Pr* = 0.71.

Nu_{av}			
Ha	$Ra = 10^3$	$Ra = 5\times10^3$	$Ra = 10^4$
5	4.38836694	6.434903	5.764501
10	4.36317068	6.413537	5.805674
20	4.26278628	6.331658	5.913316
50	3.79764503	5.890227	5.878074

Table 4.3: Average Bulk temperature for different Hartmann number while *Ha* = 5, 10, 20, 50, *Re* = 50 and *Pr* = 0.71.

θ_{av}			
Ha	$Ra = 10^3$	$Ra = 5\times10^3$	$Ra = 10^4$
5	0.593528	0.566768	0.57386
10	0.593913	0.567008	0.570757
20	0.598198	0.568812	0.561785
50	0.633216	0.585029	0.533999

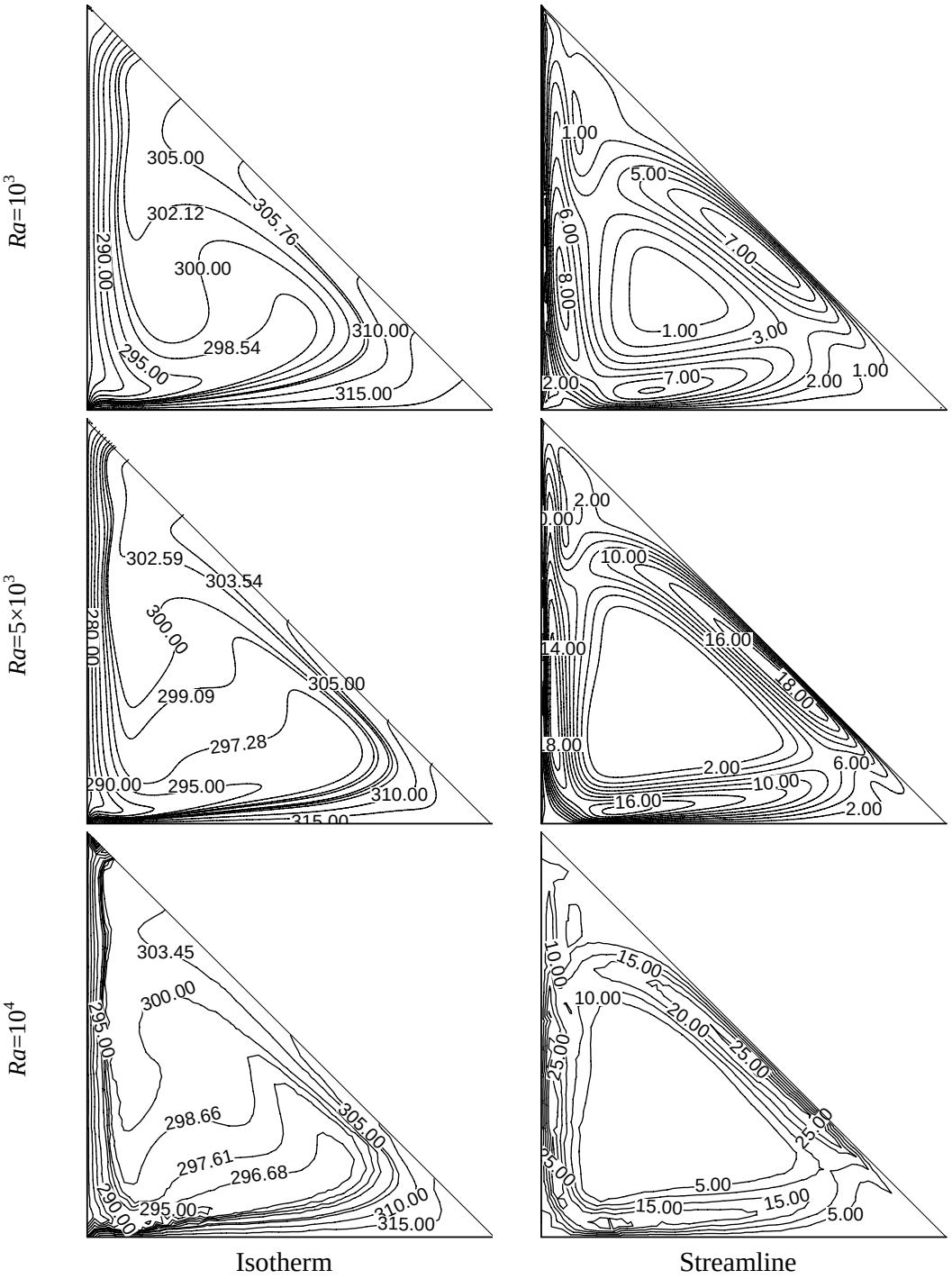

Fig 4.3: Isotherms and streamlines patterns for Re = 50, Pr = 0.71 and Ha = 5

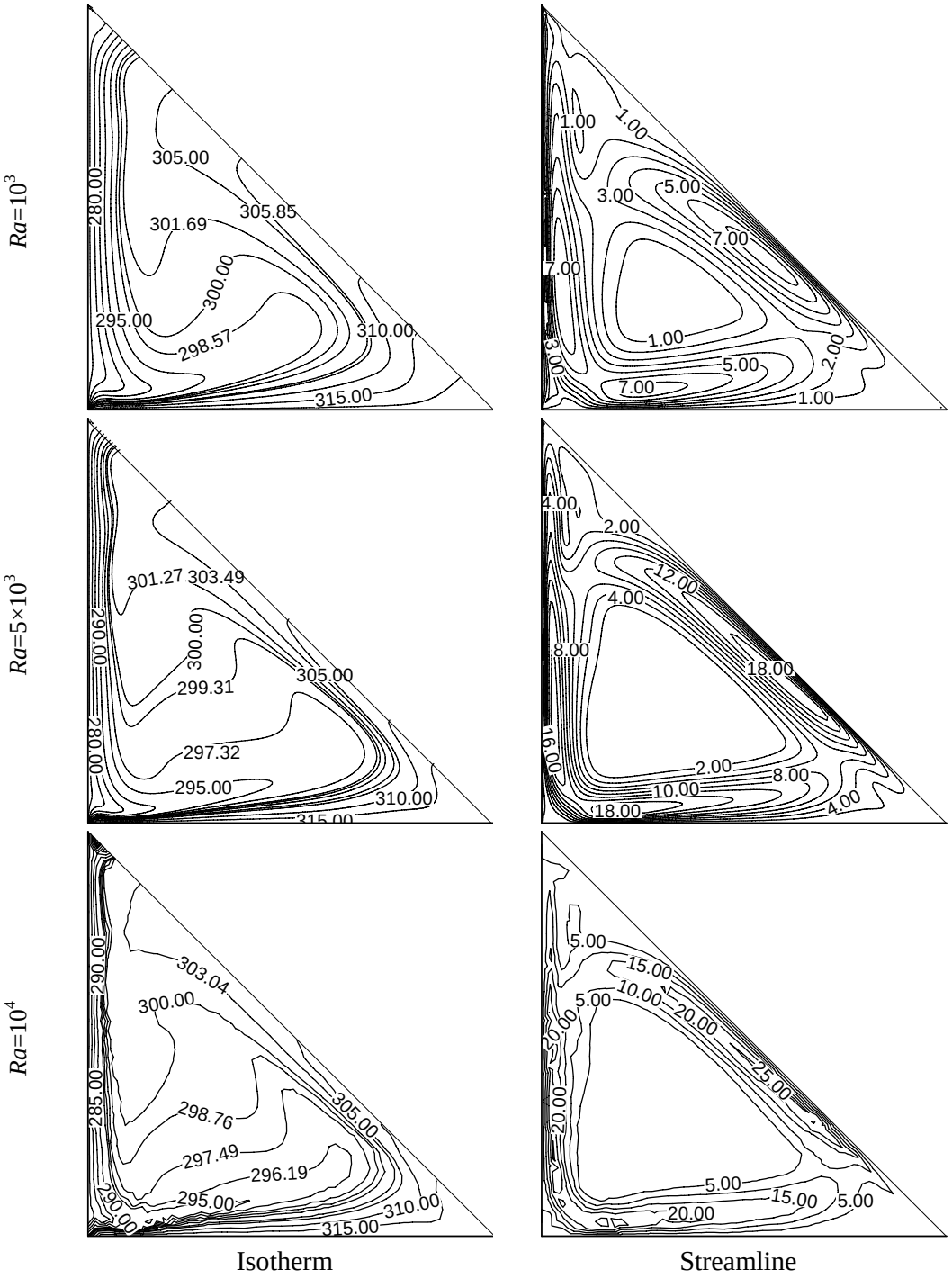

Fig 4.4: Isotherms and streamlines patterns for *Re* = 50, *Pr* = 0.71 *and Ha* = 10

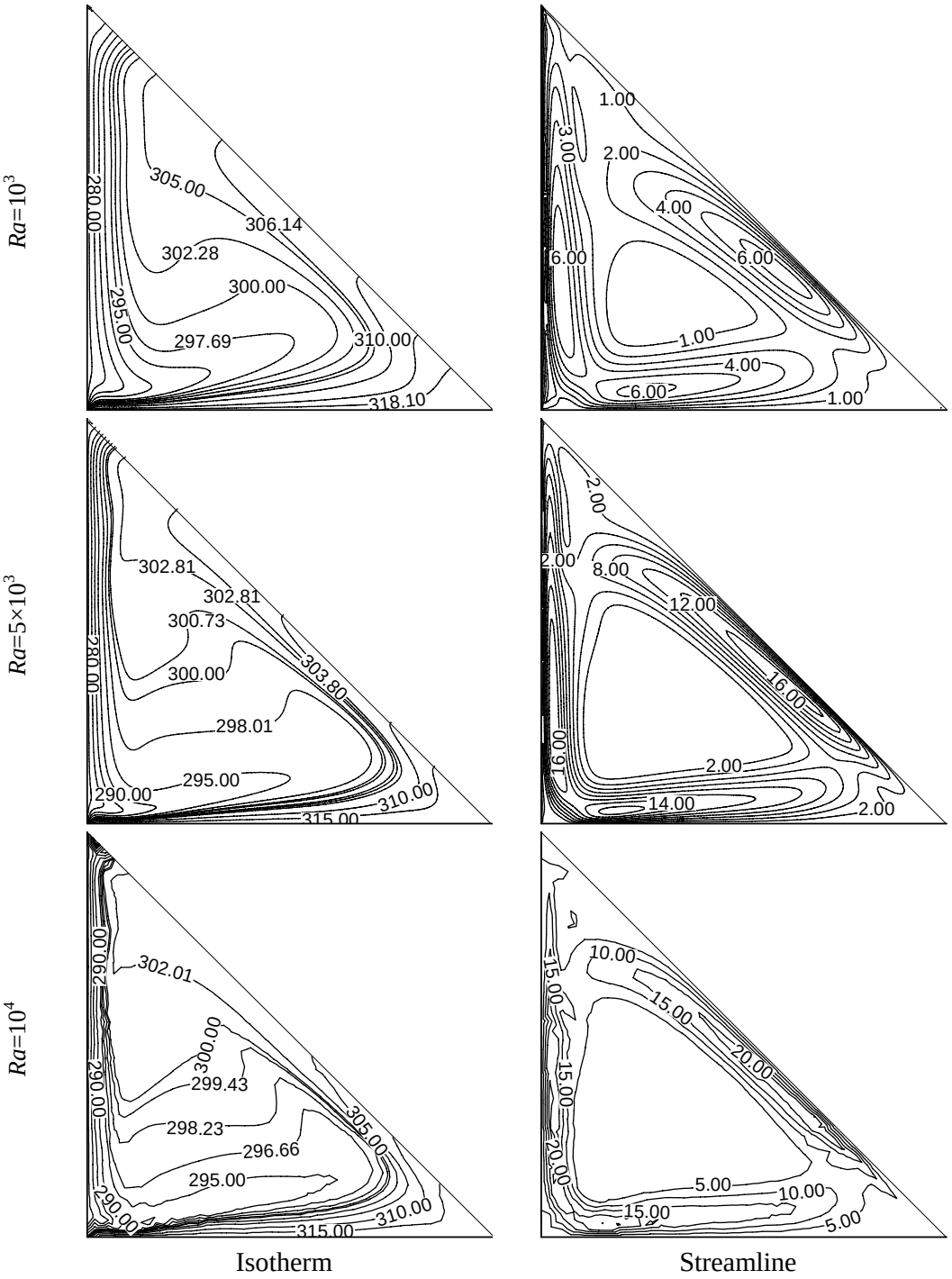

Fig 4.5: Isotherms and streamlines patterns for *Re* = 50, *Pr* = 0.71 and *Ha* = 20

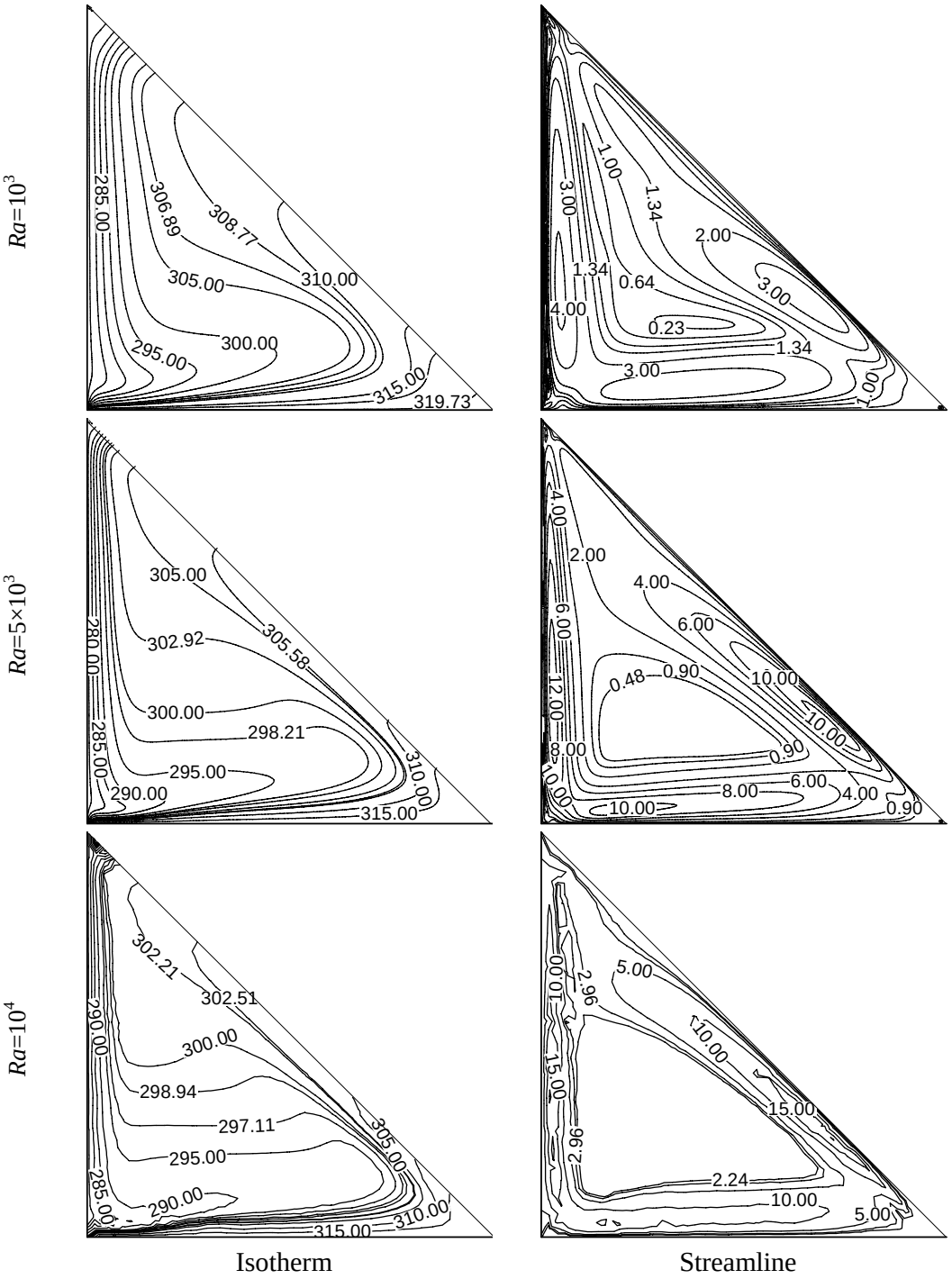

Fig 4.6: Isotherms and streamlines patterns for Re = 50, Pr = 0.71 and Ha = 50

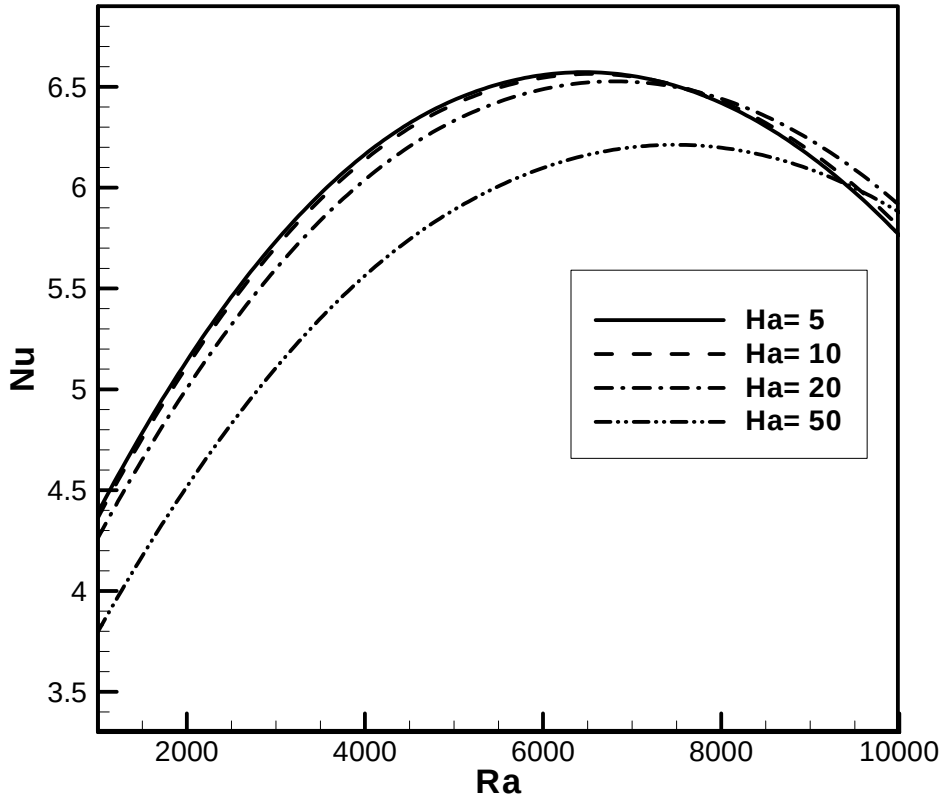

Fig.4.7: Effect of average Nusselt number and Rayleigh number while Pr = 0.71 and Re = 50.

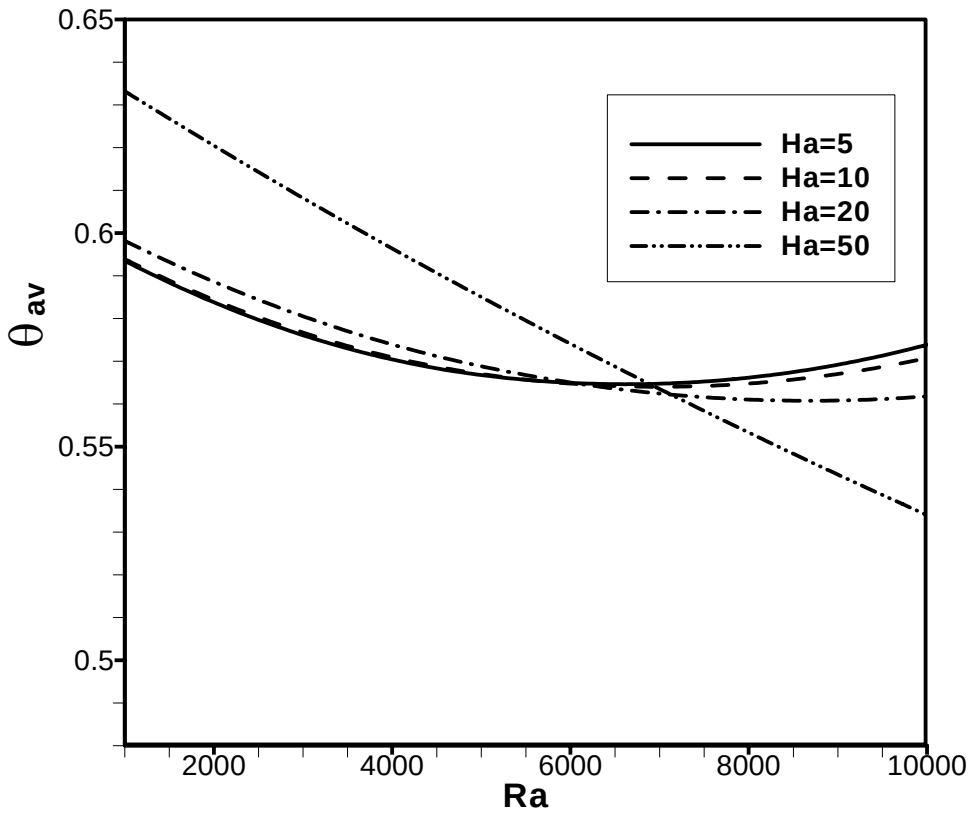

Fig.4.8: Effect of average bulk temperature and Rayleigh number while *Pr* = 0.71 and *Re* = 50.

4.5.2 EFFECTS OF REYNOLDS NUMBER

The effects of Reynolds number on the flow structure and temperature distribution are depicted in Fig. 4.9 - 4.12. The streamlines have been presented for different values of Rayleigh numbers (*Ra),* Reynolds numbers (*Re*) ranging from 10^3 to 10^4 and 40 to 100 respectively while *Pr* = 0.71, and *Ha* = 20. Now at *Re* = 40, the fluid near to the hot (bottom) wall has lower density, so it moves upward while the relatively heavy fluid near to cold (left) wall and this fluid is heated up. Thus the fluid motion completes the circulation. A very small magnitude value of contour rotating cell is observed in the middle part of the cavity as primary vortex. The secondary vortex cells are shown around the primary vortex in the cavity. The secondary vortex are more packed to the respective wall dramatically for the increasing value of *Re* that's imply the flow moves faster and the velocity boundary layer become thinner. Moreover, it is clearly seen that the center vortex become bigger with increasing *Re* due to conduction intensified gradually. The value of the magnitudes of the stream function greater due to mechanically driven circulations.

The corresponding isotherm pattern for different value of Reynolds number while *Pr* = 0.71 and *Ha* = 20 is shown in the Fig. 4.9 - 4.12. From this figure, it is found that the isotherms are more congested at the heated wall of the cavity testifying of the noticeable increase in convective heat exchange. The temperature gradients are very small due to mechanically driven circulations at the left wall of the cavity. It is also noticed that the thermal boundary layer near the heated wall becomes thinner with increasing Re. Due to high circulations, the temperature contours condensed in a very small regime at the upper portion of the left wall and this may cause greater heat transfer rates at the heated wall.

The effects of Reynolds number on average Nusselt number Nu at the heated wall and the average bulk temperature θ_{av} of the fluid in the cavity are illustrated in Fig 4.13 & 4.14, while *Pr* = 0.71, *Ha* = 20. From Fig.4.13, it is seen that the average Nusselt number Nu increases steadily with increasing Rayleigh number. This arises from the fact that physical properties of fluid changes to better heat transfer. For *Re* = 100, it is noticed that the average Nusselt number Nu increases sharply but for lower values of *Re* (= 40) then the increase of Nu befall slower.

Fig. 4.14 displays the variation of the average bulk temperature against the Rayleigh number for various Reynolds numbers. The average temperature decreases smoothly with increase of *Ra*. It is an interesting observation that at lower *Re*, the average bulk temperature is affected by Rayleigh number.

Table 4.4: Average Nusselt numbers for different Reynolds number while *Re* = 40, 50, 70, 100, Pr = 0.71 and *Ha = 20*.

	Nu_{av}		
Re	$Ra = 10^3$	$Ra = 5\times10^3$	$Ra = 10^4$
40	3.864211	5.703775	6.750194
50	4.262786	6.331658	7.510701
70	4.972487	7.448734	8.86882
100	5.910879	8.937115	10.676461

Table 4.5: Average Bulk temperature for different Reynolds number while *Re* = 40, 50, 70, 100, *Pr* = 0.71 and *Ha = 20*.

	θ_{av}		
Re	$Ra = 10^3$	$Ra = 5\times10^3$	$Ra = 10^4$
40	0.602588	0.57354	0.563087
50	0.598198	0.568812	0.558697
70	0.591386	0.562046	0.552434
100	0.584332	0.555258	0.546148

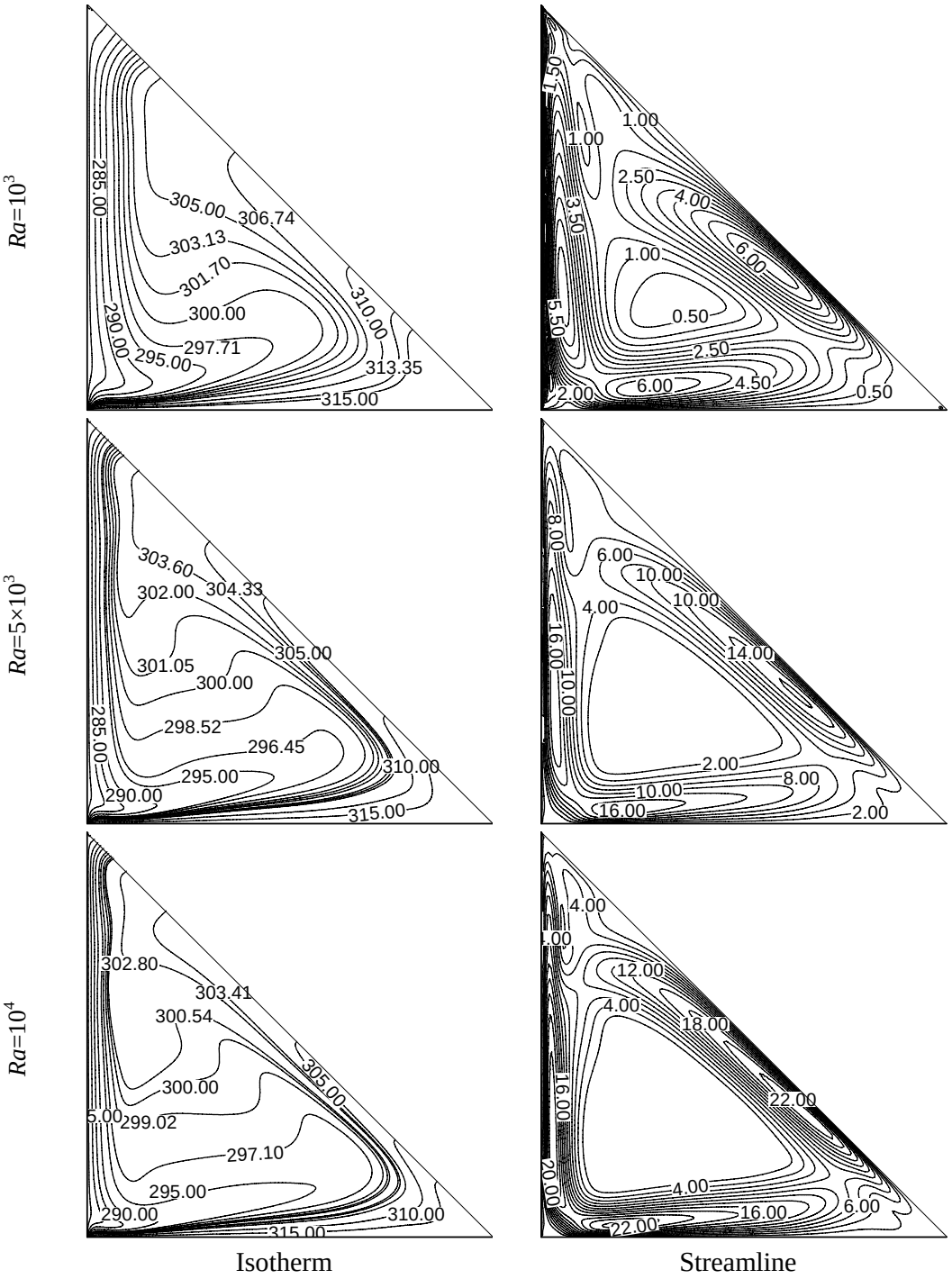

Fig 4.9: Isotherms and streamlines patterns for Re = 40, Pr = 0.71, and Ha = 20

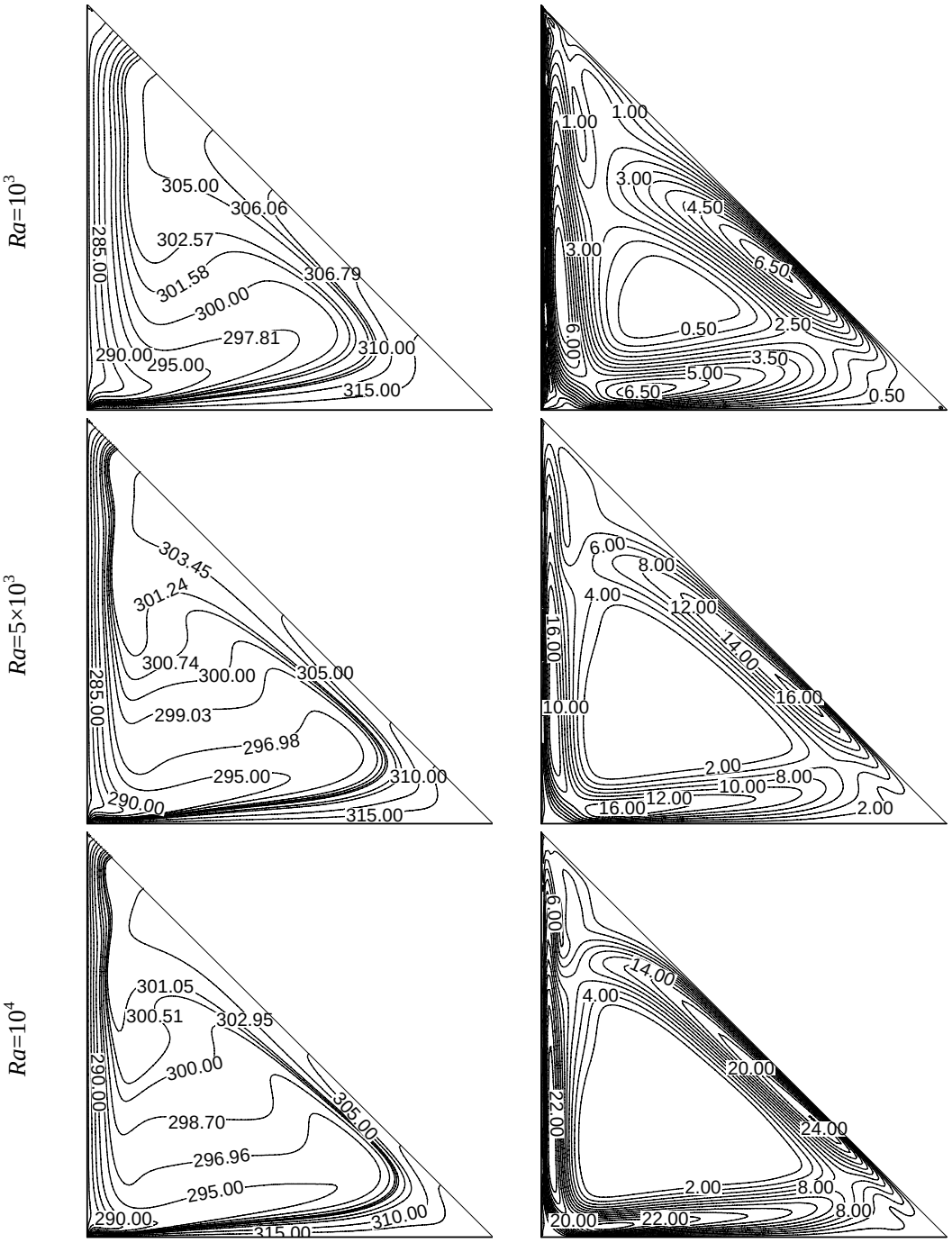

Fig 4.10: Isotherms and streamlines patterns for *Re* = 50, *Pr* = 0.71 *and Ha* = 20

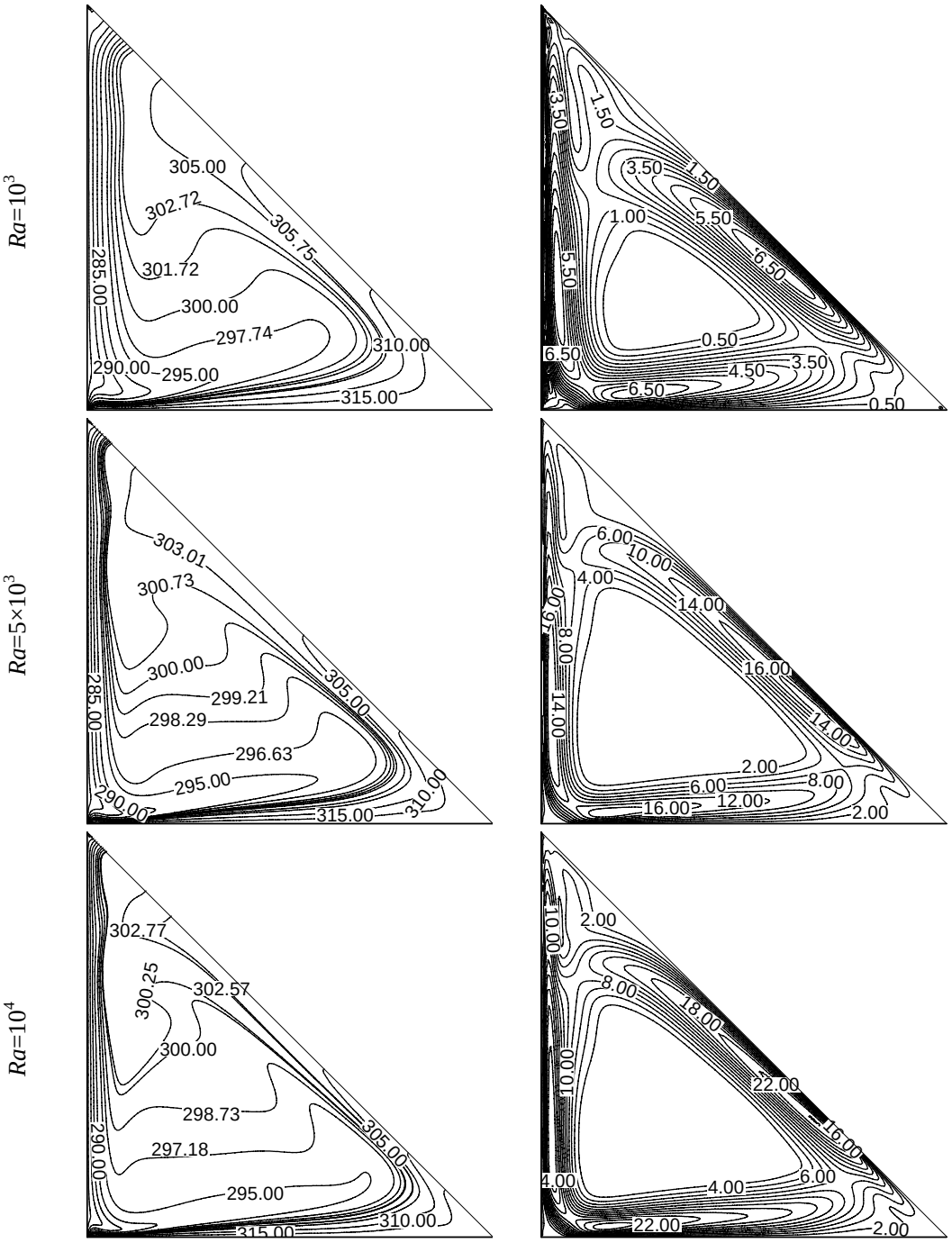

Fig 4.11: Isotherms and streamlines patterns for *Re* = 70, *Pr* = 0.71 and *Ha* = 20

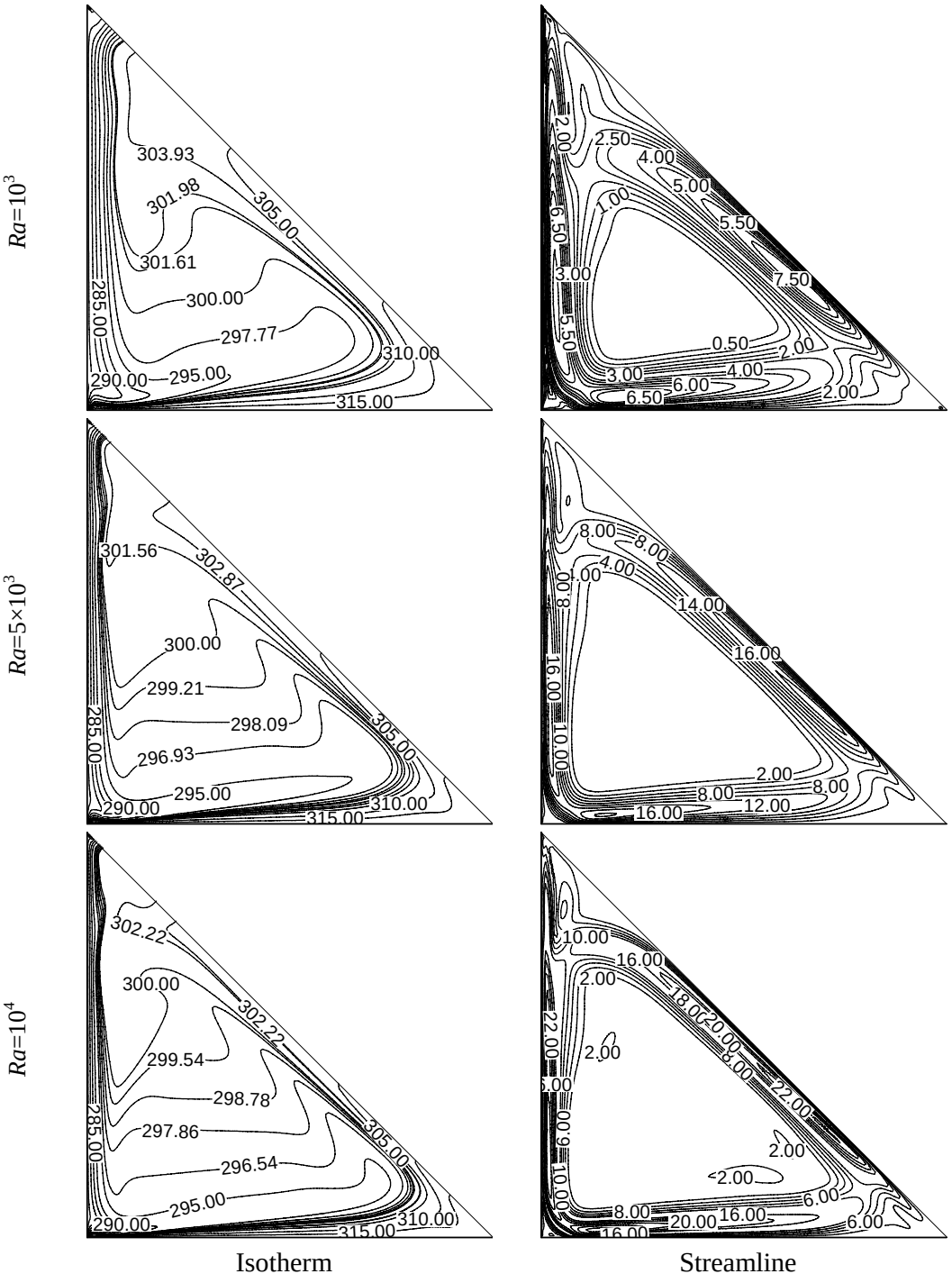

Fig 4.12: Isotherms and streamlines patterns for *Re* = 100, *Pr* = 0.71 and *Ha* = 20

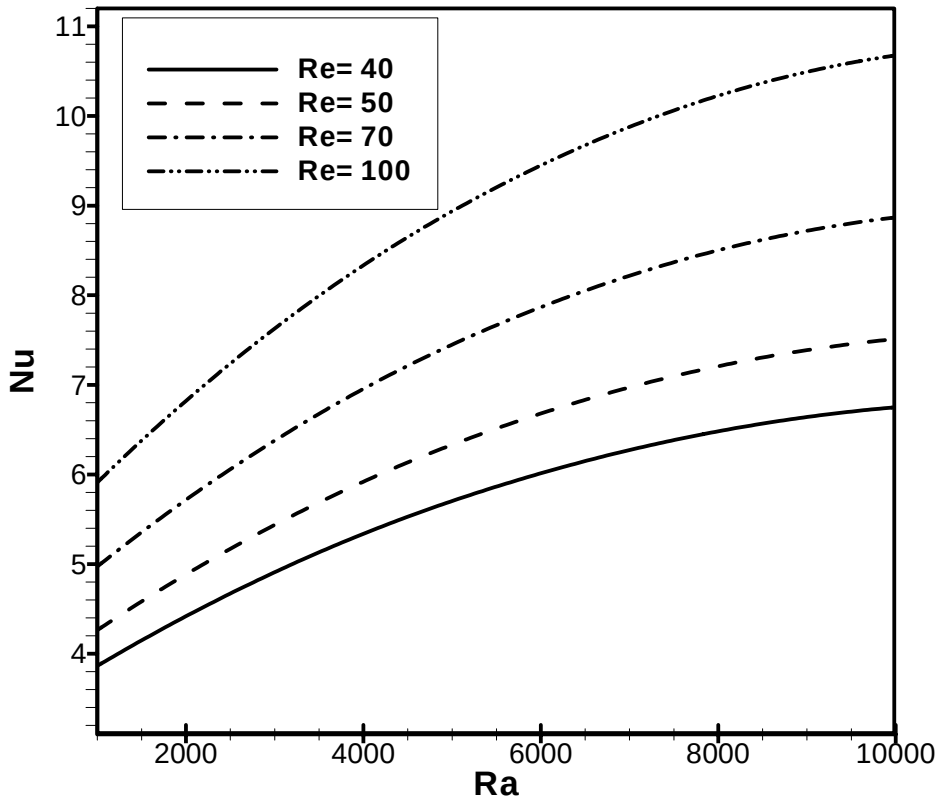

Fig.4.13: Effect of average Nusselt number and Rayleigh number while Pr = 0.71 and Ha = 20.

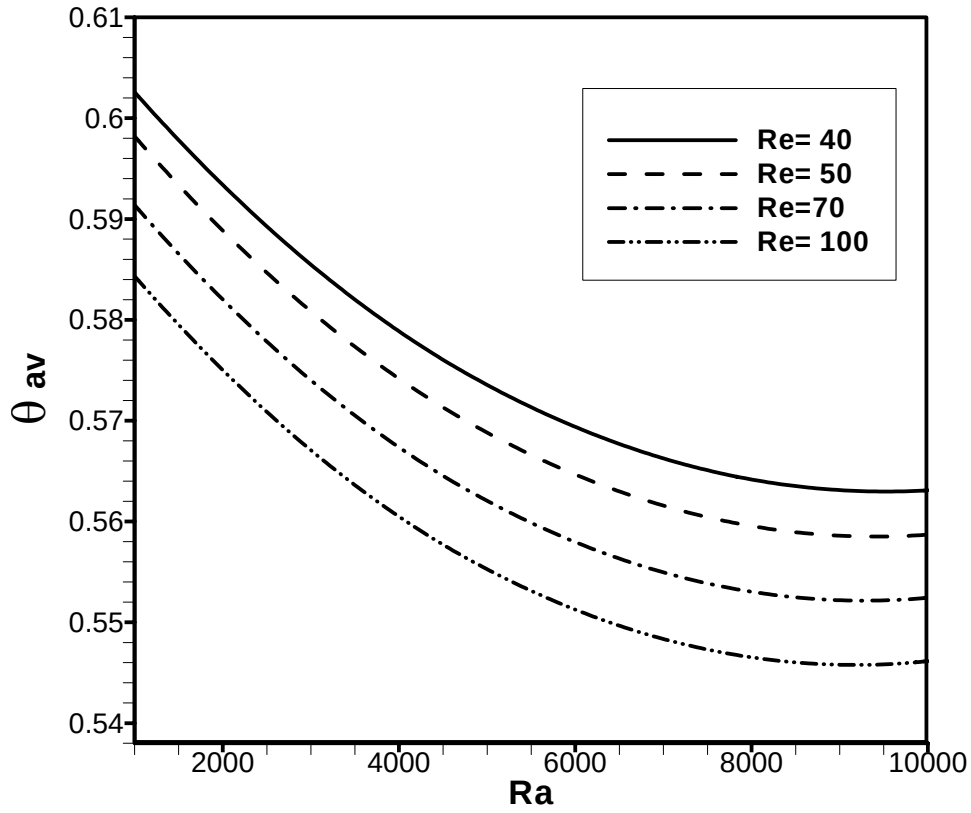

Fig.4.14: Effect of average bulk temperature and Rayleigh number while Pr = 0.71 and Ha = 20.

4.5.3 EFFECTS OF PRANDLT NUMBER

The property of Prandtl number on flow fields for the considered *Ra* is depicted in Fig.4.15 - 4.18, while *Re* = 50 and *Ha* = 20 were kept fixed. Now from the figure, it has been seen that a small vortex is formed at the center of the cavity. It is evident that the size of the vortex is increased with the increasing value of *Pr*. The influence of Prandtl number *Pr* on thermal fields for the selected value of *Ra* is displayed in Fig.4.17 for *Re* = 50 and *Ha* = 20. As expected, the thermal boundary layer decreases in thickness as *Pr* increases. This is reflected by the denser deserting of isotherms close to the heated wall and cooled wall as *Pr* increases. The spread of isotherms at low values of *Pr* is due to a strong stream wise conduction that decreases the stream wise temperature gradient in the field. At the increase of *Pr* the isotherms become linear in the cavity and impenetrable to respective wall. From the Fig. 4.18, it can easily be seen that the isotherms for different values of *Pr* at *Ra* = 10^4 are clustered near the heated horizontal wall and cooled vertical heated surface of the enclosure, indicating steep temperature gradient along the vertical direction in this region. Besides, the thermal layer near the heated wall becomes thinner moderately with increasing *Pr*.

The effects of Prandtl number on average Nusselt number *Nu* at the heated surface and average bulk temperature θ_{av} in the cavity is illustrated in Fig. 4.19 & 4.20 with *Re* = 50 and *Ha* = 20. From this figure, it is found that the average Nusselt number *Nu* goes up penetratingly with increasing *Pr*. It is to be highlighted that the highest heat transfer rate occurs for the highest values of *Pr* (= 6). The average bulk temperature of the fluid in the cavity declines very mildly for higher values of *Pr* (0.71 - 6.0). But for the lower values of *Pr*, the average bulk temperature is linear. It is to be mentioned here that the highest average temperature is documented for the lower value of *Pr* (= 0.71) in the free convection dominated region.

Table 4.6: Average Nusselt numbers for different Prandtl number while *Pr* = 0.71, 2.0, 3.0, 6.0, *Re* = 50 and *Ha = 20*.

Nu_{av}			
Pr	$Ra = 10^3$	$Ra = 5\times10^3$	$Ra = 10^4$
0.71	4.262786	6.331658	7.510701
2.0	4.998317	7.454621	8.857028
3.0	6.807629	10.118253	12.023071
6.0	8.111548	11.920293	13.940204

Table 4.7: Average Bulk temperature for different Prandtl number while *Pr* = 0.71, 2.0, 3.0, 6.0, *Re* = 50 and *Ha = 20*.

θ_{av}			
Pr	$Ra = 10^3$	$Ra = 5\times10^3$	$Ra = 10^4$
0.71	0.598198	0.568812	0.558697
2.0	0.584269	0.550002	0.538424
3.0	0.547777	0.504842	0.490760
6.0	0.524512	0.475957	0.459601

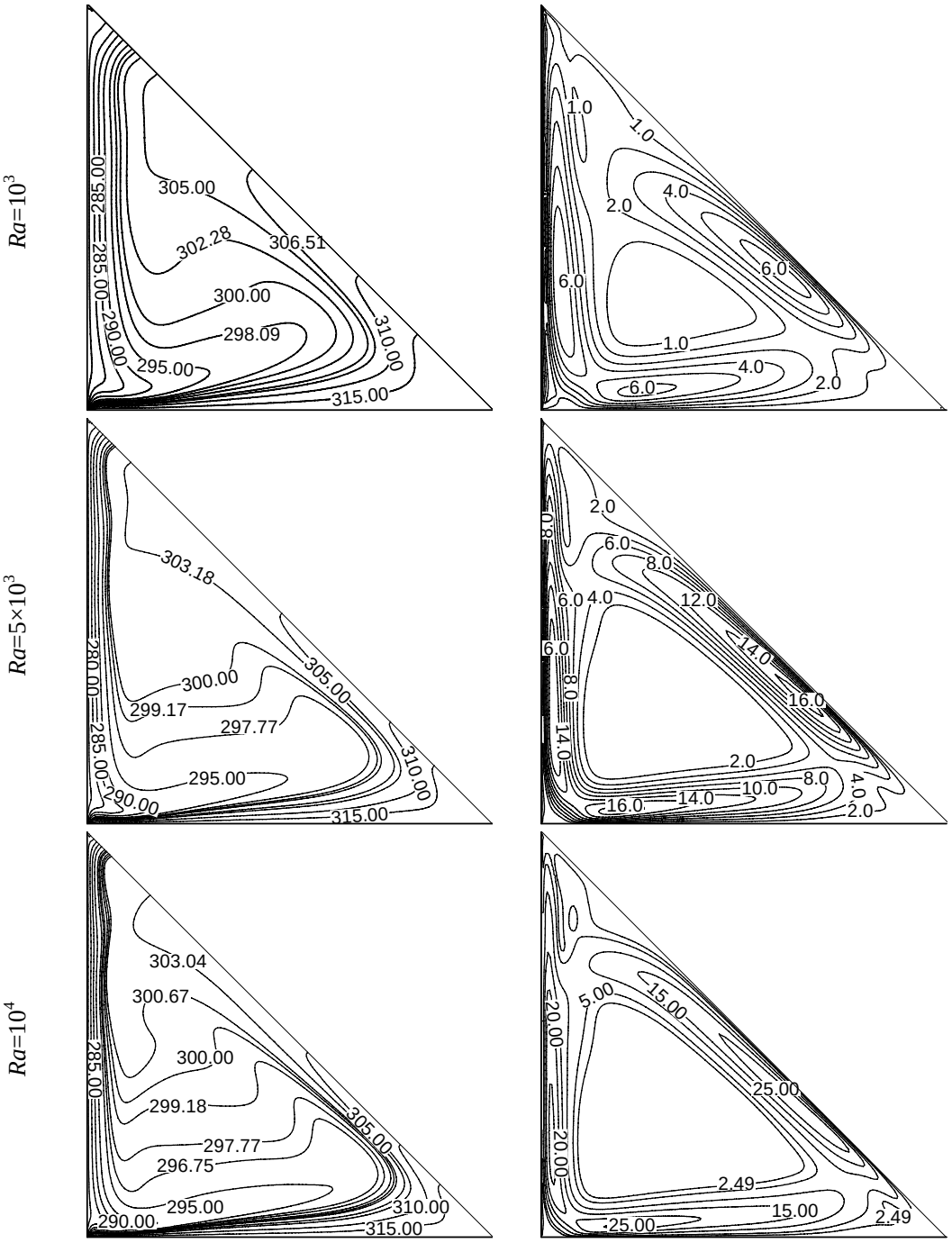

Fig 4.15: Isotherms and streamlines patterns for *Re* = 50, *Pr* = 0.71 and *Ha* = 20

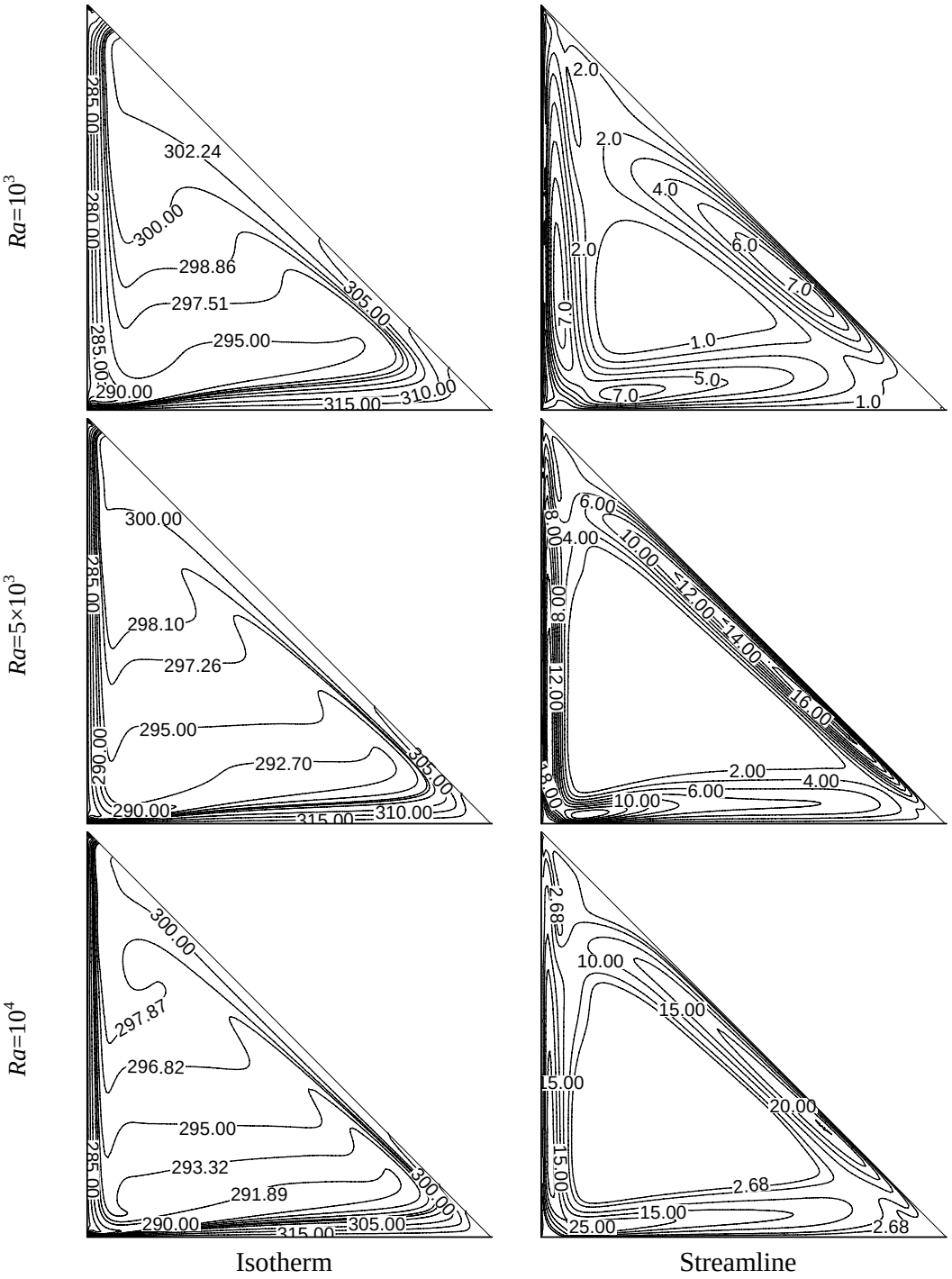

Fig 4.16: Isotherms and streamlines patterns for Re = 50, Pr = 2.0 and Ha = 20

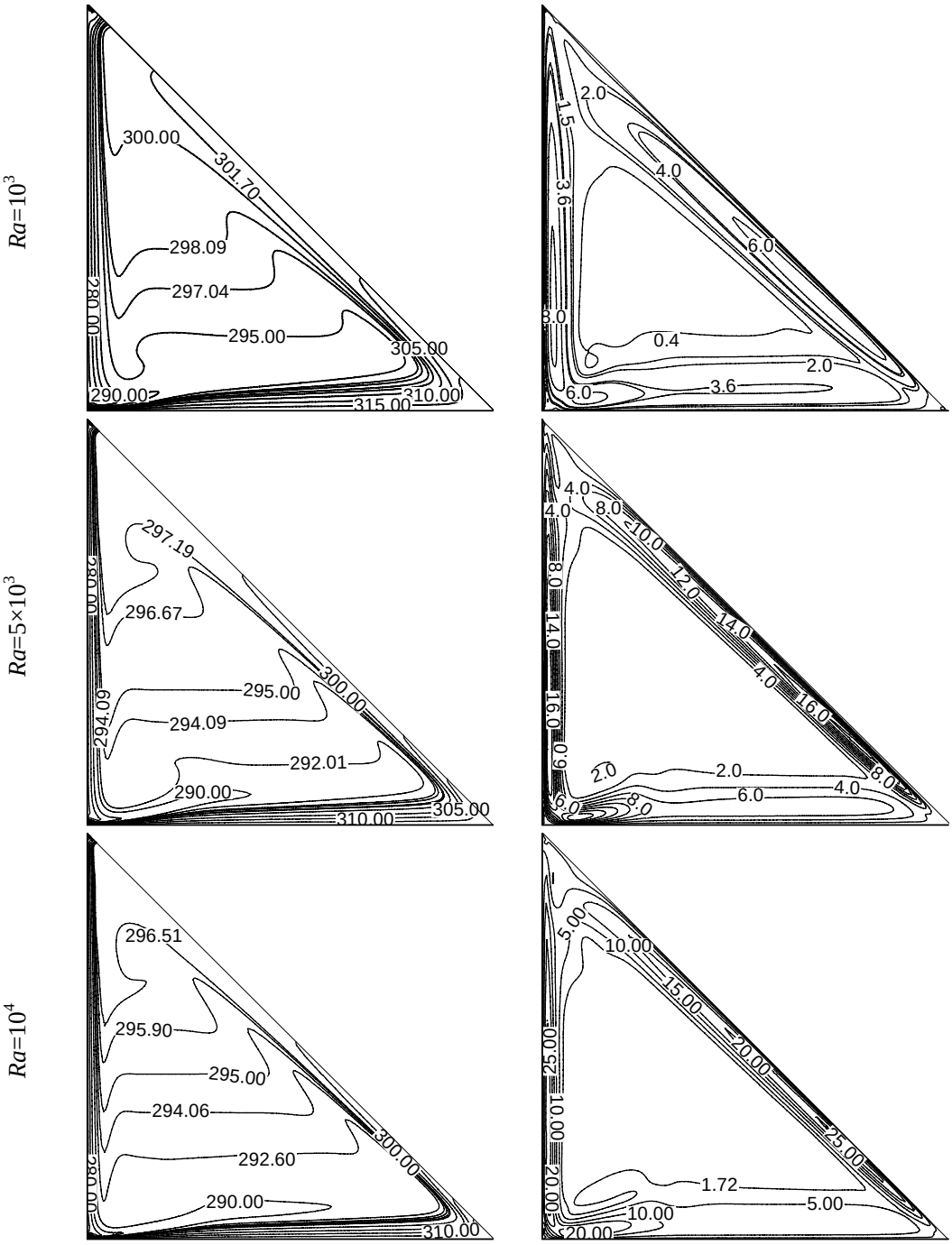

Fig 4.17: Isotherms and streamlines patterns for *Re* = 50, *Pr* = 3.0 and *Ha* = 20

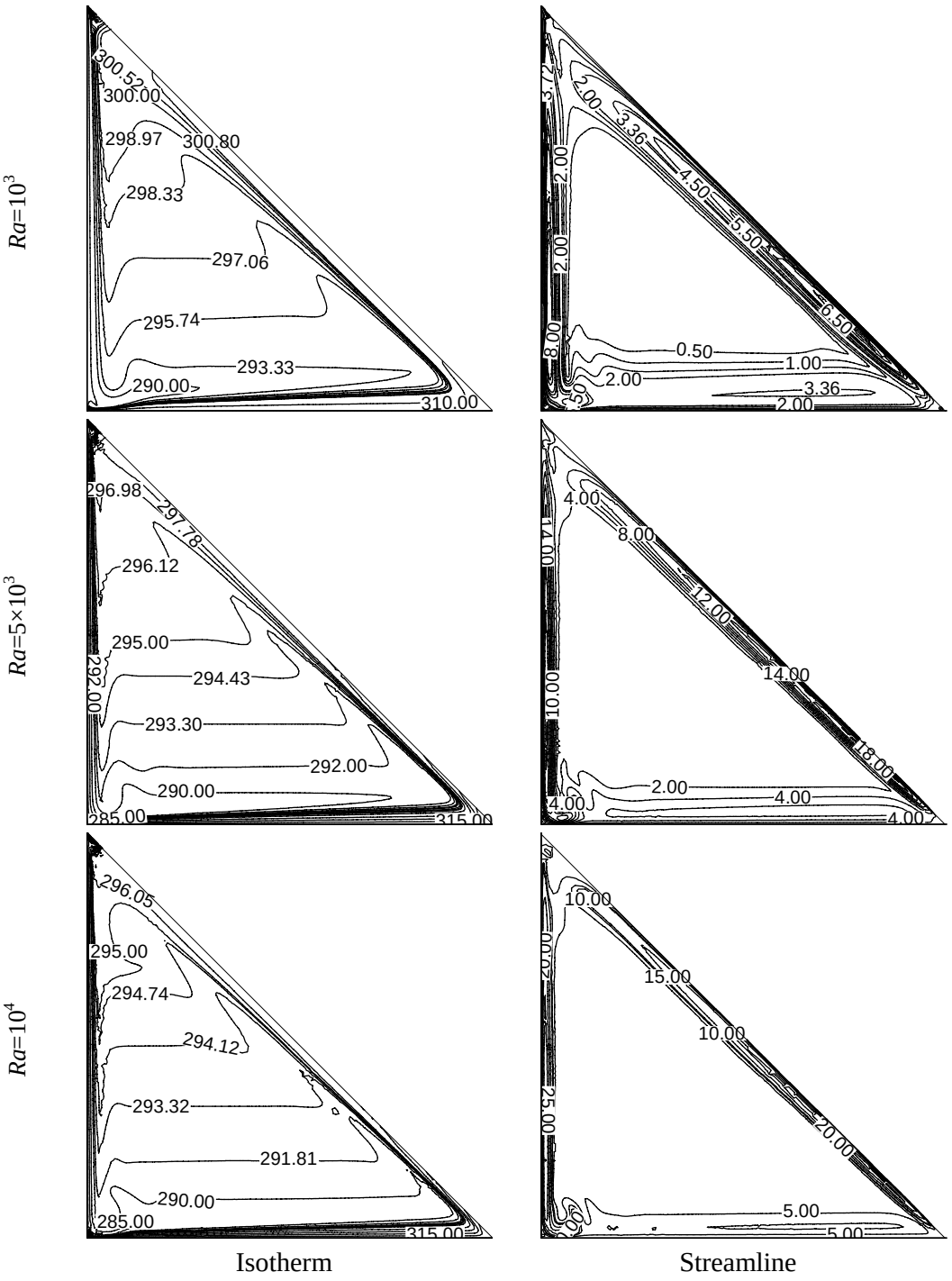

Fig 4.18: Isotherms and streamlines patterns for *Re* = 50, *Pr* = 6.0 and *Ha* = 20

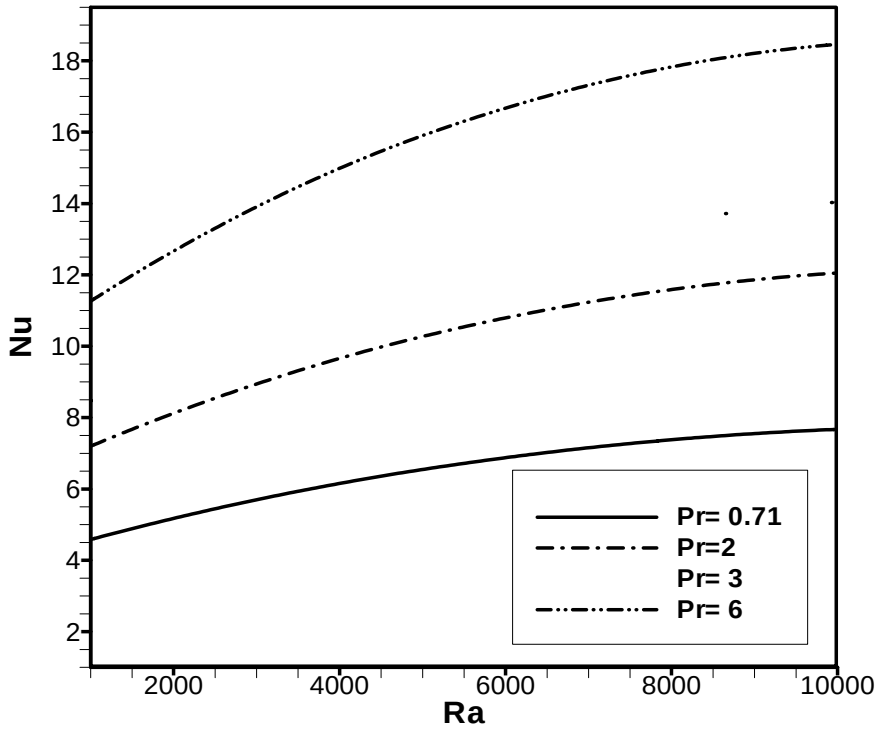

Fig.4.19: Effect of average Nusselt number and Rayleigh number while *Re* = 50 and *Ha* = 20

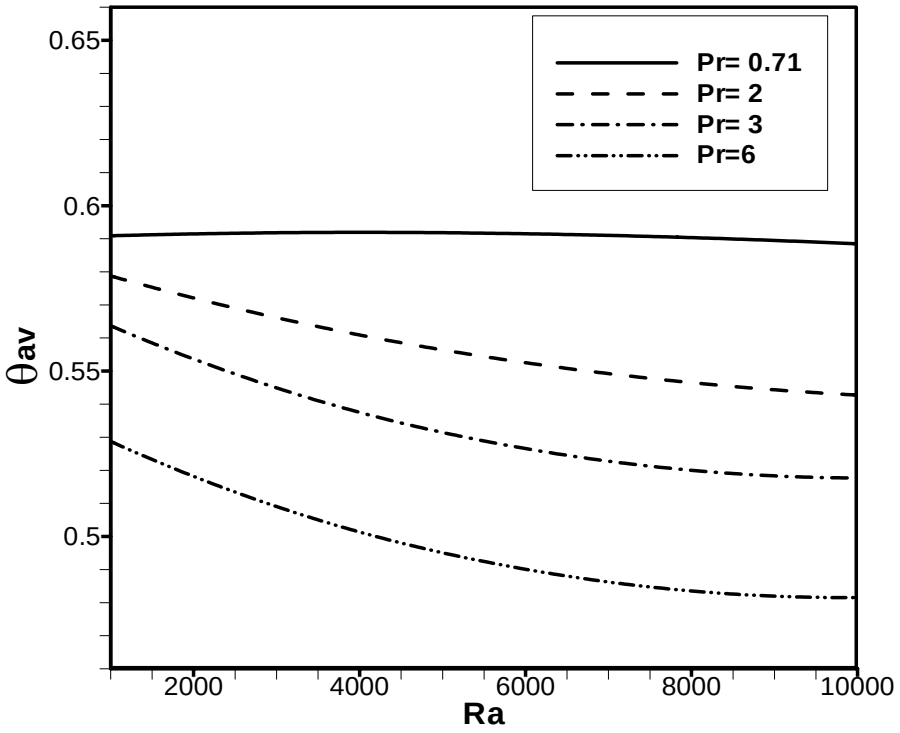

Fig.4.20: Effect of average bulk temperature and Rayleigh number while *Re* = 50 and *Ha* = 20.

4.6 CHAPTER SUMMARY

Two-dimensional laminar steady state MHD mixed convection flow in triangular cavity with the bottom wall is at iso-heat flux has been studied numerically. A finite element method for steady-state incompressible MHD mixed convection flow is presented. The finite element equations were derived from the governing flow equations that consist of the conservation of mass, momentum, and energy equations. The derived finite element equations are nonlinear requiring an iterative technique solver. The Newton-Raphson iteration method has applied to solve these nonlinear equations for solutions of the nodal velocity component, temperature, and pressure by considering Prandtl numbers of 0.71, 2.00, 3.0 and 6.00, Reynolds numbers of 40, 50, 70 and 100, Hartman numbers of 5, 10, 20 and 50, also Rayleigh numbers of 10^3 to 10^4. The results show that

- The heat transfer rate increases for Rayleigh number 10^3 to 10^4 gradually but different behave in bulk temperature for higher Reynold number.
- Heat transfer depends on Prandtl number and heat transfer rate increases but the bulk temperature decreases for higher Prandtl number.
- Thermal boundary layer thickness is thinner for increasing of Rayleigh number due to upsurge of convective heat transfer rate.
- The heat transfer rate Nu_{av} increases with the increase of Ha number in forced dominated region but sharply fall down in mixed dominated region.
- The heat transfer rate (Nu_{av}) at the hot wall is the highest for the Pr = 6.0 when Rayleigh number 10^4, whereas the lowest heat transfer rate for the Ha = 50 when Rayleigh number 10^3, while diverse item happens in the case of bulk temperature.
- Various vortices entering into the flow field and secondary vortex at the vicinity boundary wall and bottom wall of the cavity is seen in the streamlines.

CHAPTER 5
CONCLUSIONS

The conjugate effects of conduction and MHD mixed convection flow in a triangular cavity with some possible boundary conditions are the fundamental objective of this work is to study. The overall work can be summed up through the subsequent conclusions.

5.1 SUMMARY OF THE MAJOR OUTCOMES

In this testimony, the effect of conduction on mixed convection flow and the significance of conduction on MHD mixed convection flow inside a triangular cavity have been studied. Foremost, a two dimensional, steady combined convection flow in a triangular cavity, and subjected to cool at the right vertical wall which is moving, adiabatic conditions at the other inclined wall and the bottom wall considered as hot. In this cases the stream line of flow and thermal fields as well as characteristics of heat transfer process particularly its expansion has been evaluated in chapter 3.On the basis of the analysis the following conclusions have been drawn:

- The Reynolds number has major effect on the flow and thermal distributions in the triangular cavity. The average Nusselt number (*Nu*) at the hot wall is the highest for the *Re* = 100 when Rayleigh number 10^4, while the lowermost heat transfer rate for *Re* = 40 when Rayleigh number 10^3. As the Reynolds number indicates force convection, so for greater value of Reynolds number increases buoyancy force inside the cavity and increase the heat transfer rate quickly.
- Moreover, the average bulk temperature become greatest for *Re* = 40 and *Ra* = 5×10^3 and lowest for *Ra* = 10^4.Bulk temperature demonstrations counter behavior with average Nusslt number for Reaynolds number.
- The influence of Prandtl number on the flow and thermal fields in the cavity is found to be more prominent in fixed *Re*. The maximum heat transfer is experimented at the highest value of *Pr* for the considered value of *Ra*. The average bulk temperature is high for *Pr* = 0.71 in free convection region.
- Thermal and velocity boundary layer thickness is thinner for increasing of Rayleigh number

- Several vortex cells are found into the flow field and a secondary vortex at the center and bottom wall of the cavity is seen in the streamlines.

Secondly, a two dimensional, steady combined convection flow with MHD effect in the same triangular cavity has been studied and subjected to cool at the right vertical wall which is moving, adiabatic conditions at the other inclined wall and the bottom wall considered as hot. In cases of MHD effect, the stream lines of flow and thermal fields as well as characteristics of heat transfer process particularly its expansion has been evaluated in chapter 4. On the basis of the analysis the following conclusions have been drawn:

- The MHD has significant effect on the flow and thermal distributions in the triangular cavity. The average Nusselt number (*Nu*) at the hot wall is the highest for the *Pr* = 6.0 when Rayleigh number 10^4, whereas the lowest heat transfer rate for the *Ha* = 50 when Rayleigh number 10^3. Moreover, the average Nusselt number with MHD effect is considered higher than those obtained without MHD effect for different value of *Pr* number. However, the average bulk temperature at the hot wall is the lowest for the *Pr* = 6.0 when Rayleigh number 10^4, whereas the highest rate for the *Ha* = 50 when Rayleigh number 10^3
- The heat transfer rate increase steadily with the increase of *Ra*. Increasing *Ra* refers that the fluid flow switches from conductive to convective heat transfer. The bulk Temperature decreases smoothly with the increase of *Ra* because at constant conductivity bulk temperature is inversely proportional to the *Nu* (Average Heat Transfer rate).
- The heat transfers rate augment with the increase of *Ra* because when *Pr* number increases, the convective heat transfer dominated inside the flow field. The bulk Temperature remain linear at *Pr* = 0.71 because for low *Pr* number conduction heat transfer dominate in the cavity. But for higher *Pr* bulk temperature decreases due to conduction turn into convection.
- With the increase of *Ha* number electromagnetic conduction increases that slow down the heat transfer rate though it increases at forced convection dominated region for a while but fall steadily in mixed convection dominated region.

- Thermal boundary layer thickness is thinner and velocity of fluid flow increases for increasing of Rayleigh number due to convective heat transfer. .
- Various vortices inflowing into the flow field and secondary vortex at different place in the cavity.

5.2 FURTHER WORKS

The following recommendation can be put forward for the further work on the present research.

- Effect of conduction on MHD mixed convection flow in a triangular cavity with joule heating.
- Effect of conduction on MHD mixed convection flow in a closed triangular cavity with a heat conducting circular and square cylinder.
- Effect of conduction on MHD mixed convection flow in a closed cavity with a magnetic cylinder instead of heat conducting cylinder.
- Effect of conduction on MHD mixed convection flow in a trapezoidal lid-driven cavity for different boundary conditions
- Effect of conduction on MHD mixed convection flow in an open Channel.

REFERENCES

Akinsete V.A., Coleman T.A., "Heat transfer by steady laminar free convection in triangular enclosures", International Journal of Heat and Mass Transfer, Vol. 25, pp. 991–998, **1982.**

Asan H., Namli L., "Laminar natural convection in a pitched roof of triangular cross-section: summer day boundary conditions", Energy Buildings, Vol. 33, pp. 69–73, **2000**.

Asan H., Namli L., "Numerical simulation of buoyant flow in a roof of triangular cross section under winter day boundary conditions", Energy Buildings, Vol. 33, pp. 753–757**, 2000**.

Asan H., Namli L., "Laminar natural convection in a pitched roof of triangle cross-section: summer day boundary conditions", Energy and Buildings, Vol. 33, pp. 69–73, **2000.**

Angirasa D., "Mixed convection in a vented enclosure with isothermal vertical surface", Fluid Dyn. Res., Vol. 26, pp. 219-233, **2000.**

Basak T., Roy S., Krishna Babu S., Pop I., "Finite element simulations of natural convection flow in an isosceles triangular enclosure filled with a porous medium: effects of various thermal boundary conditions", International Journal of Heat Mass Transfer, Vol. 51, pp. 2733–2741, **2008.**

Basak T., Aravind G., Roy S., Balakrishnan A.R., "Heatline analysis of heat recovery and thermal transport in materials confined within triangular cavities" International Journal of Heat and Mass Transfer, Volume 53, pp. 3615-3628, **2010.**

Basak T., Aravind G., Roy S., Balakrishnan A.R., "Visualization of heat flow due to natural convection within triangular cavities using Bejan's heatline concept", International Journal of Heat and Mass Transfer, Vol. 52, pp. 2824-2833**, 2009**.

Basak T., Roy S., Balakrishnan A.R., "Effects of thermal boundary conditions on natural convection flows within a square cavity", International Journal of Heat and Mass Transfer, Vol. 49 (23–24), pp. 4525–4535, **2006**.

Basak T., Roy S., Krishna Babu S., Balakrishnan A.R., " Finite element analysis of natural convection flow in a isosceles triangular enclosure due to uniform and non-

uniform heating at the side walls", International Journal of Heat Mass Transfer, Vol. 51, pp. 4496–4505, **2008.**

Basak T., Aravind G., Roy S., Pop I., "Visualization of heat transport due to natural convection for hot materials confined within two entrapped porous triangular cavities via heatline concept" International Journal of Heat and Mass Transfer, Vol. 53, pp. 2100-2112, **2010**.

Bhoite M. T., Narasimham G. S. V. L., and Murthy, M. V. K., "Mixed convection in a shallow enclosure with a series of heat generating components", International Journal of Thermal Sciences, Vol. 44, pp. 125-135, **2005**.

Biswas G., Laschefski H., Mitra N. K. and Fiebig M., "Numerical investigation of mixed convection heat transfer in a horizontal channel with a built in square cylinder", Numer. Heat Transfer, Vol. 18, pp. 173-188, **1990**.

Calmidi V.V., Mahajan R.L., "Mixed convection over a heated horizontal surface in a partial enclosure" International Journal of Heat and Fluid Flow, Volume 19, pp. 358-367, **1998.**

Cengel Y. A., "Heat and mass transfer", Third Ed., Tata McGraw-Hill, **2007.**

Chen C., Cheng C., "Numerical study of the effects of lid oscillation on the periodic flow pattern and convection heat transfer in a triangular cavity", International Communications in Heat and Mass Transfer, Vol. 36, pp. 590-596**, 2009**.

Chamkha A. J., "Hydromagnetic combined convection flow in a vertical lid-driven cavity with internal heat generation or absorption", Numer. Heat Transfer, Part A, Vol. 41, pp. 529-546, **2002**.

Fuad K., "Numerical analysis of laminar natural convection in isosceles triangular enclosures for cold base and hot inclined walls" Mechanics Research Communications, Vol. 36, pp. 497-508, **2009**.

Gowda Y. T. K., Narayana P. A. A., and Seetharamu K. N., "Mixed convection heat transfer past in-line cylinders in a vertical duct", Numer. Heat Transfer, Part A, Vol. 31, pp. 551-562, **1997**.

Hagen K. D., "Heat transfer with applications", First Ed., Prentice-Hall International, **1999**.

Hajri I., Omri A., Nasrallah S. B., "A numerical model for the simulation of double-diffusive natural convection in a triangular cavity using equal order and control volume based on the finite element method" Original Research Article Desalination, Vol. 206, pp. 579-588, **2007**.

How S.P., and Hsu T.H., "Transient mixed convection in a partially divided enclosure", Comput. Math. Appl., Vol. 36, pp. 95-115, **1998**.

Hossain M. A., and Gorla R. S. R., "Effect of viscous dissipation on mixed convection flow of water near its density maximum in a rectangular enclosure with isothermal wall", International Journal of Numer. Methods for Heat and Fluid Flow, Vol. 16, No. 1, pp. 5-17, **2006**.

Hwang Y. M., Lin Y. K., Altan T., "Evaluation of tubular materials by a hydraulic bulge test", International Journal of Machine Tools and Manufacture, **2002**.

Hsu T.H, Wangn S.G, "Mixed convection in a rectangular enclosure with discrete heat sources", Numer. Heat Transfer, Part A, 38 pp. 627-652, **2000**.

Hajri I., Omri A., Nasrallah S. B., "A numerical model for the simulation of double-diffusive natural convection in a triangular cavity using equal order and control volume based on the finite element method" Original Research Article Desalination, Vol. 206, pp. 579-588, **2007**.

Joudi K.A., Hussein I.A., Farhan A.A., "Computational model for a prism shaped storage solar collector with a right triangular cross section", Energy Conversion and Management, Vol. 45, pp. 337–342, **2004**.

Karyakin YU.E, Sokovishin YU.A., "Transient natural convection in triangular enclosures", International Journal of Heat and Mass Transfer, Vol. 31, pp. 1759–1766, **1988.**

Khanafer K., Vafai K., and Lightstone M., "Mixed convection heat transfer in two-dimensional open-ended enclosure", International Journal of Heat and Mass Transfer, Vol. 45, pp. 5171-5190, **2002**.

Li M., and Tang T., "Steady viscous flow in a triangular cavity by efficient numerical techniques", Comput. Math. Appl., Vol. 31, pp. 55-65, **1996**.

Lin J., and Sharif M. A. R., "Numerical study of fluid flow and heat transfer in a channel with heated normal plates", Numer. Heat Transfer, Part A, Vol. 31, pp. 853-865, **1997**.

Luo W. J., and Yang R. J., "Multiple fluid flow and heat transfer solutions in a two-sided lid-driven cavity", Int. J. of Heat and Mass Transfer, Vol. 50, pp. 2394-2405, **2007**.

Manca O., Nardini S., and Vafai K., "Experimental investigation mixed convection in a channel with an open cavity". Experimental Heat Transfer, Vol. 19, pp. 53–68, **2006**.

Manca O., Nardini S., Khanafer K., and Vafai K., "Effect of heated wall position on mixed convection in a channel with an open cavity". Numer. Heat Transfer, Part A, Vol. 43, pp. 259–282, **2003**.

Omri A., and Nasrallah S. B., "Control volume finite element numerical simulation of mixed convection in an air-cooled cavity", Numer. Heat Transfer, Part A, Vol. 36, pp. 615–637**, 1999.**

Oreper G. M., Szekely J., "The effect of an externally imposed magnetic field on buoyancy driven flow in a rectangular cavity", J. of Crystal Growth, Vol. 64, pp. 505-515, **1983**.

Ozoe H., and Maruo M., "Magnetic and gravitational natural convection of melted silicon-two dimensional numerical computations for the rate of heat transfer", JSME, Vol. 30, pp. 774-784, **1987**.

Papanicolaou E., and Jaluria Y., "Computation of turbulent flow in mixed convection in a cavity with a localized heat source", ASME J. Heat Transfer, Vol. 117, pp. 649–658**, 1995**.

Papanicolaou E., and Jaluria Y., "Mixed convection from an isolated heat source in a rectangular enclosure", Numer. Heat Transfer, Part A, Vol. 18, pp. 427–461, **1990**.

Papanicolaou E., and Jaluria Y., "Mixed convection from simulated electronic components at varying relative positions in a cavity", J. Heat Transfer, Vol. 116, pp. 960–970, **1994**.

Papanicolaou E., and Jaluria Y., "Transition to a periodic regime in mixed convection in a square cavity", J. Fluid Mech., Vol. 239, pp. 489–509, **1992**.

Raji A., and Hasnaoui M., "Correlations on mixed convection in ventilated cavities". Revue Ge´ne´rale de Thermique, Vol. 37, pp. 874–884, **1998b**.

Raji A., and Hasnaoui M., "Mixed convection heat transfer in a rectangular cavity ventilated and heated from the side", Numer. Heat Transfer, Part A, Vol. 33, pp. 533–548, **1998a**.

Raji A., and Hasnaoui M., "Mixed convection heat transfer in ventilated cavities with opposing and assisting flows", Engg. Comp., International Journal of Computer-Aided Eng. Software, Vol. 17(5), pp. 556–572, **2000**.

Rahman M.M., Alim M.A., Mamun M.A.H., Chowdhury M.K. and Islam A.K.M.S., "Numerical Study of Opposing Mixed Convection in a Vented Enclosure" ARPN J. of Eng. and Applied Sci. Vol. 2, pp. 25-36, **2007**.

Rahman M.M., Mamun M.A.H., Saidur R., and Nagata S., "Effect Of a Heat Conducting Horizontal Circular Cylinder on MHD Mixed Convection In A Lid- Driven Cavity Along With Joule Heating", International Journal of Mechanical and Materials Eng. (IJMME), Vol. 4, No. 3, pp.256-265, **2009a**.

Rahman M. M., Alim M. A., "MHD mixed convection flow in a vertical lid-driven square enclosure including a heat conducting horizontal circular cylinder with Joule heating", Nonlinear Analysis: Modeling and Control, Vol. 15(2), pp. 199-211, **2010**.

Raji A., and Hasnaoui M., "Correlations on mixed convection in ventilated cavities". Revue Ge´ne´rale de Thermique, Vol. 37, pp. 874–884, **1998b**.

Ridouane E.H., Campo A., Hasnaoui M., "Benefits derivable from connecting the bottom and top walls of attic enclosures with insulated vertical side walls", Numer. Heat Transfer Part A 49, pp. 175–193, **2006**.

Ridouane E., Campo A., Hasnaoui M., "Benefits derivable from connecting the bottom and top walls of attic enclosures with insulated vertical side walls", Numerical Heat Transfer Part A-Applications, Vol. 49 (2), pp. 175–193, **2006.**

Roy S., Basak T., "Finite element analysis of natural convection flows in a square cavity with non-uniformly heated wall(s)", International Journal of Engineering Science, Vol. 43 (8–9), pp. 668–680**, 2005.**

Rudraiah N., Barron R. M., Venkatachalappa M., and Subbaraya C. K., "Effect of magnetic field on free convection in a rectangular enclosure", International Journal of Engng. Sci., Vol. 33, pp. 1075-1084, **1995b.**

Rudraiah N., Venkatachalappa M., and Subbaraya C. K., "Combined surface tension and buoyancy-driven convection in a rectangular open cavity in the presence of magnetic field", Int. J. Non-linear Mech., Vol. 30(5), pp. 759-770, **1995a**.

Singh S., and Sharif M. A. R., "Mixed convective cooling of a rectangular cavity with inlet and exit openings on differentially heated side walls". Numer. Heat Transfer, Part A Vol. 44, pp. 233–253, **2003**.

Sahoo D., and Sharif M. A. R., "Mixed-convective cooling of an isothermal hot surface by confined slot jet impingement", Numer. Heat Transfer, Part A, Vol. 45, pp. 887-909, **2004**.

Saeidi S. M., and Khodadad J. M., "Forced convection in a square cavity with inlet and outlet ports", International Journal of Heat and Mass Transfer, Vol. 49, pp. 1896-1906, **2006.**

Tzeng S.C., Liou J.H., Jou R.Y., "Numerical simulation-aided parametric analysis of natural convection in a roof of triangular enclosures" Heat Transfer Engineering, vol. 26 (8), pp. 69–79**, 2005.**

Varol Y., Oztop H.F., Varol A., "Free convection in porous media filled right-angle triangular enclosures", Int. Commun. Heat Mass Transfer, Vol. 33, pp. 1190–1197, **2006.**

Varol Y., Koca A., Oztop H.F., "Natural convection in a triangle enclosure with flush mounted heater on the wall", International Communications in Heat and Mass Transfer, Vol. 33 (8), pp. 951–958**, 2006.**

Varol Y., Oztop H.F., Pop I., "Numerical analysis of natural convection for a porous rectangular enclosure with sinusoidally varying temperature profile on the bottom wall", Int. Commun. Heat Mass Transfer, Vol. 35, pp. 56–64, **2008.**

Varol Y., Oztop H.F., Koca A., "Entropy production due to free convection in partially heated isosceles triangular enclosures", Appl. Therm. Eng., Vol. 28., pp.1502–1513, **2008.**

Wang L.B., Wakayama N.I., " Control of natural convection in non- and low conducting diamagnetic fluids in a cubical enclosure using inhomogeneous magnetic fields with different directions", Chemical Engineering Science, Vol. 57 (11), pp. 1867–1876, **2002.**

Wang Q., and Jaluria Y., “Instability and heat transfer in mixed convection flow in a horizontal duct with discrete heat sources”, Numer. Heat Transfer, Part A, Vol. 42, pp. 445-463, **2002**.

Xu Xu., Yu Zitao., Hu Yacai., Fan Liwu., Cen K., “.A numerical study of laminar natural convective heat transfer around a horizontal cylinder inside a concentric air-filled triangular enclosure”. International Journal of Heat and Mass Transfer, Vol. 53, p. 345-355, **2010**.

Zi-Tao Yu., Xu Xu., Ya-Cai Hu., Li-Wu Fan., Ke-Fa Cen., “ Unsteady natural convection heat transfer from a heated horizontal circular cylinder to its air-filled coaxial triangular enclosure” International Journal of Heat and Mass Transfer, Vol. 54, pp. 1563-1571, **2011.**